AgRISTARS

SM-T3-04436
NAG 5-31

A Joint Program for Agriculture and Resources Inventory Surveys Through Aerospace Remote Sensing

Soil Moisture

August 1983

Technical Report

A MATHEMATICAL CHARACTERIZATION OF VEGETATION EFFECT ON MICROWAVE REMOTE SENSING FROM THE EARTH

Y. Choe
L. Tsang

1. Report No.	2. Government Accession No.	3. Recipient's Catalog No.
SM-T3-04436		

4 Title and Subtitle	5. Report Date
A Mathematical Characterization of Vegetation Effect on Microwave Remote Sensing from the Earth	August 1983
	6. Performing Organization Code

7. Author(s)	8. Performing Organization Report No.
Y. Choe L. Tsang	RSC-139
	10. Work Unit No.

9. Performing Organization Name and Address	11. Contract or Grant No.
Remote Sensing Center Texas A&M University College Station, Texas 77843	NAG 5-31
	13. Type of Report and Period Covered
12. Sponsoring Agency Name and Address National Aeronautics & Space Administration Goddard Space Flight Center Greenbelt, Maryland 20771	Quarterly Report
	14. Sponsoring Agency Code

15. Supplementary Notes

.16. Abstract

In passive microwave remote sensing of the earth, a theoretical model that utilizes the radiative transfer equations has been developed to account for the volume scattering effects of the vegetation canopy.

Vegetation canopies such as alfalfa, sorghum, and corn are simulated by a layer of ellipsoidal scatterers and cylindrical structures. The ellipsoidal scatterers represent the leaves of vegetation and are randomly positioned and oriented. The orientation of ellipsoids is characterized by a probability density function of Eulerian angles of rotation. The cylindrical structures represent the stalks of vegetation and their radii are assumed to be much smaller than their lengths.The underlying soil is represented by a half-space medium with a homogeneous permittivity and uniform temperature profile. The radiative transfer equations are solved by a numerical method using a Gaussian quadrature formula to compute both the vertical and horizontal polarized brightness temperature as a function of observation angle.

The theory was applied to the interpretation of experimental data obtained from sorghum covered fields near College Station, Texas.

17. Key Words (Suggested by Author(s))	18. Distribution Statement
	Unlimited

19. Security Classif. (of this report)	20. Security Classif. (of this page)	21. No. of Pages	22. Price*
Unclassified	Unclassified	107	

*For sale by the National Technical Information Service, Springfield, Virginia 22161

SM-T3-04436

NAG 5-31

A MATHEMATICAL CHARACTERIZATION OF VEGETATION EFFECT ON MICROWAVE REMOTE SENSING FROM THE EARTH

by

Y. Choe
L. Tsang

This report describes activity carried out in support of the Soil Moisture activites of the Project.

Remote Sensing Center
Texas A&M University
College Station, Texas 77843

August 1983

TABLE OF CONTENTS

LIST OF FIGURES

LIST OF FIGURES (continued)

LIST OF FIGURES (continued)

ABSTRACT

In passive microwave remote sensing of the earth, a theoretical model that utilizes the radiative transfer equations has been developed to account for the volume scattering effects of the vegetation canopy.

Vegetation canopies such as alfalfa, sorghum, and corn are simulated by a layer of ellipsoidal scatterers and cylindrical structures. The ellipsoidal scatterers represent the leaves of vegetation and are randomly positioned and oriented. The orientation of ellipsoids is characterized by a probability density function of Eulerian angles of rotation. The cylindrical structures represent the stalks of vegetation and their radii are assumed to be much smaller than their lengths. The underlying soil is represented by a half-space medium with a homogeneous permittivity and uniform temperature profile. The radiative transfer equations are solved by a numerical method using a Gaussian quadrature formula to compute both the vertical and horizontal polarized brightness temperature as a function of observation angle.

The theory was applied to the interpretation of experimental data obtained from sorghum covered fields near College Station, Texas.

INTRODUCTION

In recent years, remote sensing techniques utilizing microwave sensors are being developed for numerous applications. Major emphasis has been placed on measuring soil moisture for use in global monitoring of renewable resources using satellite based sensor systems. In addition, there is considerable interest in using microwave sensors for geological exploration as well as for tracking systems in military ordinance. For all of these applications, the effect of vegetation on the microwave signal is significant and must be understood to utilize the potential of microwave remote sensing techniques. The majority of the experimental and theoretical work in this area has been in relationship to the measurement of soil moisture [1]-[24].

Remote sensing, in general, can be classified into two areas: passive and active. In passive microwave remote sensing, one measures the electromagnetic power intensity naturally emitted by the medium due to turmoil agitation. This measurement is specified by a parameter termed the radiometric brightness temperature. The brightness temperature of a body is defined as the physical temperature that a blackbody must have in order to emit the same amount of radiation as the original body. In active remote sensing, one provides a source (e.g. radar) of electromagnetic radiation and measures the radiation that is scattered, usually in the backward direction.

In remote sensing of a scattering medium such as vegetation, the volume scattering has long been recognized as a dominant factor in both active and passive cases. Accordingly, the development of a theoretical model is essential both in understanding how the physical properties of the medium affect the measurements, and in interpreting the remote sensing data.

The volume scattering can be accounted for by modeling the vegetation canopy with either a random medium (random medium approach) or a homogeneous medium containing discrete scatterers (discrete scatterer approach). In the former case, a random medium has an average permittivity ε_1 and its random part is characterized by a correlation function with variance δ, horizontal correlation length ℓ_p and a vertical correlation length ℓ. In the discrete scatterer approach, vegetation canopy is modeled as a layer of such scattering medium bounded by air above and half-space below, and the scatterers are characterized with their sizes, permittivities and effective fractional volume imbedded inside a homogeneous medium.

In the theoretical development of the random medium approach for passive remote sensing, the volume scattering effect due to medium inhomogeneity was first accounted for by Gurvich et al. [25]. Assuming the constant temperature profile, they derived the expressions for the brightness temperature of a random medium with laminar structure in the single scattering approximation. Incorporating nonuniform temperature profiles, Tsang and Kong [26] studied the problem with a radiative transfer approach. They [27] also derived the emissivity of a half-space random medium with a three-dimensional variation. They then

solved the radiative transfer equation to obtain the brightness temperatures for a half-space random medium with three-dimensional variation [28]. From the Dyson and Bethe-Salpeter equations, they derived modified radiative transfer equations for a two-layer random medium [29]. With the method of invariant imbedding, Tsang and Kong [30] studied the thermal microwave emission from a slab random medium with non-uniform scattering, absorption, and temperature profile in the vertical direction. Djermakoye and Kong [31] also used the random medium approach and the radiative transfer theory to obtain results for a N-scattering layer model with a laminar structure.

For active remote sensing, Stogryn [32] studied scattering by random dielectric constant fluctuations in the low frequency limit using the distorted Born approximation. The bistatic scattering cross sections for a random medium with lateral and vertical correlations were calculated by Tsang and Kong [33]. Fung and Fung [34] obtained the bistatic scattering coefficients from a vegetation-like half-space random medium. Zuniga and Kong [35] studied the scattering from a slab of random medium using the Born approximation. Then Zuniga et al. [36] extended the result to the second order in albedo to see the depolarization effect in the backscattering direction. Zuniga et al. [37] also studied the scattering from a generalized N-layered random medium using the Born approximation.

In developing the discrete approach for passive remote sensing, England [38] examined thermal emission darkening caused by randomly distributed isotropic point scatterers in a uniform low-loss dielectric half-space medium with a radiative transfer approach. He [39] then

solved the radiative transfer equation for a scattering layer containing Rayleigh particles. Using Mie scattering phase functions the problem has been solved for a half-space medium by Tsang and Kong [40]. Tsang et al. [41] applied the Mie scattering model to a layer of cloud and rainfall. Chang et al. [42] treated the problem of microwave emission from a layer of snow and glacier ice at the nadir viewing angle.

For active remote sensing case, Shin et al. [43] used an iterative and a numerical approach to solve the radiative transfer equation with a Rayleigh phase function. Using Foldy's and distorted Born approximations, Lang [44] calculated the backscattering cross section. Tsang et al. [45] applied the radiative transfer theory within the Rayleigh approximation to calculate the backscattering cross section of a layer of randomly positioned and oriented small ellipsoids.

The radiative transfer theory has been used extensively in theoretical studies for remote sensing from scattering medium because it is simple and includes multiple scattering effects. It starts with the radiative transfer equations which govern the propagation of energy through the scattering medium.

In this thesis, the volume scattering effects of vegetation canopies are studied by introducing a theoretical model that utilizes the radiative transfer equation defined for a medium containing discrete scatterers as shown in Fig. 1. The model is interpreted in terms of microwave emission. Vegetation canopies such as alfalfa, sorghum, and corn are simulated by a layer of ellipsoidal scatterers [45] and cylindrical structures. The ellipsoidal scatterers represent the leaves of vegetation and are randomly positioned and oriented. The orientation

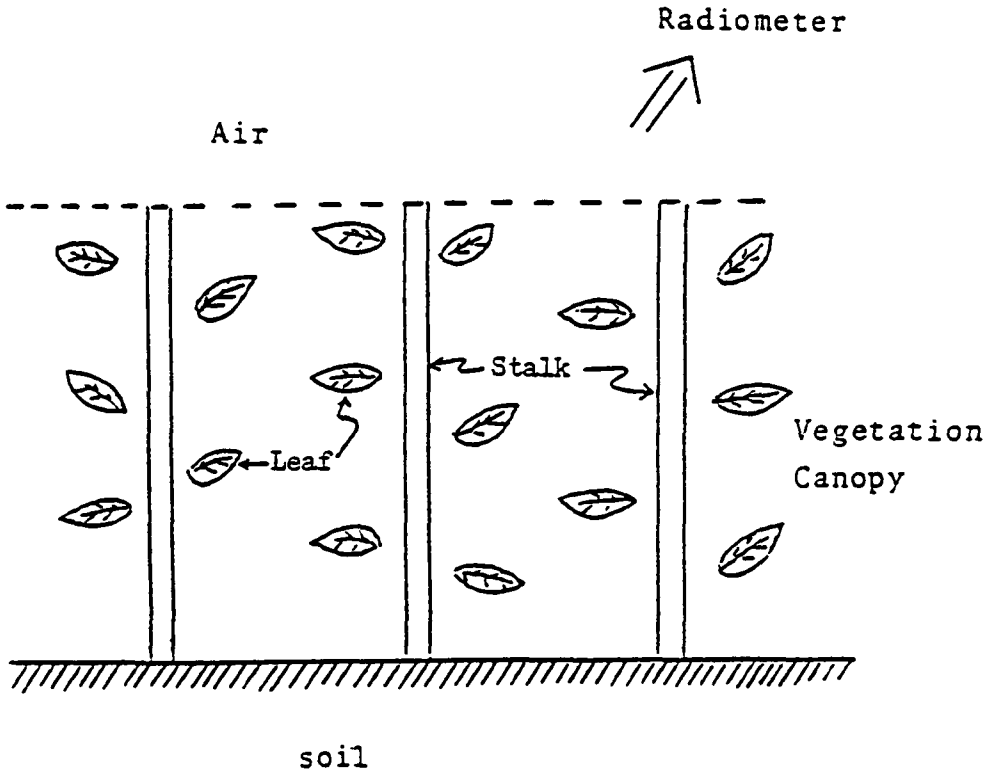

Fig. 1. Geometry of vegetation canopy.

of the ellipsoids is characterized by a probability density function of Eulerian angles of rotation [46]. The cylindrical structure represents the stalks of the vegetation and has a small radius in the horizontal direction and a large length in the vertical direction. The underlying soil is represented by half-space medium with a homogeneous permittivity and a uniform temperature profile. The model computes both the vertical and horizontal polarized brightness temperature as a function of the emission angle.

The second section of this report describes the experimental measurements obtained at the Texas A&M University Experimental Research Farm near College Station, Texas. The passive microwave and ground truth data collected from bare soil and vegetation fields are tabulated. Also, the information of test vegetation (sorghum) such as the shape, size and leaf inclination angle is described.

In the section entitled Radiative Transfer Theory, the radiative transfer equations that describe the electromagnetic emission and scattering are derived for a homogeneous medium containing randomly distributed cylindrical and ellipsoidal scatterers, respectively. For each discrete scatterers model, the absorption and scattering coefficients, the loss per unit length due to absorption and scattering, respectively, as well as scattering functions are derived. Then, the radiative transfer equations are solved by numerical technique.

The next section describes the numerical technique used to solve the radiative transfer equations using the Gaussian quadrature formula.

In the section entitled Data Matching, the theoretical results of the radiative transfer equations are matched to the experimental

measurements. First, experimental measurements obtained from bare soil are used to calculate the permittivity of bare soil. These permittivities are used to compute the theoretical results for a vegetated soil. These computations are matched to experimental measurements of the vegetated fields by adjusting the model input parameters such as size, permittivity and volumetric density of each scatterer.

DESCRIPTION OF MEASUREMENT AND VEGETATION

Background

There has been a series of experimental ground-based microwave measurements at the Texas A&M University Experimental Research Farm near College Station, Texas [8]-[12]. An experiment was performed in 1974 during which simultaneous active and passive microwave measurements were acquired over controlled bare and vegetated soil as a function of soil moisture and surface roughness. The NASA Johnson Space Center L-band (1.4 GHz) and X-band (10.69 GHz) truck mounted radiometer was used to obtain the passive microwave data. This thesis deals only with passive microwave remote sensing.

Data Acquisition

Ground truth and microwave data were obtained from ten plots of land in the Texas A&M University Experimental Research Farm in Burleson County, Texas [12]. Fig. 2 shows the field layout. Textural analysis of soil within the test field revealed that the average soil texture was 3% sand, 35% silt and 62% clay. The soil was uniform across the test fields and is classified as Miller clay.

In Fig. 2, nine of ten plots were 15 m by 46 m (sets A, B, C) and one was 46 m square (plot D). The nine smaller plots were in sets of three with each set having one plot prepared with a smooth surface, one with a medium rough surface, and one with a rough surface. Set C was bare while sets A and B were uniformly planted in a sorghum hybrid.

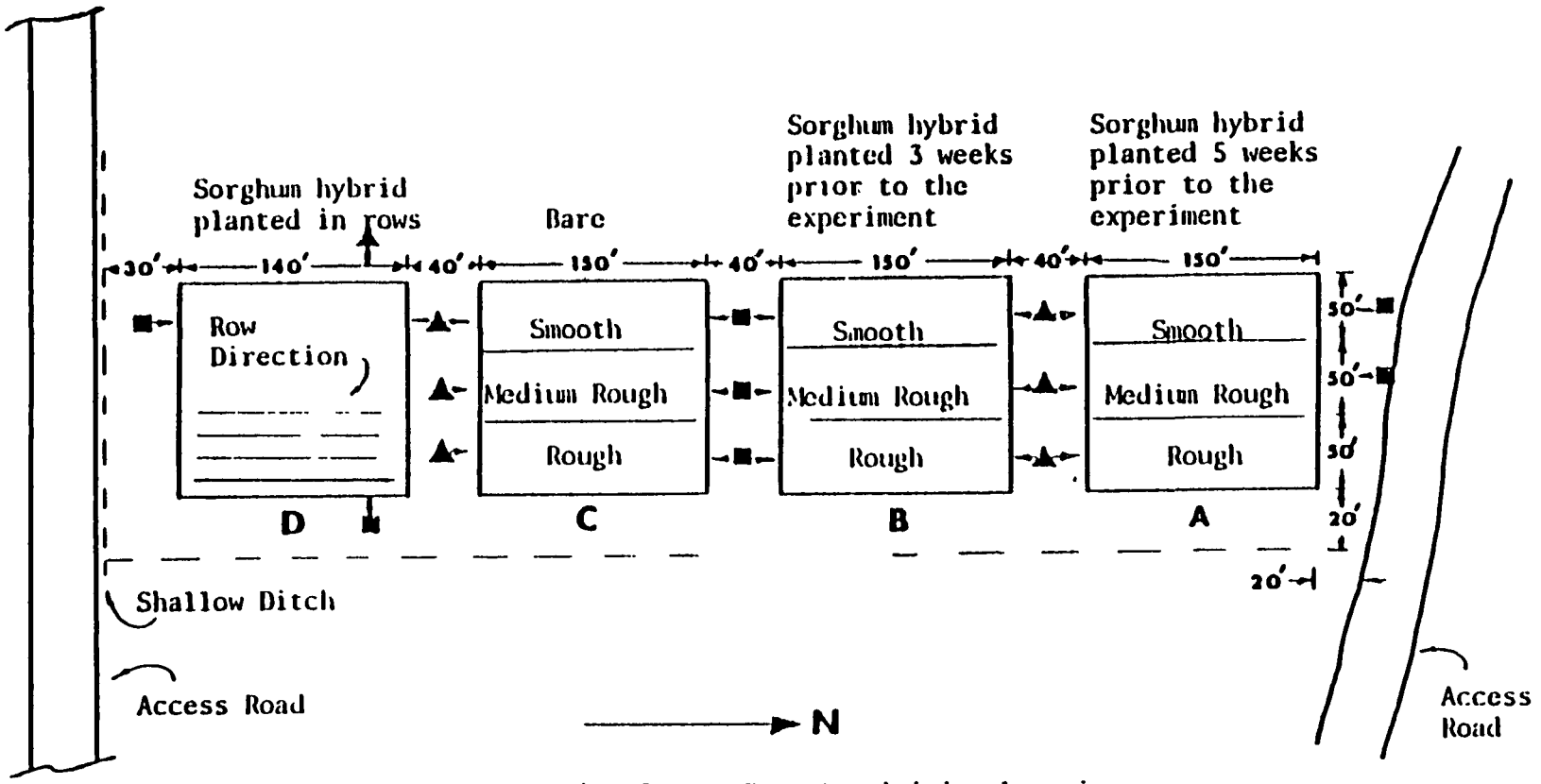

Fig. 2. Layout of the 1974 Experimental Plots.

Set A was planted approximately five weeks prior to the field measurements and set B was planted three weeks before. Plot D was also planted in sorghum hybrid, but in row running north and south.

Passive microwave data were recorded simultaneously at each field as a function of soil moisture, incident angles, polarization and frequency [9]. Passive microwave measurements were acquired at 0°, 20°, 35° and 50° incident angles for both horizontal and vertical polarizations at 1.4 GHz and 10.69 GHz. The 1.4 GHz data obtained from bare soil (CS field) and vegetation-covered (sorghum hybrid) soil (BS field) with smooth surfaces are used in this research and tabulated in Appendix A.

Ground truth measurements of soil moisture and temperature profile were made simultaneously with the microwave measurements [9]. Soil moisture samples were obtained at several depths down to 15 cm and are tabulated in Appendix A. There are 15 profiles for bare soil (CS 1 - CS 15) and 7 profiles for vegetated soil (BS 1 - BS 7). The various soil moisture conditions were a result of irrigation and the various rainfall events that occurred in that time period. Surface roughness and vegetation height were obtained at numerous locations throughout the experiment. The smooth surface had an rms surface height of 0.88 cm, the medium 2.6 cm, and the rough 4.3 cm. The average heights of vegetation in fields A and B were 188 cm and 125 cm, respectively, and the volumetric density of vegetation in each of these fields was approximately 1 %.

Description of Vegetation

Before the formulation of a theoretical model, the vegetation canopy must be specified. Since sorghum was chosen as the vegetation to be modeled, informaton such as shape, size and leaf inclination angle for sorghum is needed.

Havelka [47] studied the effect of leaf type, plant density and row spacing to evaluate the performance of several erect and normal leaved grain sorghum selections and hybrids. In his research, two erect leaf strains from the World Sorghum Collection, P 407 and SC 170, and a normal leaved variety, Caprock, were used. Fig. 3 shows the hemispherical photographs taken of the 3 different canopies 2 weeks prior to anthesis. Examination of the photographs showed that a greater percentage of leaf area of the erect leaf selections tended toward a more acute inclination, while Caprock exibited most of its leaves in a horizontal plane. In Fig. 3, we observe that the shape of sorghum leaf is long and thin. Although the length and width of leaf are different with the populations of sorghum, those values are within the range of 40-80 cm and 4-8 cm, respectively. Therefore, the effective leaf area is within the range of 200π-500π cm^2. The stalk diameters of the three sorghums were within the range of 10-25 mm.

Leaf angle measurements were taken by Havelka from the horizontal plane at 2 growth stages: 57 days after planting and 103 days after planting. Leaf angle distribution measurements made 57 days after planting show that leaves of the erect leaf selections became more inclined with increased population density. The greatest prepondence

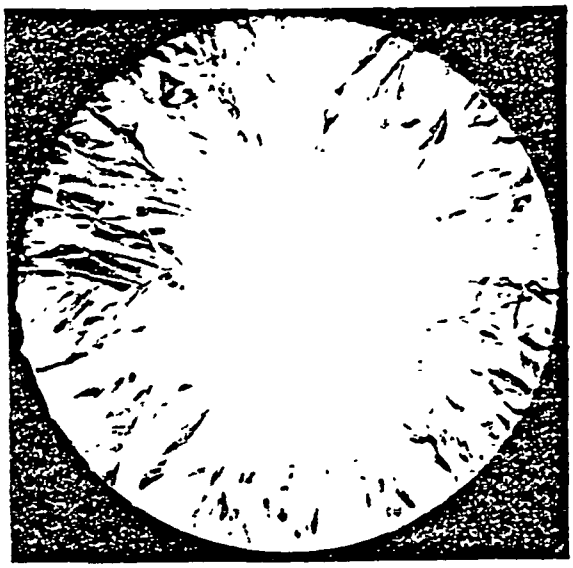

P 407

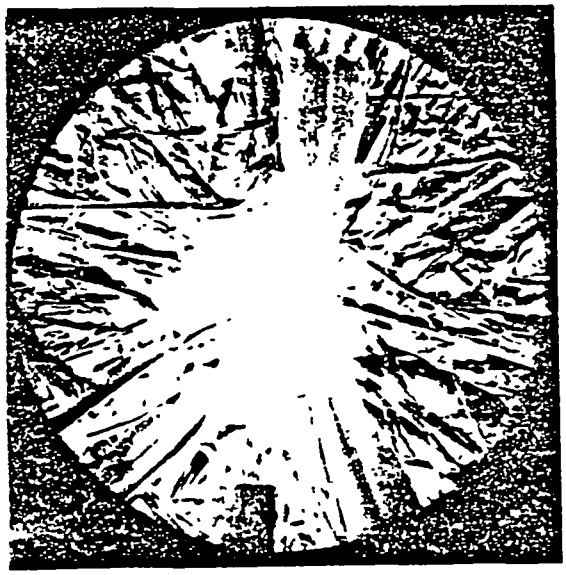

SC 170

Caprock

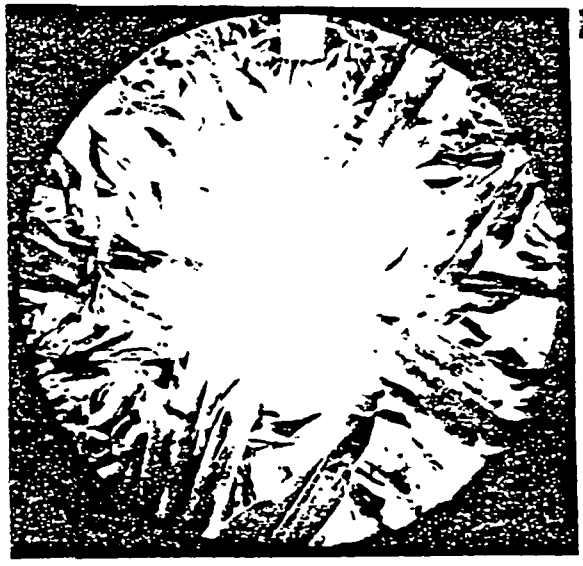

Fig. 3. Hemispherical photograph of foliage selections 2 weeks before anthesis planted 14 cm apart in equidistant spacing pattern.

of leaf angle measured from the horizontal plane fell into the 45° - 90° angle classes for P 407 and SC 170. About 70% of the leaf areas of P 407 and SC 170 occurred in the 60° - 90° angle classes. Caprock had its greatest percentage of leaf area in the 30° - 60° angle classes for populations of $129X10^3$, $172X10^3$ and $258X10^3$ plants/ha. At a population of $517x10^3$ plants/ha, 48% of its leaf area occurred in the 60° - 90° classes. The leaf area of Caprock was distributed mostly in the 30° - 75° range of classes. The 0° - 30° angle classes accounted for approximately 18% of leaf area in each population. At 103 days after planting, the leaf inclinations had decreased sharply from those measured previously. Leaf angles of the two erect leaf strains were mostly in the 30° - 75° angle classes, while the leaf angle of Caprock were distributed mostly in 0° - 60° angle classes.

For the theoretical simulation to be performed later, the length and width of leaf were chosen as 64.8 cm and 5 cm which correspond to the effective leaf area of 324π cm^2. Since th leaf is represented by a circular disk, the radius of disk can be assumed to be 18 cm which corresponds to the effective leaf area of 324π cm^2. Furthermore, for the convenience of problem, we assume the leaves are uniformly distributed along the height of sorghum.

From the Havelka's study, the leaf angles of erect leaved sorghum and Caprock were distributed mostly in 60° - 90° and 30° - 75° from the horizontal plane, respectively. Thus, a leaf angle of 60° from the horizontal plane (30° from the vertical direction) can be chosen for the theoretical modeling.

RADIATIVE TRANSFER THEORY

In this section, the radiative transfer equations that govern the electromagnetic propagation through the homogeneous medium containing discrete scatterers are derived.

In general, two theories are currently being used to incorporate scattering effects: wave theory and the radiative transfer theory. In the wave theory one starts out with Maxwell's equations, introduces the scattering and absorption characteristics of the medium, and tries to solve the problem for the quantities of interest, such as brightness temperatures or backscattering cross sections. This is mathematically rigorous in a sense that in principle all of the multiple scattering, diffraction, and interference effects can be included. However, in practice, it is impossible to obtain a formulation which completely includes all these effects, and various theories which yield useful solutions are all approximations, each being useful over a specific range of parameters.

Radiative transfer theory, on the other hand, starts with the radiative transfer equations which govern the propagation of energy through the scattering medium. It is assumed that there is no correlation between electromagnetic vector fields and therefore, the addition of intensities is considered rather than the addition of vector fields. However, it has an advantage in that it is simple and, more importantly, includes multiple scattering effects.

Therefore, in this chapter the radiative transfer equations are derived for the homogeneous medium containing sparsely distributed cylindrical and ellipsoidal scatterers. Then, the absorption and scattering coefficients, loss per unit length due to absorption, and scattering, respectively, as well as the scattering function matrix are derived for each model of scatterer. In the cylindrical scatterer case, the radius of cylinder is assumed to be much smaller than the length of the cylinder. In the ellipsoidal scatterer case, the radiative transfer theory is applied within the Rayleigh approximation. The Rayleigh scattering model can be used when the size of the scatterers is small compared to the electromagnetic wavelength of interest. To solve the radiative transfer equations, the boundary conditions must be satisfied.

Radiative Transfer Equations

We now derive the radiative transfer equations which are the fundamental equations governing the variation of intensities in the medium which absorbs, emits and scatters radiation.

Consider a small element of cross section da and length ds in the medium as shown in Fig. 4. From a phenomenological point of view, energy conservation requires that the change in intensity I in a distance ds be given by

$$dI = - k_a I ds - k_s I ds + E_t ds + k_s J ds \qquad (1)$$

where k_a and k_s are the absorption and scattering coefficients. The term $-k_a I ds$ accounts for extinction due to absorption, the term $-k_s I ds$ accounts for extinction due to scattering out of the direction

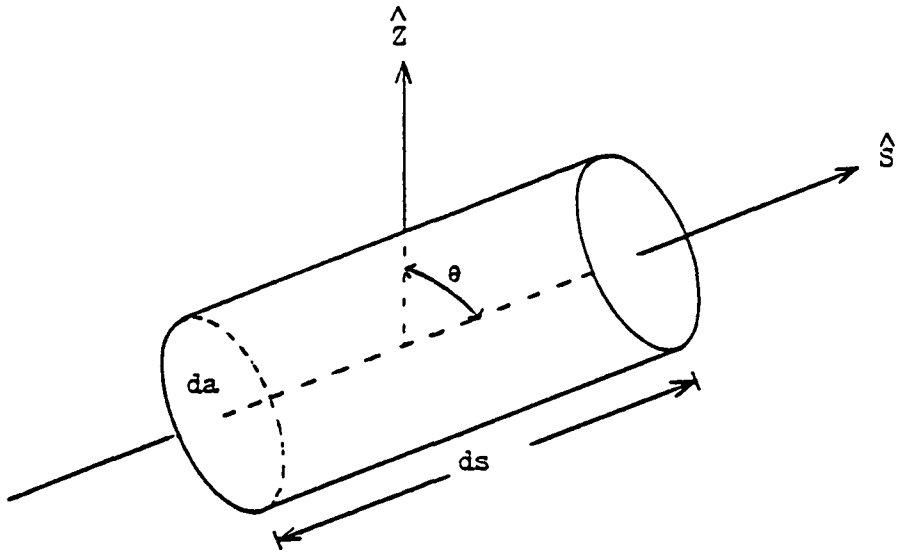

Fig. 4. Geometry used in derivation of radiative transfer equation.

of propagation, the term $E_t ds$ arises from thermal emission and the term $k_s J ds$ accounts for the increase in the intensity due to scattering from all other directions into the direction of propagation.

We can generalize the above equation to the case of radiation with an arbitrary polarization. Consider a scattering dielectric slab of thickness d, permittivity ε_1 and temperature T, overlying a homogeneous half-space of permittivity ε_2 and temperature T_2 (Fig. 5). Both the scattering layer and the homogeneous half-space are emitting thermal radiation. Using the Stokes parameters, the radiative transfer equations in matrix form can be written down readily. In the following, we take z to be the vertical direction and denote the direction of propagation by solid angle variable Ω, where

$$\Omega = (\theta, \phi) \tag{2}$$

Then,

$$\cos\theta \frac{d}{dz} \bar{I}(\Omega,z) = -\bar{\bar{k}}_e(\Omega) \cdot \bar{I}(\Omega,z) + \bar{E}_t + \int d\Omega' \bar{\bar{P}}(\Omega,\Omega') \cdot \bar{I}(\Omega',z) \tag{3}$$

where $\bar{I}(\Omega,z)$ is a four-component vector which represents the four Stokes parameters, and the extinction coefficient, $\bar{\bar{k}}_e(\Omega) = \bar{\bar{k}}_a(\Omega) + \bar{\bar{k}}_s(\Omega)$, forms a diagonal matrix.

$$\bar{\bar{k}} = [k_v, k_h, k_3, k_4] \tag{4}$$

$\bar{\bar{P}}(\Omega,\Omega')$, the scattering function matrix, represents the scattering coupling coefficients from the direction $\Omega' = (\theta',\phi')$ into the direction $\Omega = (\theta,\phi)$[48]. The coefficients $\cos\theta$ on the left hand side of (3) arises from the fact that the propagating direction is inclined

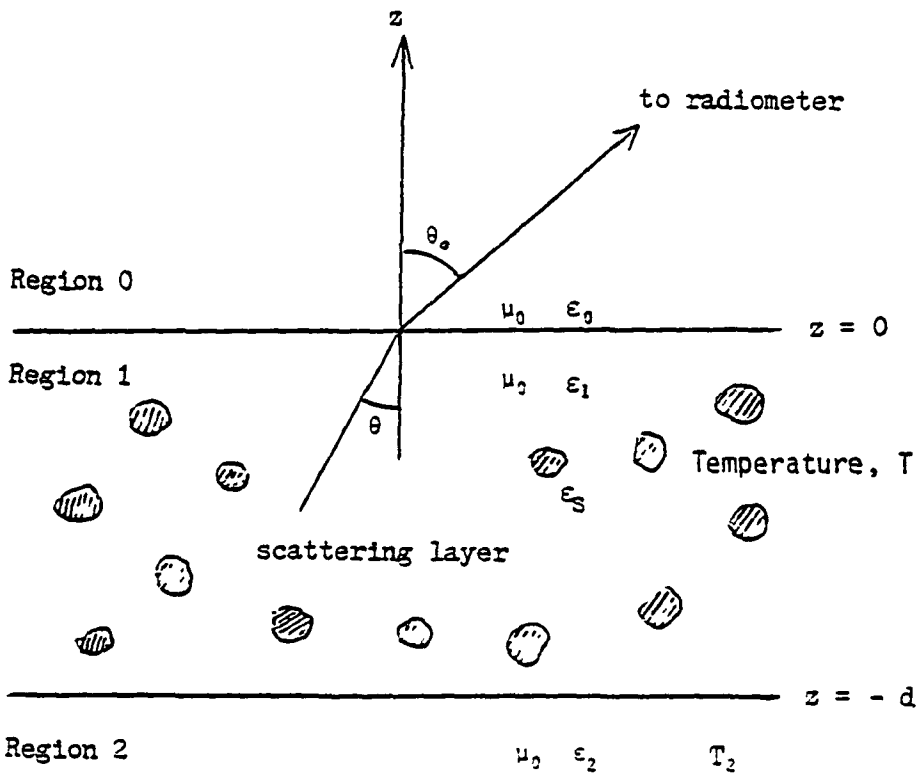

Fig. 5. Geometry used in derivation of general radiative transfer equation.

at angle θ to the vertical direction $\hat{z}$ direction, so that $ds=\sec\theta\, dz$. Stokes vector $\bar{I}(\Omega,z)$ contains four Stokes parameters which are

$$\bar{I}(\Omega,z) = \begin{bmatrix} I_v(\Omega,z) \\ I_h(\Omega,z) \\ U(\Omega,z) \\ V(\Omega,z) \end{bmatrix} \tag{5}$$

The first component, I_v, denotes the specific intensity for vertical polarization and the second component, I_h, denotes the specific intensity for horizontal polarization. The third and fourth components, U and V, represent the correlation between the two polarizations. For a time harmonic field given by $\bar{E} = \hat{v}\, E_v + \hat{h}\, E_h$ where $\hat{v}$ and $\hat{h}$ denote the two orthogonal polarizations which are perpendicular to the propagation direction $\hat{k}$, (i.e. $\hat{v} \times \hat{h} = \hat{k}$), the Stokes parameters are defined as

$$I_v = \frac{1}{\eta} < |E_v|^2 > \tag{6}$$

$$I_h = \frac{1}{\eta} < |E_h|^2 > \tag{7}$$

$$U = \frac{2}{\eta} \text{Real} < E_v E_h^* > \tag{8}$$

$$V = \frac{2}{\eta} \text{Imag} < E_v E_h^* > \tag{9}$$

where η is the wave impedance of the medium and the bracket <> denotes the time average. The average is necessary because of the fluctuation in the amplitude and phase of the wave.

The thermal emission coefficient $\bar{E}_t$ in (3) can be derived assuming that each point in the medium is in local thermodynamic equilibrium. In that case, it is assumed that the circumstances are such that we can

define at each point in the medium a local temperature $\bar{T}$ such that the emission coefficient at each point is given by Kirchhoff's law.

$$\bar{E}_t = \bar{\bar{k}}_a (\Omega)\, \bar{B} \tag{10}$$

where $\bar{B}$ is the Plank function,

$$\bar{B} = \frac{h\nu^3}{\lambda^2} \frac{1}{\exp[h\nu/kT]-1} \begin{bmatrix} 1 \\ 1 \\ 0 \\ 0 \end{bmatrix} \tag{11}$$

where K and h are the Boltzmann and Plank constants, ν is frequency, c is the speed of light in the medium, and T is the temperature of the medium. The last two elements of the Plank function $\bar{B}$ are zero since the emitted thermal radiation is uncoupled.

In the Rayleigh-Jeans approximation, which is valid in microwave frequencies ($h\nu/KT \ll 1$), we obtain from (11)

$$\bar{B} = C\bar{T} \tag{12}$$

where

$$\bar{T} = \begin{bmatrix} T \\ T \\ 0 \\ 0 \end{bmatrix} \tag{13}$$

$$C = \frac{K}{\lambda^2} \frac{\varepsilon_1'}{\varepsilon_0} \tag{14}$$

and λ is the free space wavelength and ε_1' is the real part of the permittivity of the scattering medium.

In passive remote sensing case, only two Stokes parameters I_v and I_h are necessary for the radiative transfer equations. Therefore, the radiative transfer equations inside the scattering medium take the following form. For $0 < \theta < \pi$

$$\cos\theta \frac{d}{dz} I_v(\theta,\phi,z) = k_{av}(\theta,\phi)\, CT - k_{ev}(\theta,\phi)\, I_v(\theta,\phi,z)$$
$$+ \int_0^{\pi} d\theta' \sin\theta' \int_0^{2\pi} d\phi' \,[(v,v')\, I_v(\theta',\phi',z)$$
$$+ (v,h')\, I_h(\theta',\phi',z)] \qquad (15)$$

$$\cos\theta \frac{d}{dz} I_h(\theta,\phi,z) = k_{ah}(\theta,\phi)\, CT - k_{eh}(\theta,\phi)\, I_h(\theta,\phi,z)$$
$$+ \int_0^{\pi} d\theta' \sin\theta' \int_0^{2\pi} d\phi' \,[(h,v')\, I_v(\theta',\phi',z)$$
$$+ (h,h')\, I_h(\theta',\phi',z)] \qquad (16)$$

where the subscripts v and h represent vertical polarization and horizontal polarization, respectively, the extinction coefficient $k_e(\theta,\phi) = k_a(\theta,\phi) + k_s(\theta,\phi)$ is the loss due to absorption and scattering, and the scattering function (v,v'), (v,h'), (h,v') and (h,h') denote the scattering coupling coefficients from the direction θ', ϕ' into the direction θ, ϕ.

Boundary Conditions

The boundary conditions for the Stokes parameters at planar dielectic interface have been derived by Tsang and Kong [33] from the continuity of tangential electric magnetic fields. For passive remote sensing, the boundary conditions that have to be satisfied by the solutions to the equations of (15) and (16) are (Fig. 5), for $0<\theta<\pi/2$, at $z = 0$.

$$I_v(\pi-\theta, z=0) = 0 \qquad (17)$$

$$I_h(\pi-\theta, z=0) = 0 \qquad (18)$$

and at $z = -d$

$$I_v(\theta, z=-d) = r_{v12}(\theta)\, I_v(\pi-\theta, z=-d) + t_{v21}(\theta)\, CT_2 \tag{19}$$

$$I_h(\theta, z=-d) = r_{h12}(\theta)\, I_h(\pi-\theta, z=-d) + t_{h21}(\theta)\, CT_2 \tag{20}$$

where

$$t_{v21}(\theta) = 1 - r_{v21}(\theta) \tag{21}$$

$$t_{h21}(\theta) = 1 - r_{h21}(\theta) \tag{22}$$

and for $\ell, m = 1,2$

$$r_{v\ell m}(\theta) = \left|S_{\ell m}(\theta)\right|^2 \tag{23}$$

$$r_{h\ell m}(\theta) = \left|R_{\ell m}(\theta)\right|^2 \tag{24}$$

where $R_{\ell m}$ and $S_{\ell m}$ are the TE and TM reflection coefficients, respectively, and

$$R_{\ell m}(\theta) = \frac{k_{\ell z} - k_{mz}}{k_{\ell z} + k_{mz}} \tag{25}$$

$$S_{\ell m}(\theta) = \frac{\varepsilon_m k_{\ell z} - \varepsilon_\ell k_{mz}}{\varepsilon_m k_{\ell z} + \varepsilon_\ell k_{mz}} \tag{26}$$

with

$$k_{\ell z} = k_\ell \cos\theta_\ell \tag{27}$$

$$k_\ell = w\sqrt{\mu_o \varepsilon_\ell} \tag{28}$$

Once the specific intensities I_v and I_h are obtained, the brightness temperatures are given as

$$T_{Bv}(\theta) = \frac{1}{c}(1 - r_{v10})\, I_v(\theta, z=0) \tag{29}$$

$$T_{Bh}(\theta) = \frac{1}{c}(1 - r_{h10})\, I_h(\theta, z=0) \tag{30}$$

Cylindrical scatterer Model

Formulation

Consider a collection of sparsely distributed cylinders with permittivity ε_s embedded in region 1 with permittivity $\varepsilon_1=\varepsilon_0$ above a half space of homogeneous dielectric with permittivity ε_2 as shown in Fig. 6. The radiative transfer equations inside region 1 for $0<\theta<\pi$ take the form of equations in (15) and (16). These equations can be simplified by assuming that its radius and length are small and long in horizontal and vertical directions, respectively. Since the configuration and the sources are azimuthal symmetric, the intensities are independent of angle ϕ.

Using the above assumptions, we find the specific intensities for different θ are decoupled, and the radiative transfer equations of (15) and (16) assume the following forms for $0<\theta<\pi$

$$\cos\theta \frac{d}{dz} I_v(\theta,z) = [Q_1(\theta) - k_{ev}^{(c)}(\theta)]I_v(\theta,z) + Q_2(\theta)\, I_h(\theta,z) + k_{av}^{(c)}(\theta)\, CT \tag{31}$$

$$\cos\theta \frac{d}{dz} I_h(\theta,z) = [Q_2(\theta)\, I_v(\theta,z) + [Q_3(\theta) - k_{eh}^{(c)}(\theta)]\, I_h(\theta,z) + k_{ah}^{(c)}(\theta)\, CT \tag{32}$$

where the absorption coefficients are:

$$k_{av}^{(c)}(\theta) = \frac{-4\ Na\ \ell}{k_1\cos\theta}\, \pi a^2 \left[\frac{k_{1\rho}^2}{4}\, I_m\left(\frac{\varepsilon_1-\varepsilon_s}{\varepsilon_1}\right) + \frac{k_{1z}^2}{2}\, I_m\left(\frac{\varepsilon_1-\varepsilon_s}{\varepsilon_1+\varepsilon_s}\right)\right] \tag{33}$$

$$k_{ah}^{(c)}(\theta) = \frac{-4\ Na\ \ell}{\cos\theta}\, \pi a^2\, \frac{k_1}{2}\, I_m\left(\frac{\varepsilon_1-\varepsilon_s}{\varepsilon_1+\varepsilon_s}\right) \tag{34}$$

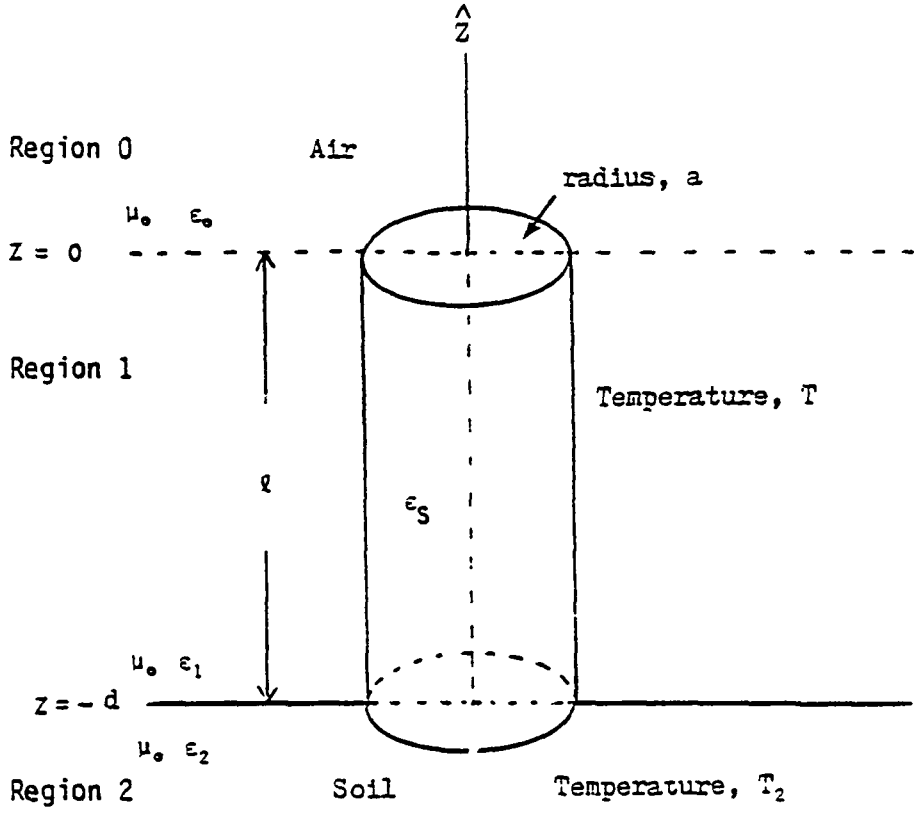

Fig. 6. Geometry of cylindrical scatterer model.

and the extinction coefficients are:

$$k_{ev}^{(c)}(\theta) = k_{av}^{(c)}(\theta) + k_{sv}^{(c)}(\theta) \tag{35}$$

$$k_{eh}^{(c)}(\theta) = k_{ah}^{(c)}(\theta) + k_{sh}^{(c)}(\theta) \tag{36}$$

with the scattering coefficients,

$$k_{sv}^{(c)}(\theta) = \frac{4\ Na\ \ell}{k_1 \cos\theta}\left[\left|C_0^{TM}\right|^2 + 2\left|C_1^{TM}\right|^2 + 2\left|C_1^{ME}\right|^2\right] \tag{37}$$

$$k_{sh}^{(c)}(\theta) = \frac{4\ Na\ \ell}{k_1 \cos\theta}\left[2\left|C_1^{ME}\right|^2 + 2\left|C_1^{TE}\right|^2\right] \tag{38}$$

and the scattering functions,

$$Q_1(\theta) = \frac{4\ Na\ \ell}{k_1 \cos\theta}\left[\left|C_0^{TM}\right|^2 + 2\left|C_1^{TM}\right|^2\right] \tag{39}$$

$$Q_2(\theta) = \frac{4\ Na\ \ell}{k_1 \cos\theta}\ 2\left|C_1^{ME}\right|^2 \tag{40}$$

$$Q_3(\theta) = \frac{4\ Na\ \ell}{k_1 \cos\theta}\ 2\left|C_1^{TE}\right|^2 \tag{41}$$

where

$$C_0^{TM} = \frac{i\pi a^2 k_{1\rho}^{\ 2}}{4}(\varepsilon_s - 1) \tag{42}$$

$$C_1^{TM} = \frac{i\pi a^2 k_{1z}^{\ 2}}{4}\ \frac{\varepsilon_s - 1}{\varepsilon_s + 1} \tag{43}$$

$$C_1^{ME} = \frac{i\pi a^2 k_1 k_{1z}}{4}\ \frac{\varepsilon_s - 1}{\varepsilon_s + 1} \tag{44}$$

$$C_1^{TE} = \frac{i\pi a^2 k_1^{\ 2}}{4}\ \frac{\varepsilon_s - 1}{\varepsilon_s + 1} \tag{45}$$

with

$$k_{1\rho} = k_1 \sin\theta \tag{46}$$

$$k_{1z} = k_1 \cos\theta \tag{47}$$

In (33)-(41), N_a is the number of scatterers per unit area. These coefficients are derived in Appendix B in detail.

The Solution for Cylindrical Model

The radiative transfer equations for the cylindrical scatterer model can be solved explicitly by obtaining the particular solution and homogeneous solution, and by summing them. Then, the solution of radiative transfer equations, (31) and (32), subject to the boundary conditions in section B are:

for the upward intensities ($0<\theta<\pi/2$),

$$I_v(\theta,z) = CT + A_u\, e^{\alpha_1 z/\cos\theta} + B_u\, e^{\alpha_2 z/\cos\theta} \tag{48}$$

$$I_h(\theta,z) = CT + A_u \frac{C_1+\alpha_1}{C_2}\, e^{\alpha_1 z/\cos\theta} + B_u \frac{C_1+\alpha_2}{C_2}\, e^{\alpha_2 z/\cos\theta} \tag{49}$$

and for downward intensities ($\pi/2<\theta<\pi$),

$$I_v(\theta,z) = CT + A_d\, e^{-\alpha_1 z/\cos\theta} + B_d\, e^{\alpha_2 z/\cos\theta} \tag{50}$$

$$I_h(\theta,z) = CT + A_d \frac{C_1+\alpha_1}{C_2}\, e^{\alpha_1 z/\cos\theta} + B_d \frac{C_1+\alpha_2}{C_2}\, e^{-\alpha_2 z/\cos\theta} \tag{51}$$

where the subscript u and d represent the upward direction and downward direction, respectively and

$$A_d = [C_2 - (C_1 + \alpha_2)]\, CT/(\alpha_2-\alpha_1) \tag{52}$$

$$B_d = [C_2 - (C_1 + \alpha_1)]\, CT/(\alpha_1-\alpha_2) \tag{53}$$

$$\begin{aligned} A_u = {} & \{[r_{v12} - (C_1 + \alpha_2) - r_{h12}\,(C_1 + \alpha_1)]\, A_d\, e^{\alpha_1 d/\cos\theta} \\ & + (r_{v12} - r_{h12})\,(C_1 + \alpha_2)\, B_d\, e^{\alpha_2 d/\cos\theta} \\ & + [t_{v12}\,(C_1 + \alpha_2) - t_{h12}\, C_2]\,(CT_2 - CT)\}\, e^{\alpha_1 d'/\cos\theta} / (\alpha_2 - \alpha_1) \end{aligned} \tag{54}$$

$$B_u = \{ (r_{v12} - r_{h12}) (C_1 + \alpha_1) A_d e^{\alpha_1 d/\cos\theta}$$

$$+ [r_{v12} (C_1 + \alpha_1) - r_{h12} (C_1 + \alpha_2)] B_d e^{\alpha_2 d/\cos\theta}$$

$$+ [t_{v12} (C_1 + \alpha_1) - t_{h12} C_2] (CT_2 - CT)\} e^{\alpha_2 d/\cos\theta} / (\alpha_1 - \alpha_2) \quad (55)$$

with

$$\alpha_1 = -[C_1 + C_3 - \sqrt{(C_1-C_3)^2 + 4C_2^2}] / 2 \quad (56)$$

$$\alpha_2 = -[C_1 + C_3 - \sqrt{(C_1-C_3)^2 + 4C_2^2}] / 2 \quad (57)$$

$$C_1 = Q_1 (\theta) - k_{ev}^{(c)}(\theta) \quad (58)$$

$$C_2 = Q_2 (\theta) \quad (59)$$

$$C_3 = Q_3 (\theta) - k_{eh}^{(c)}(\theta) \quad (60)$$

The brightness temperature for the vertical and horizontal polarization can be obtained by applying the boundary conditions at z=0. Then,

$$T_{Bv}(\theta) = \frac{1}{C} (A_u + B_u + CT) \quad (61)$$

$$T_{Bh}(\theta) = \frac{1}{C} [A_u(C_1 + \alpha_1)/C_2 + B_u(C_1 + \alpha_2)/C_2 + CT] \quad (62)$$

The results

The formulas derived in this section were used to simulate the emissivity for various soil moisture contents at a frequency of 1.4 GHz. Before matching the measurement data, the sensitivity of the emissivity to changes in fractional volume and permittivity of the cylindrical scatterers (or stalks) is studied.

In Figs. 7-9, the vertical polarized emissivity and the horizontal polarized emissivity are plotted as a function of observation angle by changing the fractional volume from 0.01% to 0.1% at soil moisture contents of 4.4% , 10.2% and 25.3% by weight. The permittivity of the scatterer is $\varepsilon_s = (2 + i0.1)\ \varepsilon_0$ which is an assumed value. The radius and length of the scatterers are 1 cm and 125 cm, respectively. The permittivities of underlying soil are $\varepsilon_2 = (3.65 + i0.3)\ \varepsilon_0$, $(8.13 + i0.68)\varepsilon_0$ and $(27.3 + i2.06)\varepsilon_0$, respectively and the surface temperatures are 302.1°K, 299.9°K and 292.1°K, respectively. The depth of the scattering medium is 125 cm which is the same value as the cylinder length. In Figs. 7-9, by changing fractional volume from 0.01% to 0.1%, emissivity was increased by 20% at the observation angle of 20° for each soil moisture content.

In Figs. 10-12, the sensitivity of the emissivity to the real part of scatterer permittivity, ε_s', is shown. An increase in ε_s' results in a decrease of emissivity. For the higher soil moisture contents, emissivities were decreased more than for the drier soil moisture content.

In Figs. 13-15, the sensitivity of the emissivity to the imaginary part of scatterer permittivity, ε_s'', is shown. An increase in ε_s'' results in an increase in emissivity. For higher soil moisture contents, emissivities were increased more. In Figs. 10-15, fractional volume was 0.1% and other parameters were the same as those in Figs. 7-9.

In the sensitivity analysis, we observe that small changes of fractional volume and permittivity of the cylindrical scatterer (or stalk) result in relatively large changes in emissivity.

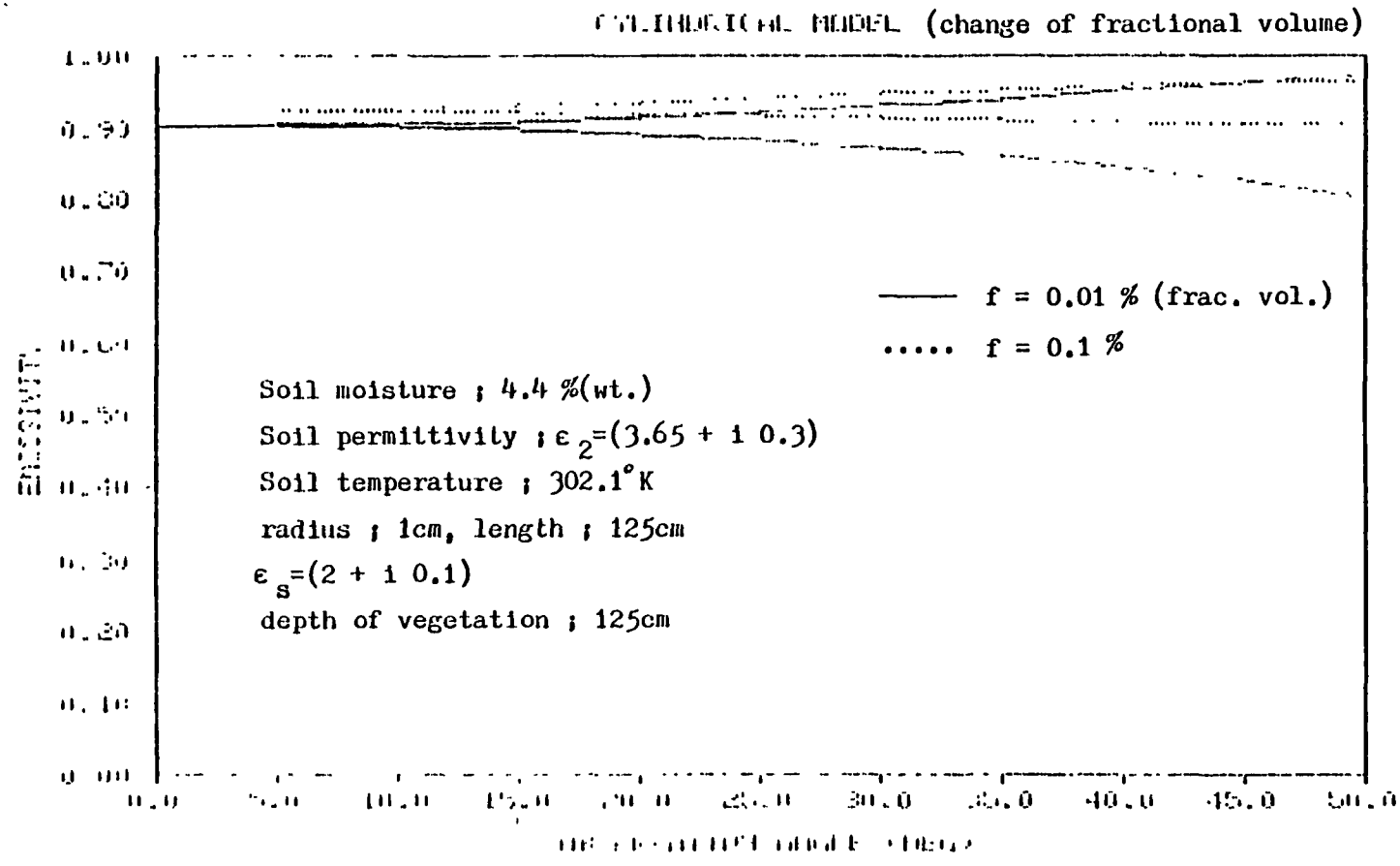

Fig. 7. Sensitivity plot of cylindrical scatterer model with different fractional volumes at soil moisture 4.4 %.

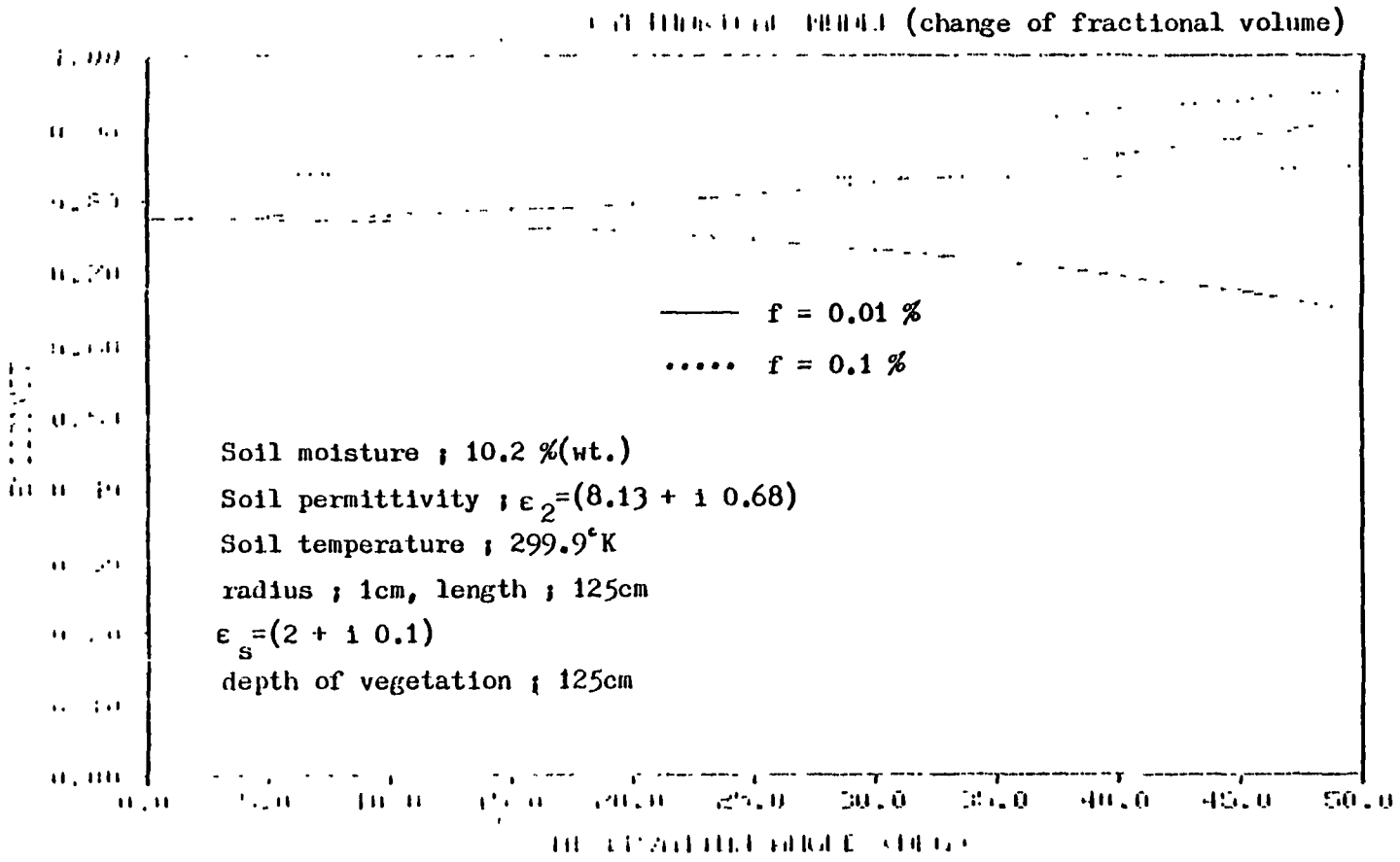

Fig. 8. Sensitivity plot of cylindrical scatterer model with different fractional volumes at soil moisture 10.2 %.

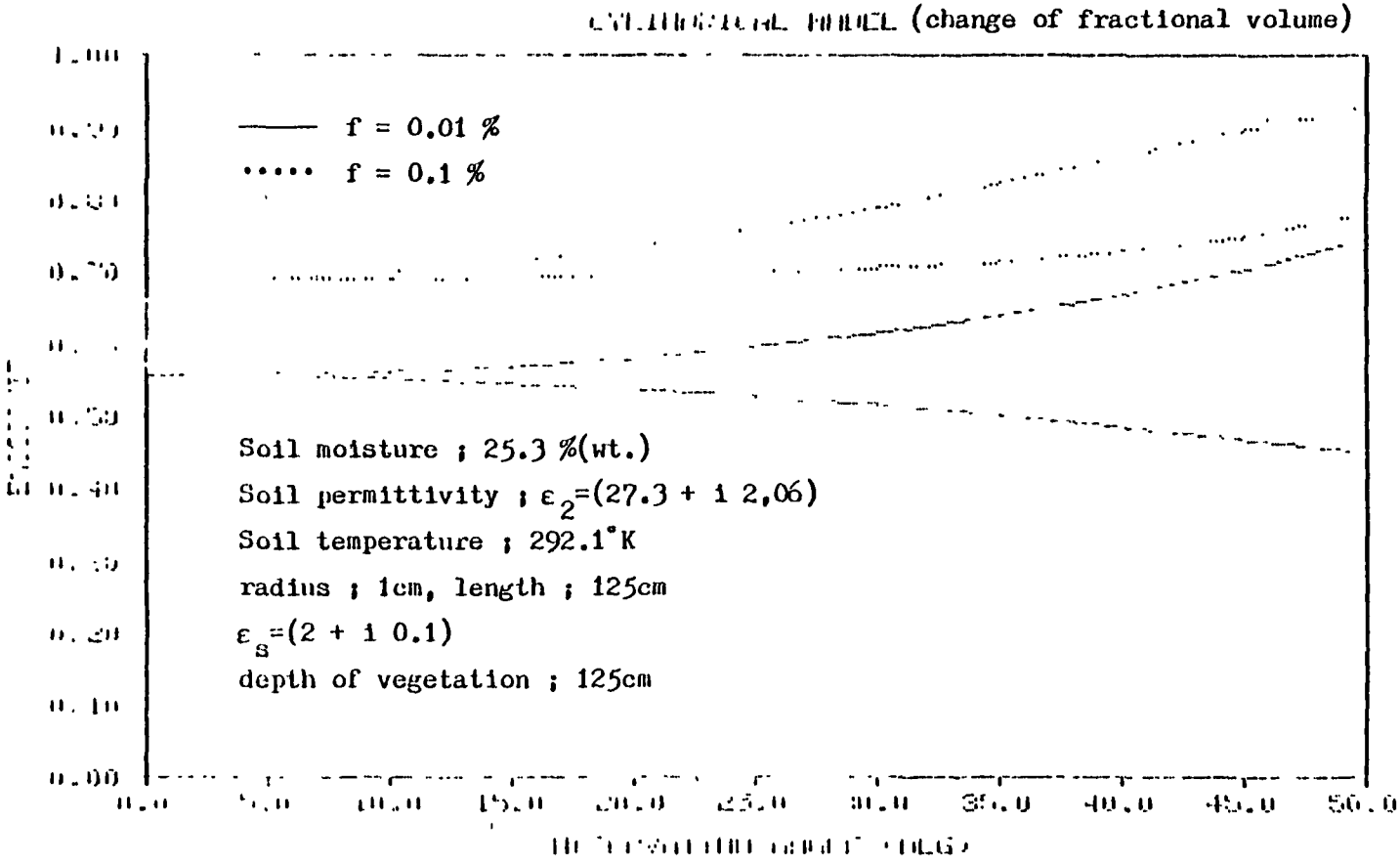

Fig. 9. Sensitivity plot of cylindrical scatterer model with different fractional volumes at soil moisture 25.3 %.

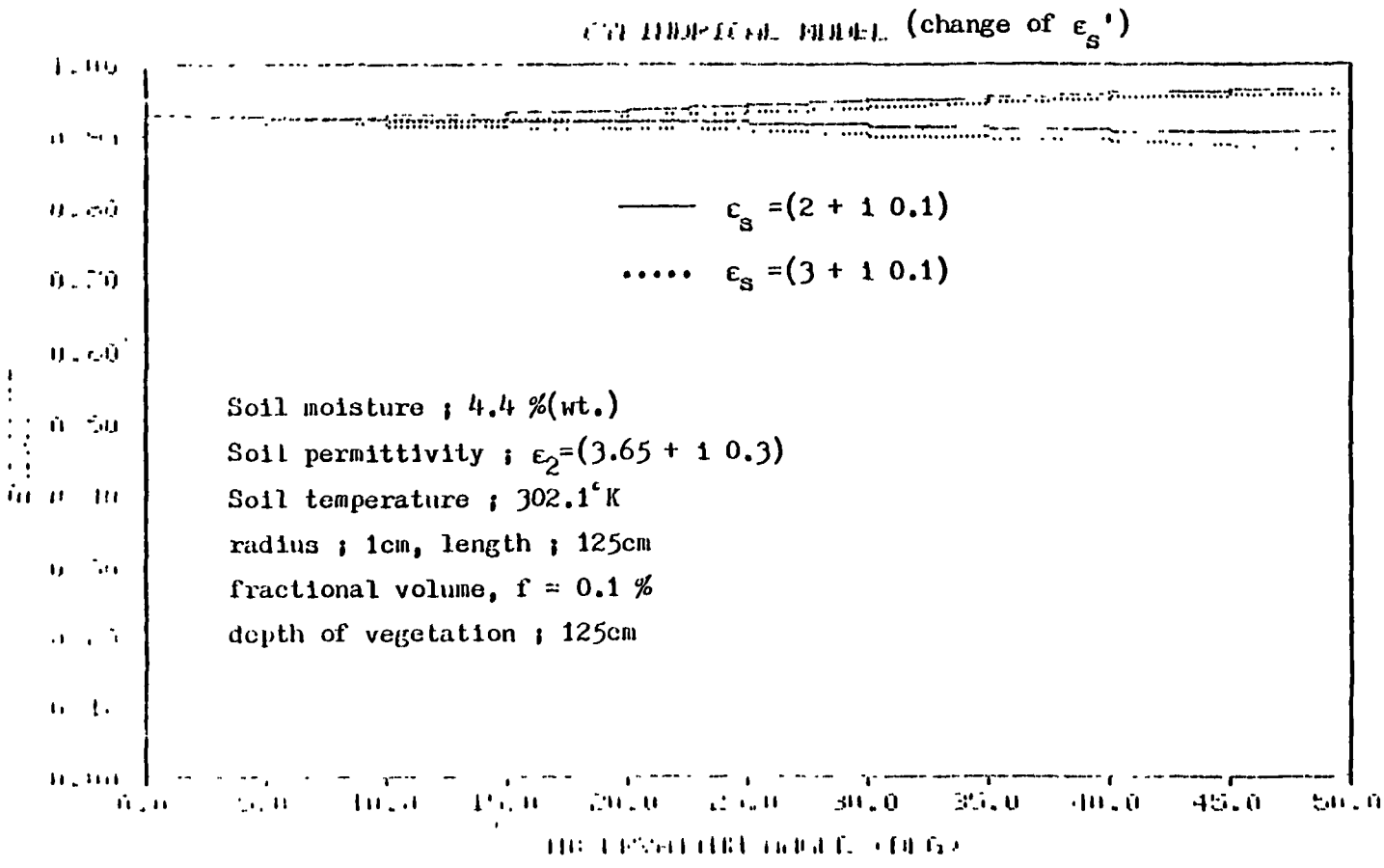

Fig. 10. Sensitivity plot of cylindrical scatterer model with different ε_s' at soil moisture of 4.4 %.

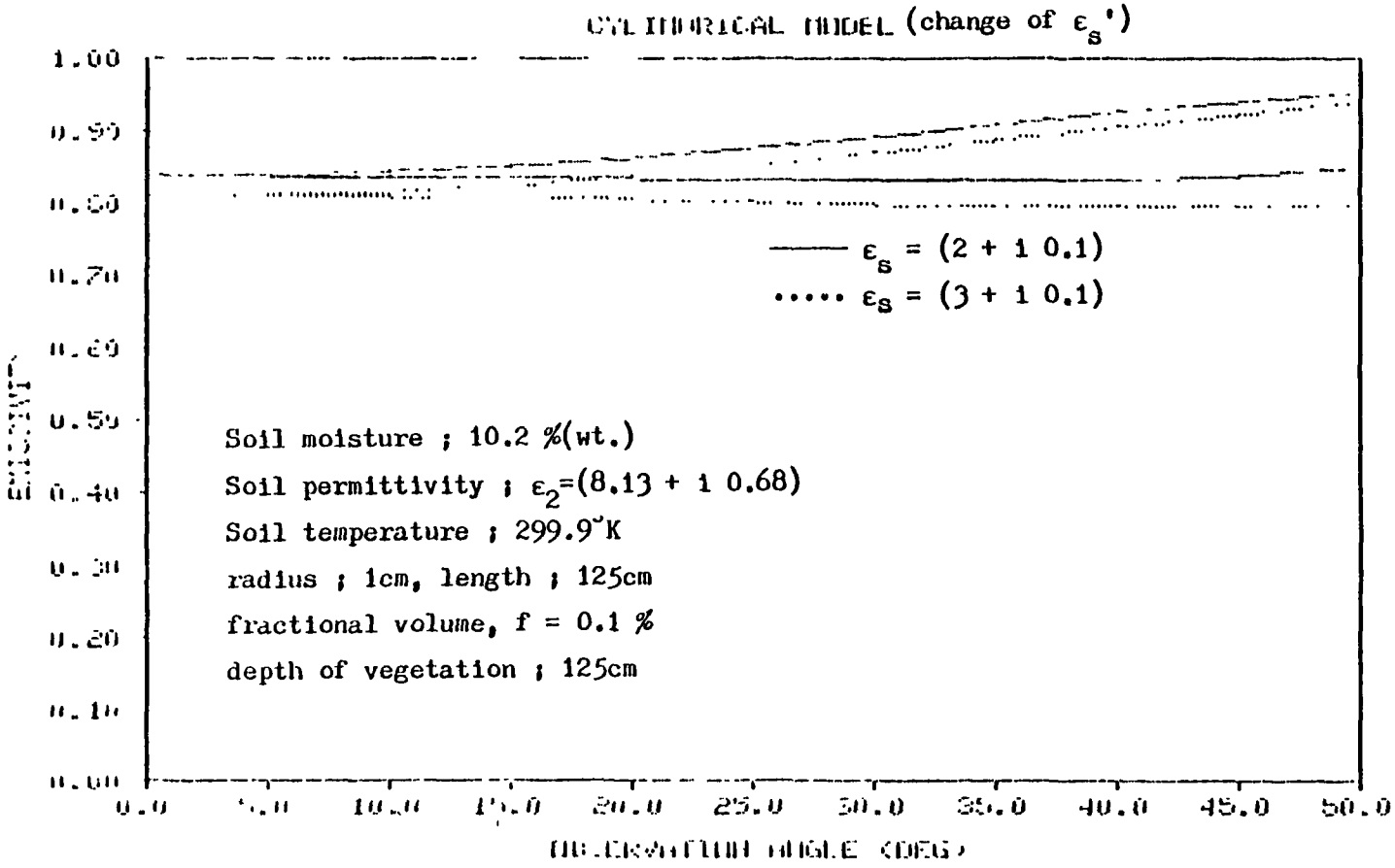

Fig. 11. Sensitivity plot of cylindrical scatterer model with different ε_s' at soil moisture of 10.2 %.

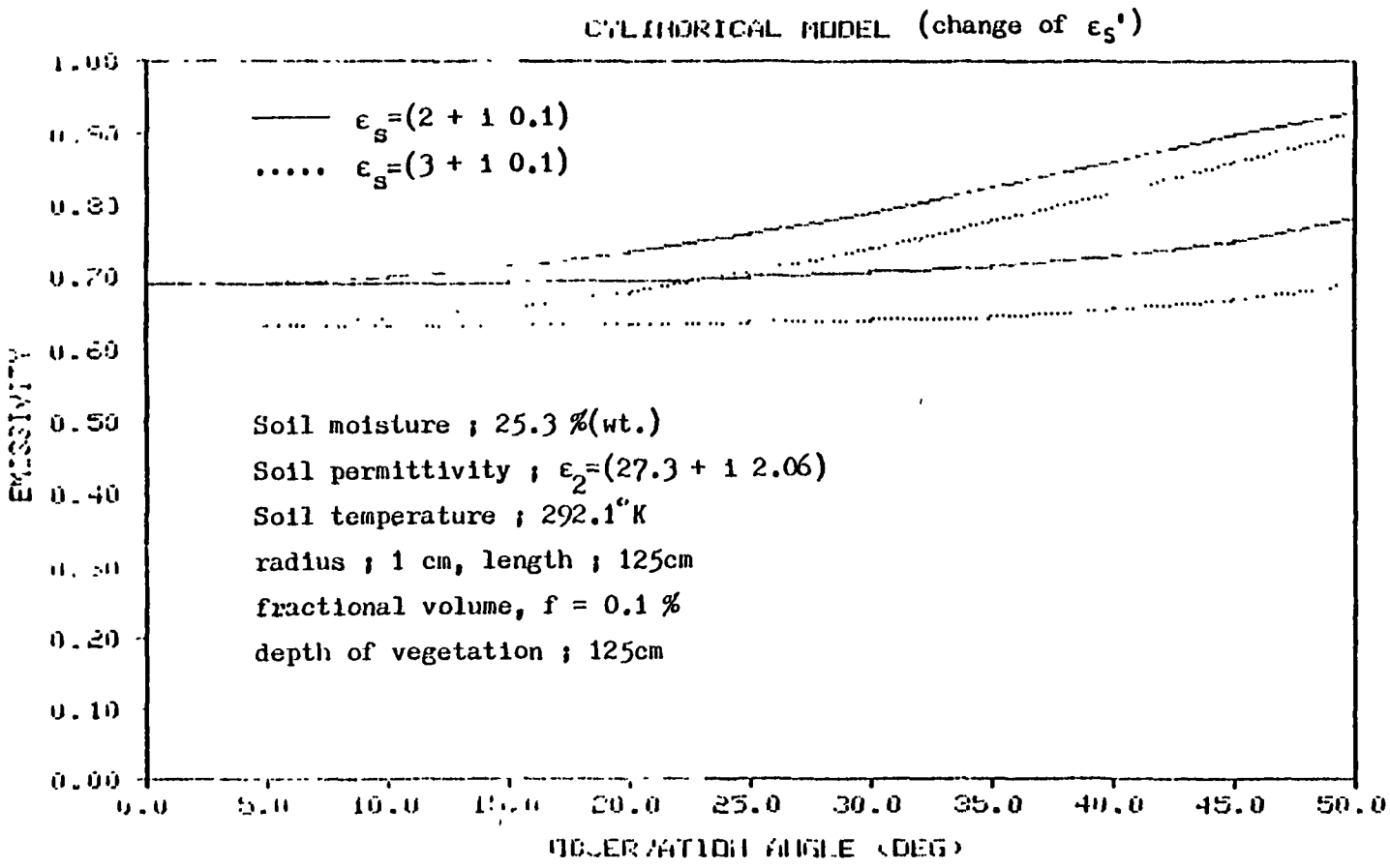

Fig. 12. Sensitivity plot of cylindrical scatterer model with different ϵ_s' at soil moisture of 25.3 %.

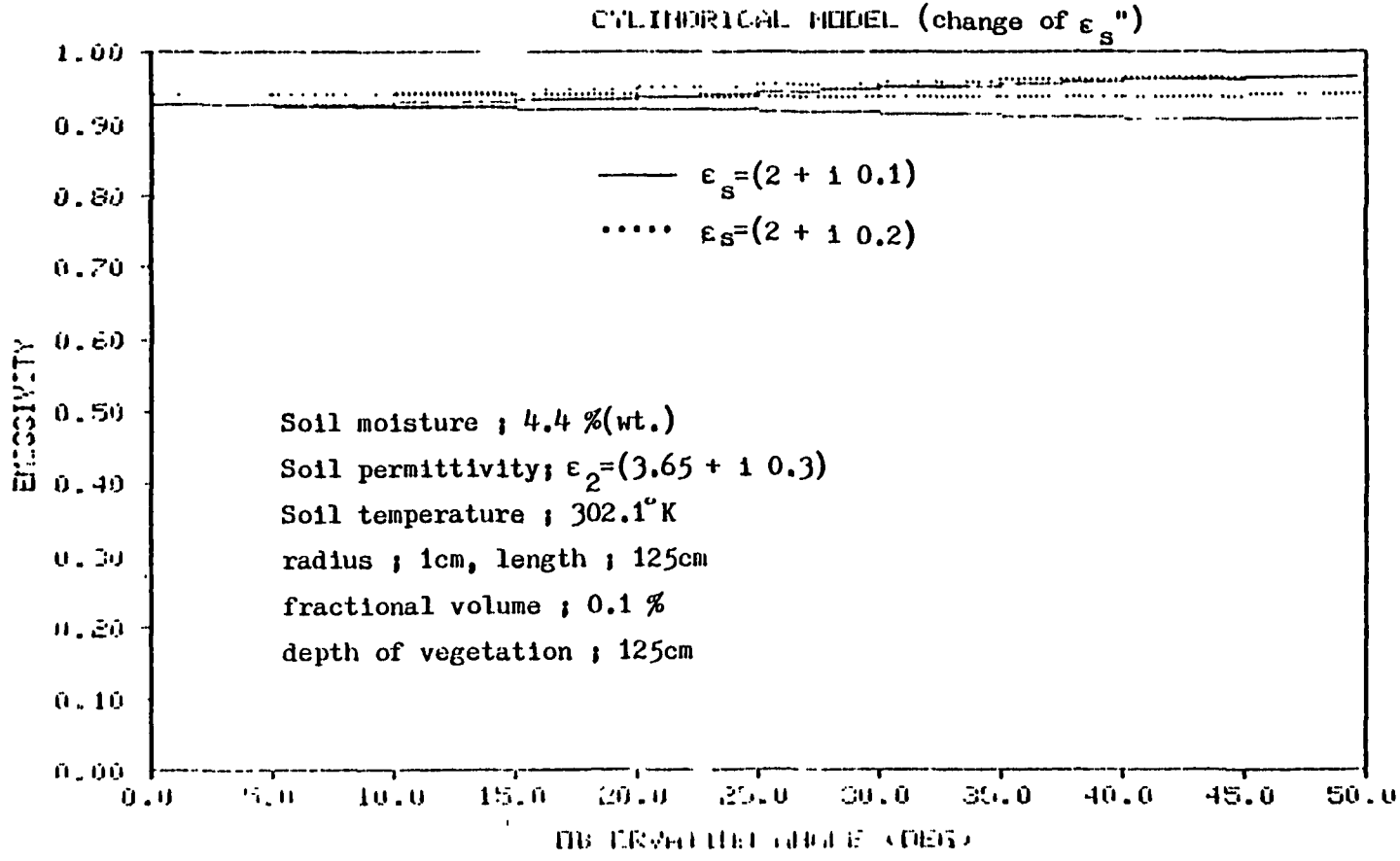

Fig. 13. Sensitivity plot of cylindrical scatterer model with different ε_s" at soil moisture of 4.4 %.

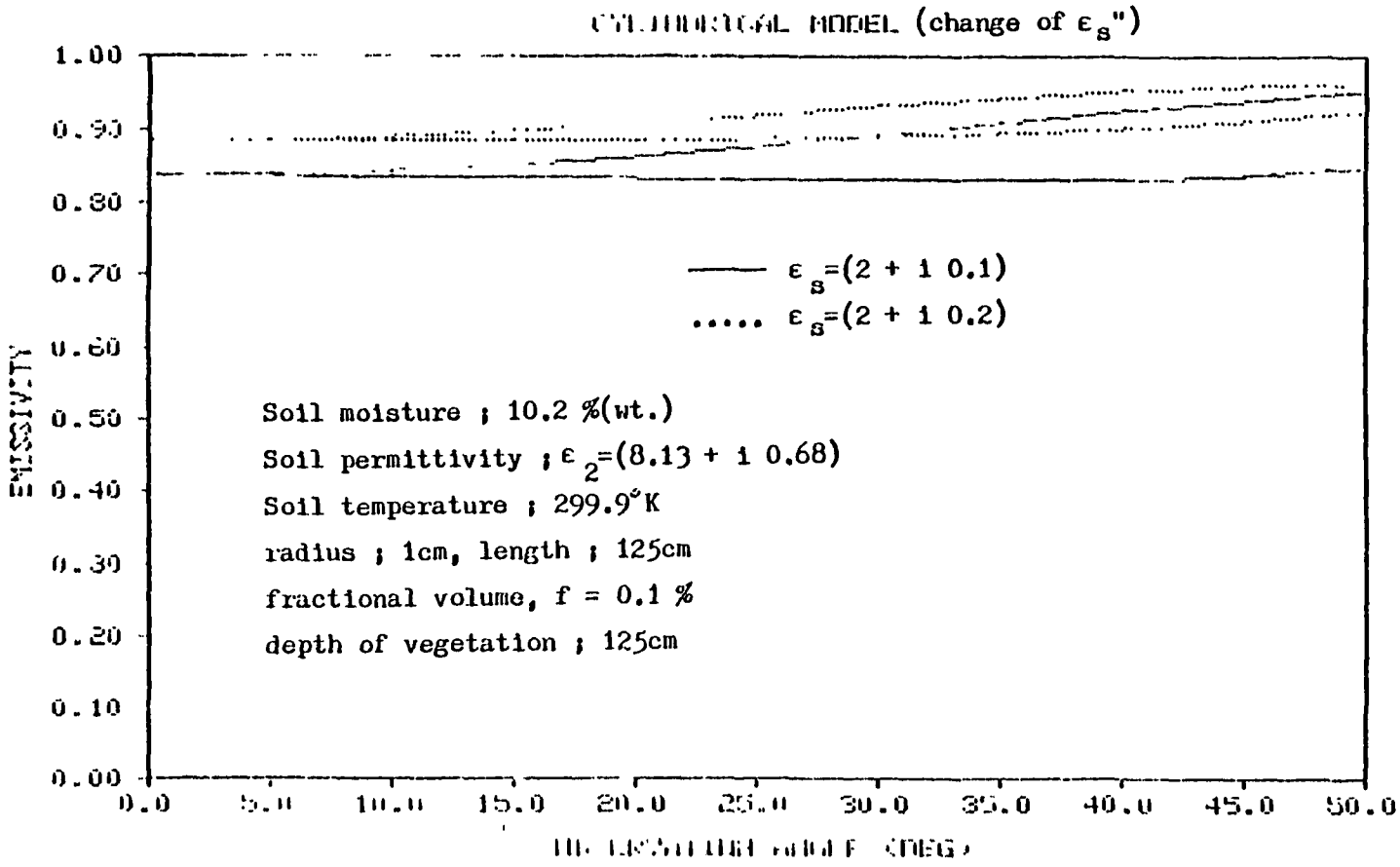

Fig. 14. Sensitivity plot of cylindrical scatterer model with different ε_s" at soil moisture of 10.2 %.

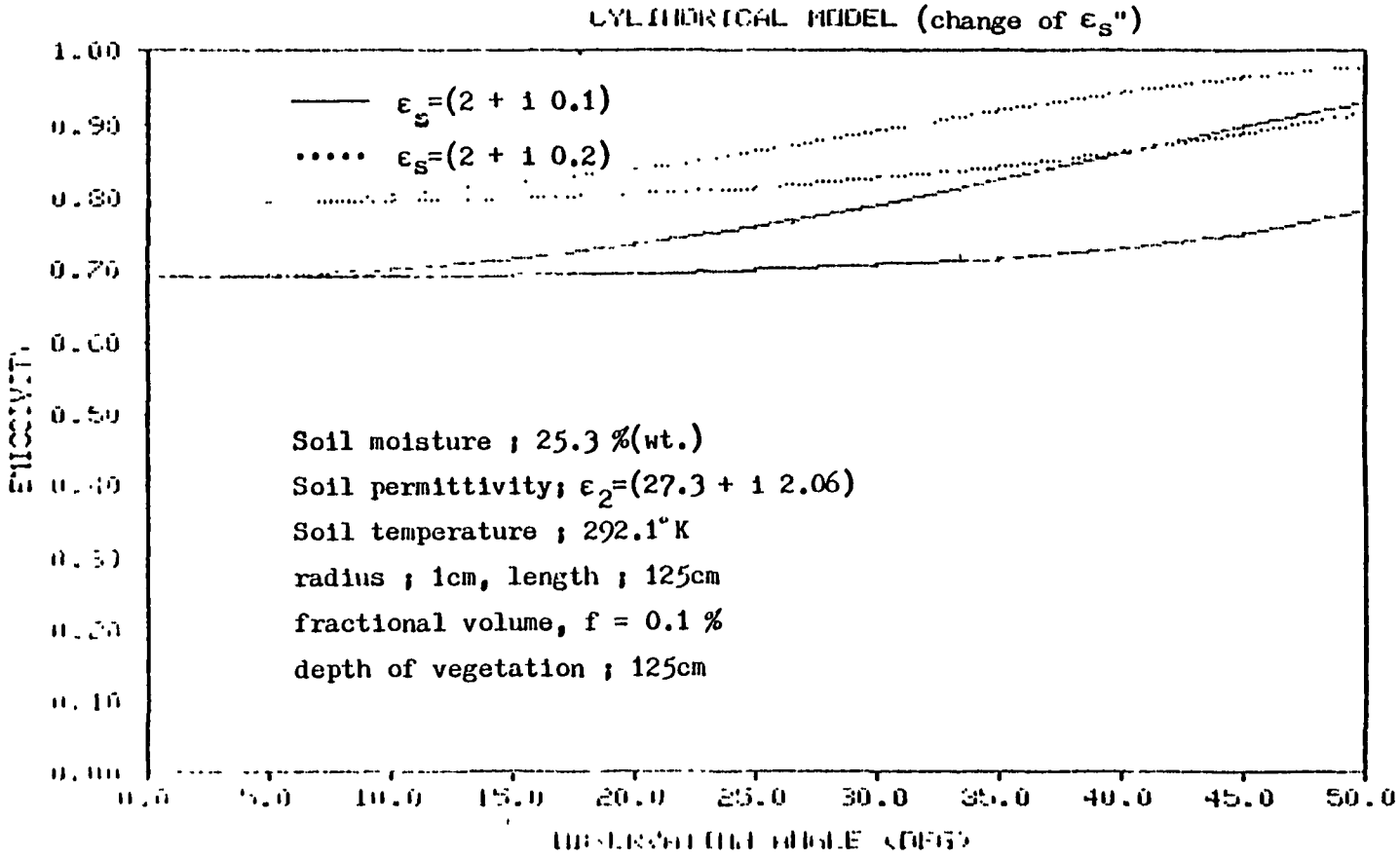

Fig. 15. Sensitivity plot of cylindrical scatterer model with different ϵ_s" at soil moisture of 25.3 %.

Ellipsoidal Scatterer Model

In this section we apply the radiative transfer approach to calculate the brightness temperature of a layer of randomly positioned and oriented ellipsoids over a homogeneous dielectric half space. The orientation of the ellipsoids is characterized by a probability density function of the Eulerian angles of rotation.

Formulation

Consider a collection of sparsely distributed ellipsoids with permittivity embedded in region 1 with permittivity $\varepsilon_1 = \varepsilon_0$ above a half space of homogeneous dielectric with permittivity ε_2 (Fig. 16). The radiative transfer equations inside the region 1 for $0<\theta<\pi$ take the form of equations (15) and (16) with

$$k_{ev}(\theta,\phi) = k_{ev}^{(e)}(\theta,\phi) \tag{63}$$

$$k_{eh}(\theta,\phi) = k_{eh}^{(e)}(\theta,\phi) \tag{64}$$

where the extinction coefficient is a summation of the absorption and scattering coefficients.

Consider an electromagnetic wave incident from the angular direction $\Omega' = (\theta',\phi')$ on a small ellipsoid with semiaxes a, b, and c with the axes pointing in the $\hat{x}_b$, $\hat{y}_b$, and $\hat{z}_b$ directions, respectively. The orientation of the body of the ellipsoid is specified by the Eulerian angles of rotation α, β and γ [46] (Fig. 17).

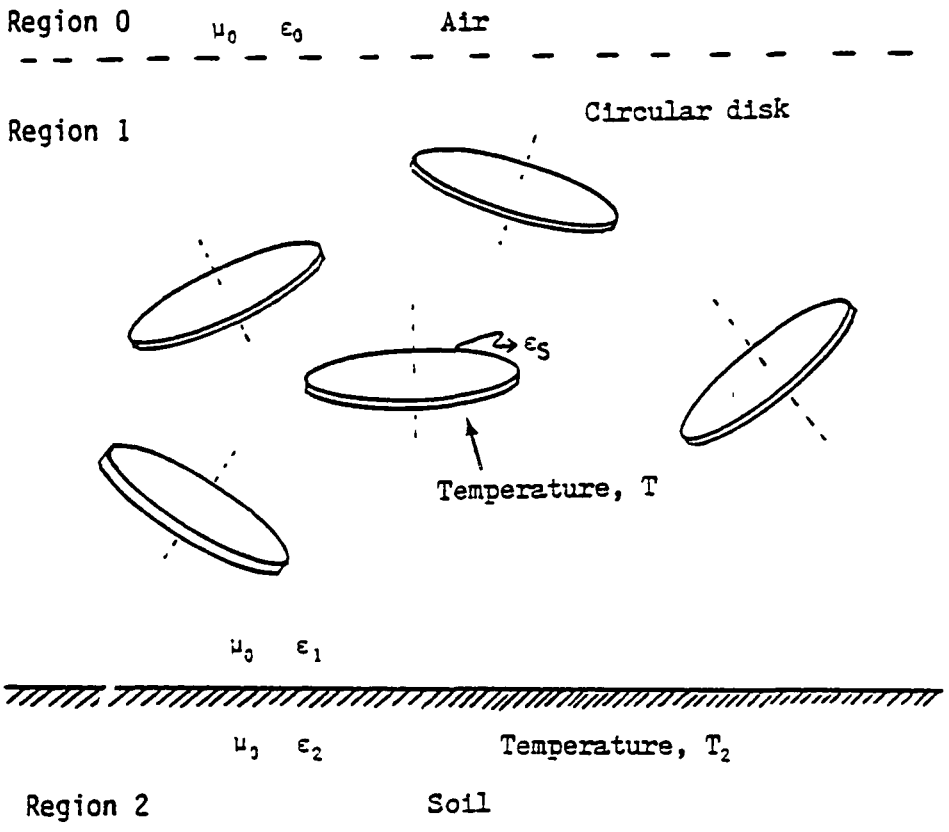

Fig. 16. Geometry of ellipsoidal scatterer model.

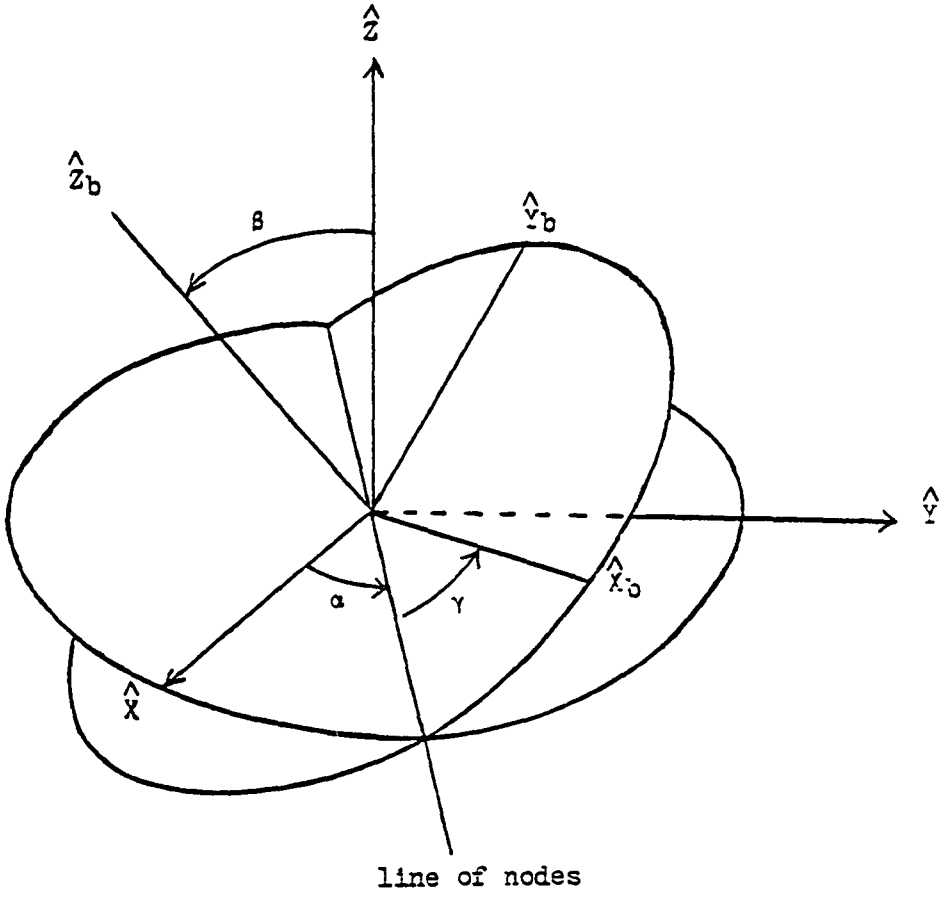

Fig. 17. Orientation of ellipsoid as specified by the Eulerian angle of rotation α, β and γ.

$$\hat{x}_b = \hat{x}\ (\cos\gamma\cos\alpha - \sin\gamma\cos\beta\sin\alpha)$$

$$+ \hat{y}\ (\cos\gamma\sin\alpha + \sin\gamma\cos\beta\cos\alpha)$$

$$+ \hat{z}\ \sin\gamma\sin\beta \tag{65}$$

$$\hat{y}_b = -\hat{x}\ (\sin\gamma\cos\alpha + \cos\gamma\cos\beta\sin\alpha)$$

$$+ \hat{y}\ (-\sin\gamma\sin\alpha + \cos\gamma\cos\beta\cos\alpha)$$

$$+ \hat{z}\ \cos\gamma\sin\beta \tag{66}$$

$$\hat{z}_b = \hat{x}\ \sin\beta\sin\alpha - \hat{y}\ \sin\beta\cos\alpha + \hat{z}\ \cos\beta \tag{67}$$

To obtain the scattering matrix and extinction coefficients for a collection of randomly oriented ellipsoids, we further average over the Eulerian angles of rotation α, β, and γ [45]. The derivation of these coefficients will be treated in Appendix C. Since the ellipsoidal scatterers represent the leaves of vegetation, a good approximation can be obtained by assuming the ellipsoid to be a circular disk characterized by $a = b$ and $c << a$ [45]. In this case, the Eulerian angle γ is immaterial and the orientation of the ellipsoid can be characterized by α and β. We further assume that the joint probability density $p(\alpha,\beta)$ is uniform in α. Thus

$$p(\alpha,\beta) = \frac{p(\beta)}{2\pi} \qquad 0 \leq \alpha \leq 2\pi \tag{68}$$

Then the scattering functions are, for $0 < \theta,\theta' < \pi$, $0 < \phi,\phi' < 2\pi$:

$$(v,v') = \frac{k^4}{16\pi^2} v_0 \int_0^{\pi} d\beta\ p(\beta)\ \{[\sin\theta\sin\theta' + \cos\theta\cos\theta'$$

$$\cos(\phi - \phi')]^2 \left|a_\theta\right|^2 + \left[\frac{\cos^2\theta\cos^2\theta'\sin^4\beta}{8}(1 + 2\cos^2(\phi-\phi'))\right.$$

$$\left. + \frac{\sin^2\theta\cos^2\theta'\sin^2\beta\cos^2\beta}{2}\right. +$$

$$2 \sin\theta' \cos\theta' \sin\theta \cos\theta \sin^2\beta \cos^2\beta \cos(\phi-\phi') + \frac{\sin^2\theta' \cos^2\theta \sin^2\beta \cos^2\beta}{2} + \sin^2\theta \sin^2\theta' \cos^4\beta] \cdot |a_\gamma - a_\theta|^2 + 2 [\sin\theta \sin\theta' + \cos\theta \cos\theta' \cos(\phi-\phi')] \cdot [\frac{\cos\theta \cos\theta' \sin^2\beta \cos(\phi-\phi')}{2} + \sin\theta \sin\theta' \cos^2\beta] \cdot \mathrm{Re}[a_\theta^* (a_\gamma - a_\theta)]\} \quad (69)$$

$$(v,h') = \frac{k^4}{16\pi^2} v_0 \int_0^\pi d\beta\, p(\beta) \{\cos^2\theta \sin^2(\phi-\phi') |a_\theta|^2 + [\frac{\cos^2\theta \sin^4\beta}{8} (1 + 2\sin^2(\phi-\phi')) + \frac{\sin^2\theta \sin^2\beta \cos^2\beta}{2}] \cdot |a_\gamma - a_\theta|^2 + \cos^2\theta \sin^2\beta \sin^2(\phi-\phi') \mathrm{Re}[a_\theta^*(a_\gamma - a_\theta)]\} \quad (70)$$

$$(h,v') = \frac{k^4}{16\pi^2} v_0 \int_0^\pi d\beta\, p(\beta) \{\cos^2\theta' \sin^2(\phi-\phi') |a_\theta|^2 + [\frac{\cos^2\theta' \sin^4\beta}{8} (1 + 2\sin^2(\phi-\phi')) + \frac{\sin^2\beta \cos^2\beta \sin^2\theta'}{2}] \cdot |a_\gamma - a_\theta|^2 + \cos^2\theta \sin^2\beta \sin^2(\phi-\phi') \mathrm{Re}[a_\theta^*(a_\gamma - a_\theta)]\} \quad (71)$$

$$(h,h') = \frac{k^4}{16\pi^2} v_0 \int_0^\pi d\beta\, p(\beta) \{\cos^2(\phi-\phi') |a_\theta|^2 + [\frac{\sin^4\beta}{8} (1 + 2\cos^2(\phi-\phi'))] |a_\gamma - a_\theta|^2 + \sin^2\beta \cos^2(\phi-\phi') \mathrm{Re}[a_\theta^*(a_\gamma - a_\theta)]\} \quad (72)$$

where, following Lang [44], we define

$$a_\gamma = \frac{\varepsilon_s - 1}{1 + \nu_d A_3} \quad (73)$$

$$a_\theta = \frac{\varepsilon_s - 1}{1 + \nu_d A} \quad (74)$$

$$k = w\sqrt{\mu_0 \varepsilon_0} \quad (75)$$

with

$$v_d = \frac{abc}{2}(\epsilon_s - 1) \tag{76}$$

$$A = \frac{\pi}{2a^3} \tag{77}$$

$$A_3 = \frac{2}{a^2 c} \tag{78}$$

In (69)-(72), f is the fractional volume occupied by the disks and,

$$f = n_0 v_0 \tag{79}$$

where n_0 is the number of circular disks per unit volume, and v_0 is the volume of one circular disk.

$$v_0 = \frac{4\pi}{3} a^2 c \tag{80}$$

$$k_{sv}^{(e)}(\theta',\phi') = \frac{k^4}{6\pi^2} v_0 f \int_0^\pi d\beta\, p(\beta) \{|a_\theta|^2 + [1/2 \cos^2\theta' \sin^2\beta + \sin^2\theta' \cos^2\beta] |a_\gamma - a_\theta|^2 + 2[\sin^2\theta' \cos^2\beta + 1/2 \cos^2\theta' \sin^2\beta] \operatorname{Re}[a_\theta^* (a_\gamma - a_\theta)]\} \tag{81}$$

$$k_{sh}^{(e)}(\theta',\phi') = \frac{k^4}{6\pi^2} v_0 f \int_0^\pi d\beta\, p(\beta) \{|a_\theta|^2 + 1/2 \sin^2\beta |a_\gamma - a_\theta|^2 + \sin^2\beta \operatorname{Re}[a_\theta^* (a_\gamma - a_\theta)]\} \tag{82}$$

and the absorption coefficients are

$$k_{av}^{(e)}(\theta',\phi') = \int_0^\pi d\beta\, p(\beta)[b_\theta + [1/2 \cos^2\theta' \sin^2\beta + \sin^2\theta' \cos^2\beta)] (b_\gamma - b_\theta)] \tag{83}$$

$$k_{ah}^{(e)}(\theta',\phi') = \int^\pi d\beta\, p(\beta) [b_\theta + 1/2 \sin^2\beta (b_\gamma - b_\theta)] \tag{84}$$

where

$$b_\gamma = kf \quad \text{Imag}(a_\gamma) \tag{85}$$

$$b_\theta = kf \quad \text{Imag}(a_\theta) \tag{86}$$

From (81)-(84), it is obvious that the extinction coefficients are dependent of ϕ and the following relations hold

$$k_{sv}^{(e)}(\pi-\theta) = k_{sv}^{(e)}(\theta) \tag{87}$$

$$k_{sh}^{(e)}(\pi-\theta) = k_{sh}^{(e)}(\theta) \tag{88}$$

$$k_{av}^{(e)}(\pi-\theta) = k_{av}^{(e)}(\theta) \tag{89}$$

$$k_{ah}^{(e)}(\pi-\theta) = k_{ah}^{(e)}(\theta) \tag{90}$$

The Solution and the Results.

The radiative transfer equations in (15) and (16) together with the boundary conditions of (17)-(20) can be solved by a numerical approach. The numerical approach using a Gaussian quadrature formula will be described in the section entitled Numerical Approach.

In simulating the theoretical model, a probability density function $p(\beta)$ is needed to describe the leaf angle distribution. We shall use one of the following four probability density functions for the Eulerian angle:

$$P_1(\beta) = \begin{cases} 1/\Delta\beta_{11}, & 0 \le 0 \le \Delta\beta_{11} \\ 0 & \text{elsewhere} \end{cases} \tag{91}$$

$$P_2(\beta) = \begin{cases} \sin\beta/[1-\cos(\Delta\beta_{11})], & 0 \le 0 \le \Delta\beta_{11} \\ 0 & \text{elsewhere} \end{cases} \tag{92}$$

$$P_3(\beta) = \begin{cases} 1/2\Delta\beta\perp, & \pi/2-\Delta\beta\perp \le \beta \le \pi/2 + \Delta\beta\perp \\ 0 & \text{elsewhere} \end{cases} \tag{93}$$

$$P_4(\beta) = \begin{cases} \sin \beta / [2 \sin \Delta\beta^{\perp}], & \pi/2 - \Delta\beta^{\perp} \leq \beta \leq \pi/2 + \Delta\beta^{\perp} \\ 0 & \text{elsewhere} \end{cases} \quad (94)$$

Probability $p_1(\beta)$ and $p_3(\beta)$ were used by Lang [44]. Tsang et al. [45] introduced the probabilities $p_2(\beta)$ and $p_4(\beta)$ to take into account the smaller angle around $\beta=0$. For a vegetation field, probability $p_4(\beta)$ can be used by assuming that the leaves are inclined more in the vertical direction.

Here, like the case of the cylindrical scatterer model, a sensitivity analysis of the input parameters were performed. Fig. 18 shows the effect of the change of ellipsoidal scatterer (or leaf) size on emissivity at a soil moisture content of 13.8%. Emissivities are compared for two different cases; for the nominal values a, b and c chosen to be 18 cm, 18 cm and 0.05 cm, respectively and 10% increases of each value. The underlying soil was assumed to have a permittivity of $\varepsilon_2 = (14.06 + i0.95)\varepsilon_0$ and a surface temperature 291.2°K. The fractional volume of the ellipsoidal scatterers was 1% and leaves were assumed to be inclined by 30° from the vertical direction. The depth of the scattering medium was 125 cm. In Fig. 18, the emissivities were almost the same for both cases. For a 10% increase of size, the comparison was almost the same as shown in Fig. 19. From the above results, the emissivity computed by the ellipsoidal scatterer model was not affected by a 10% change of scatterer size. The same result was obtained for a soil moisture content of 25.3% as shown in Fig. 20.

Figs. 21-23 show the sensitivity of emissivity to fractional volume for different soil moisture contents. By changing the fractional

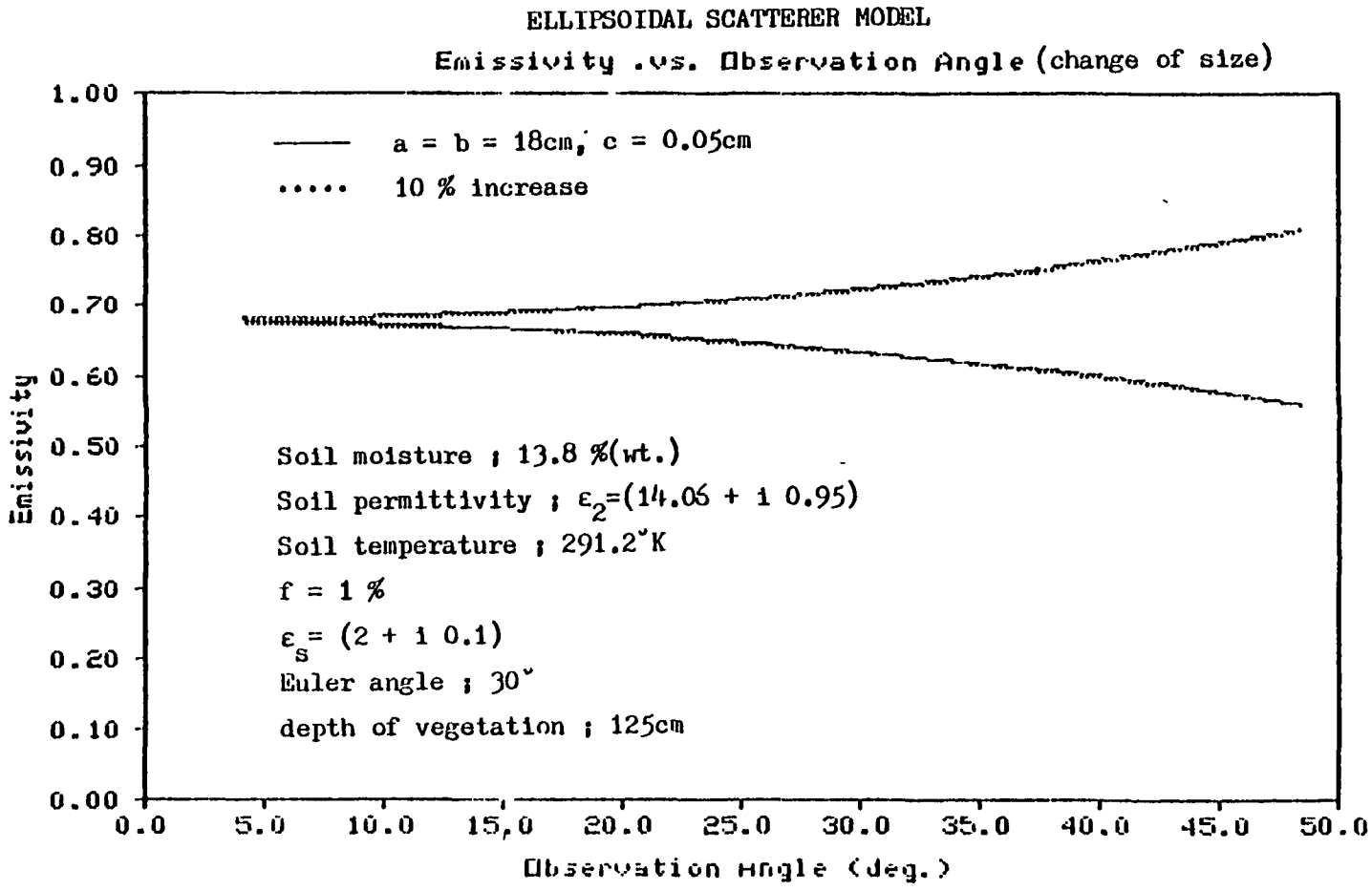

Fig. 18. Sensitivity plot of ellipsoidal scatterer model with 10 % increase of size at soil moisture 13.8 %.

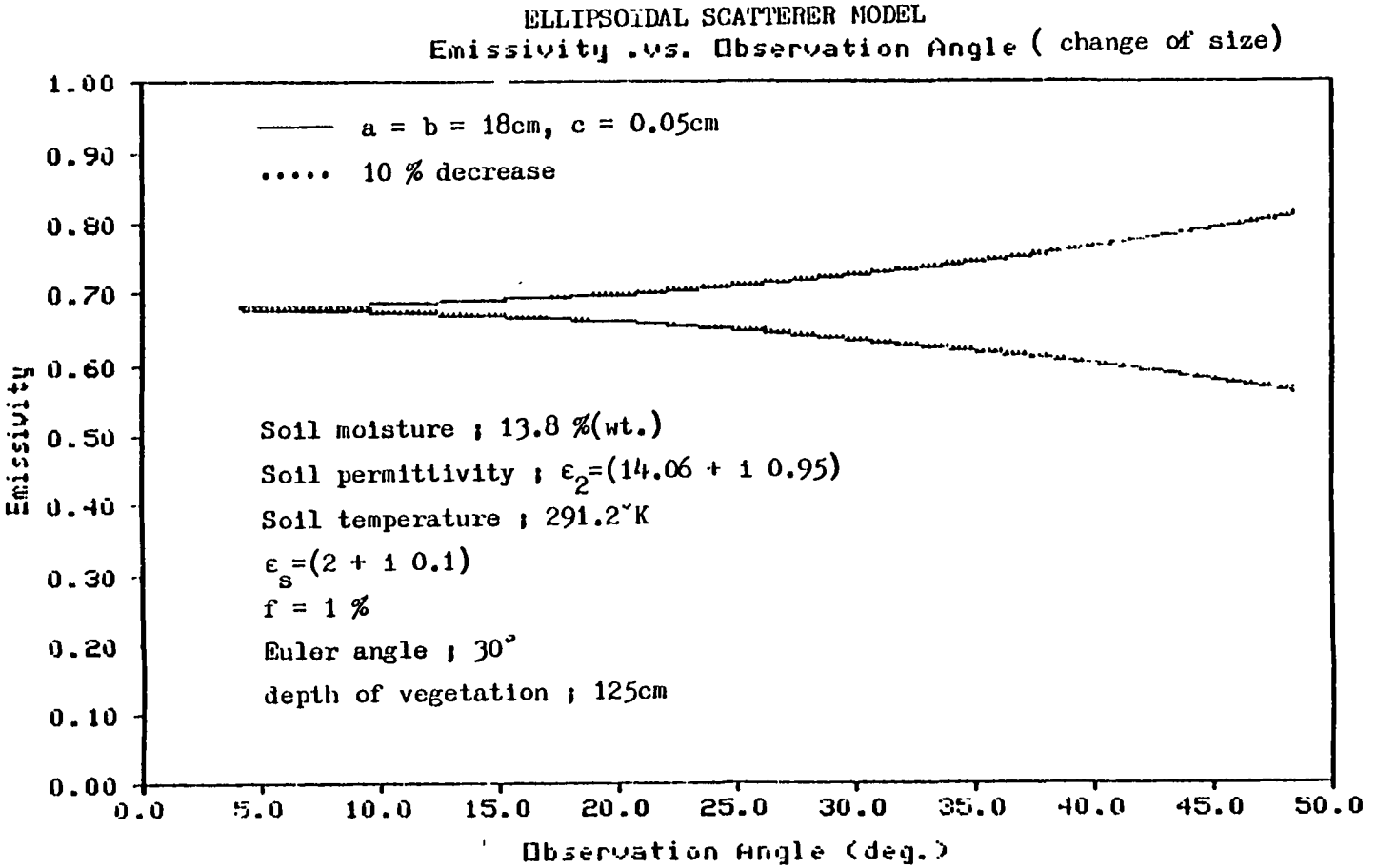

Fig. 19. Sensitivity plot of ellipsoidal scatterer model with 10 % decrease of size at soil moisture 13.8 %.

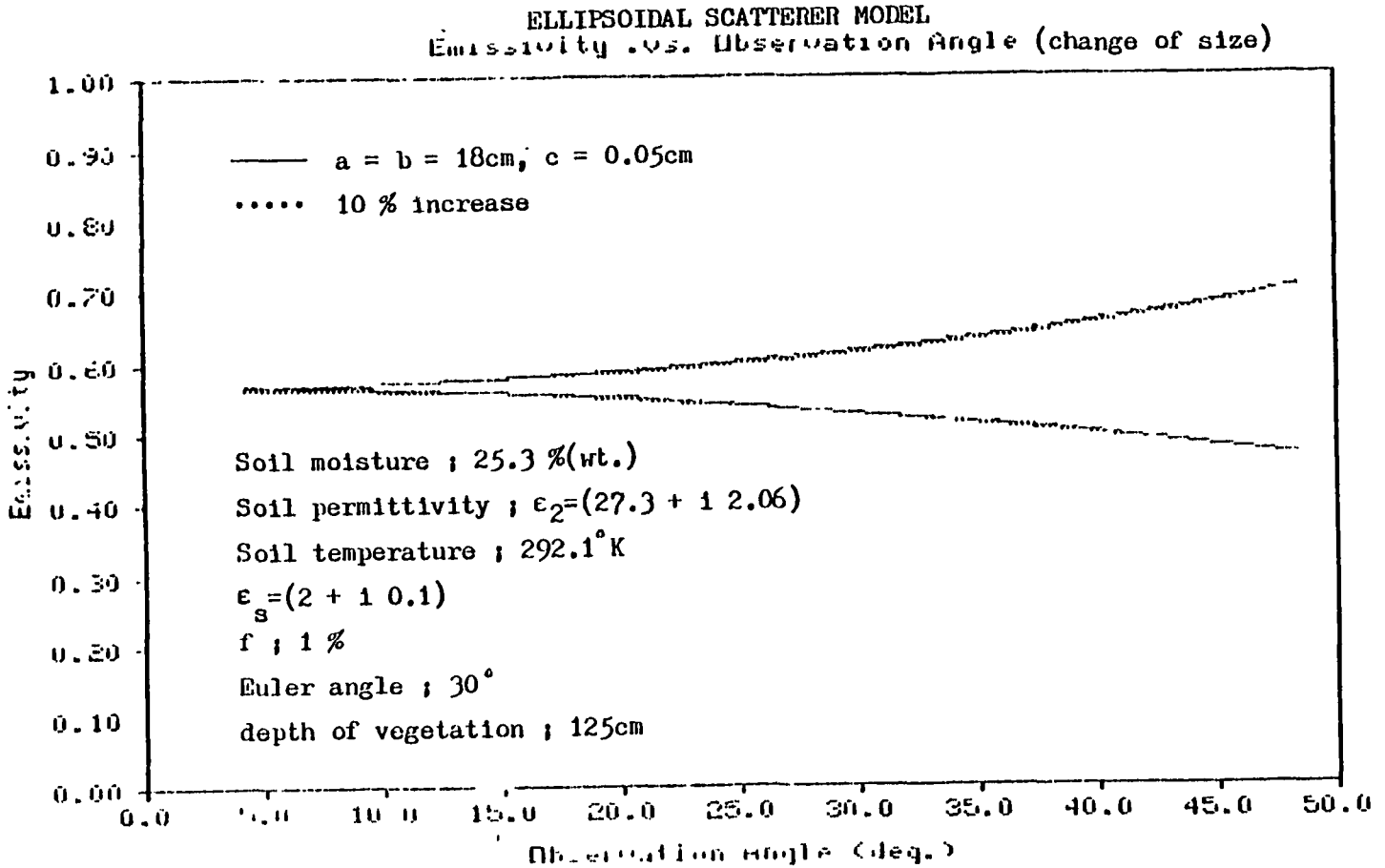

Fig. 20. Sensitivity plot of ellipsoidal scatterer model with 10 % increase of size at soil moisture 25.3 %.

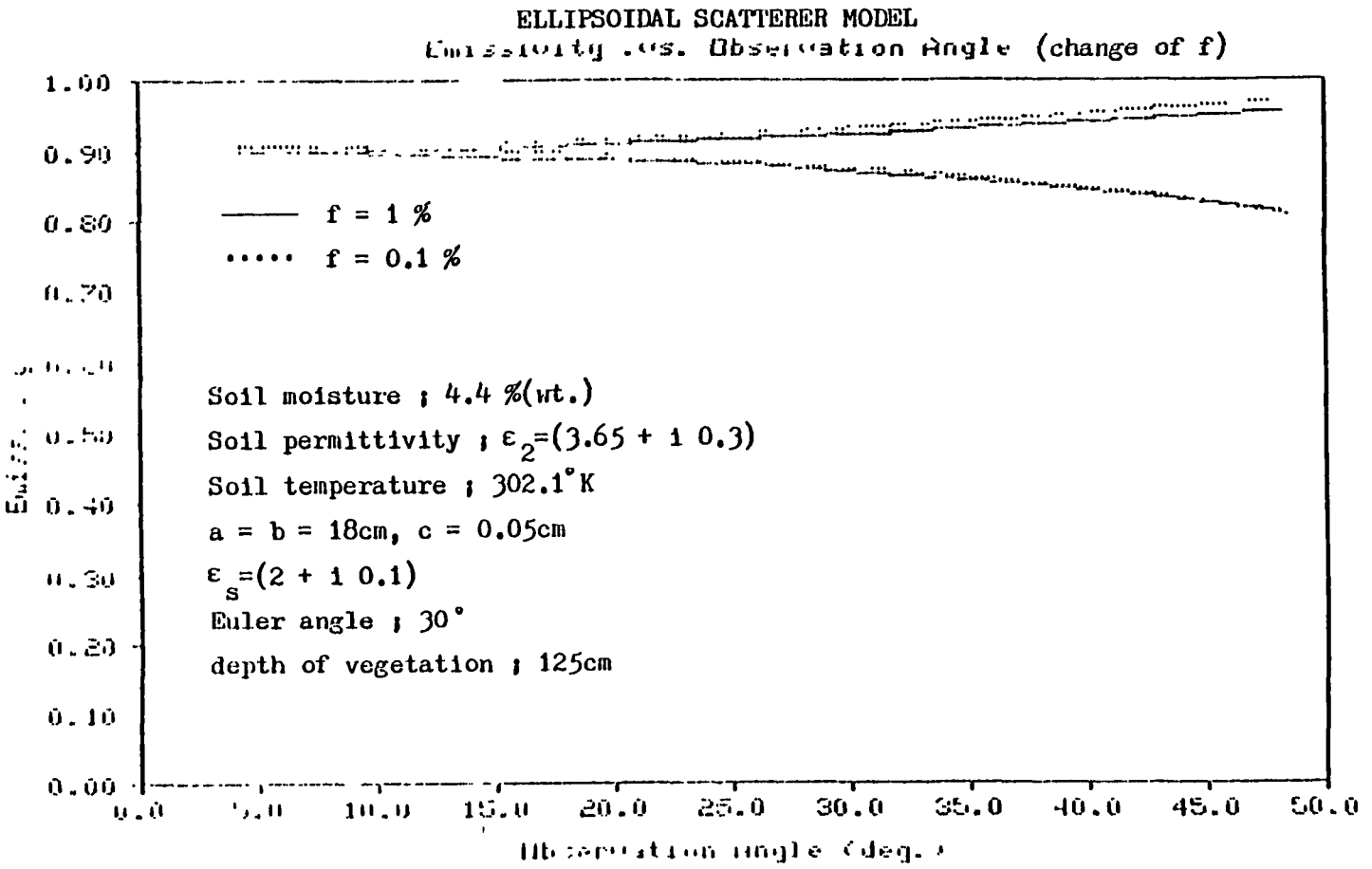

Fig. 21. Sensitivity plot of ellipsoidal scatterer model with different fractional volumes at soil moisture 4.4 %.

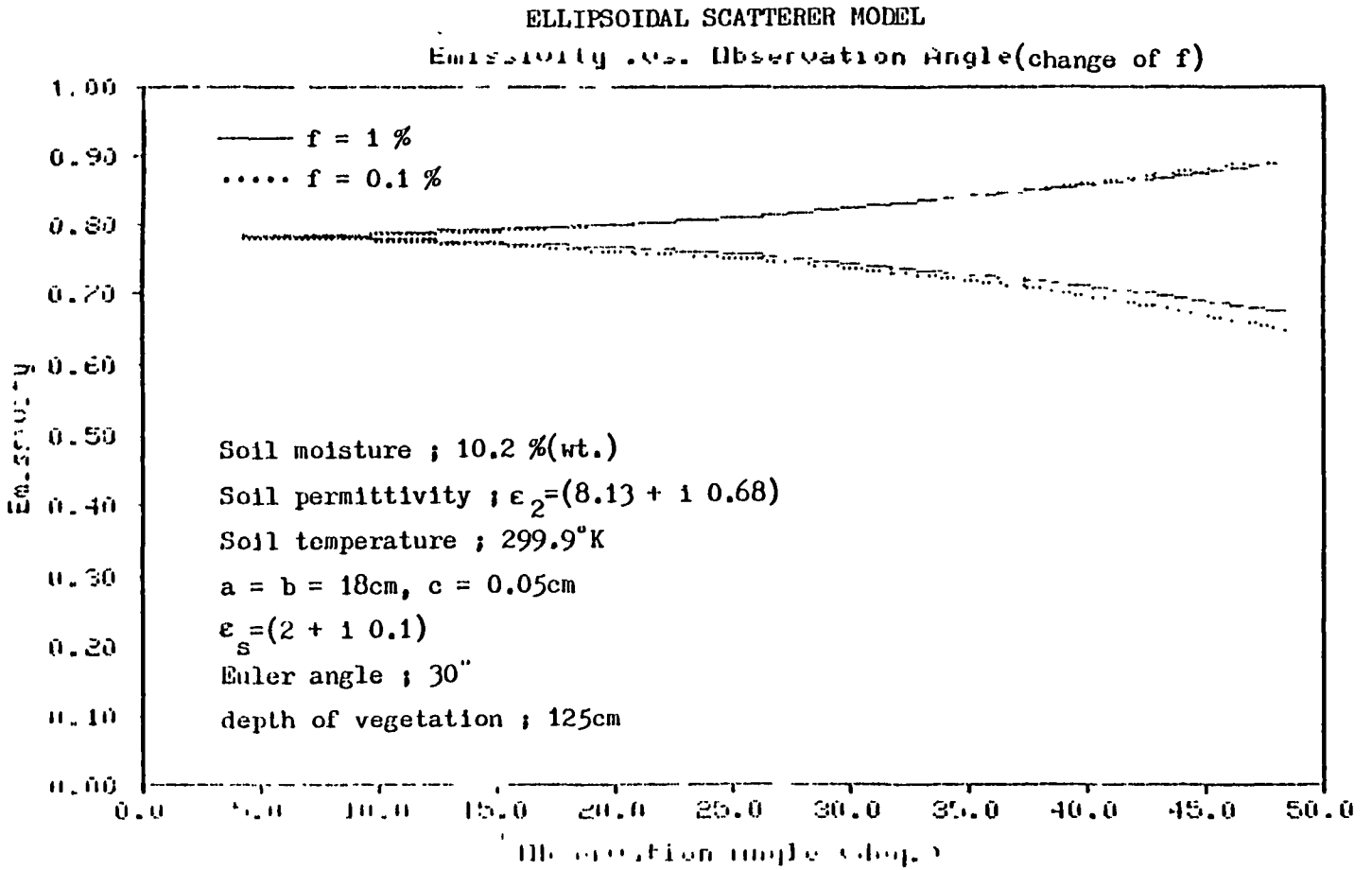

Fig. 22. Sensitivity plot of ellipsoidal scatterer model with different fractional volumes at soil moisture 10.2 %.

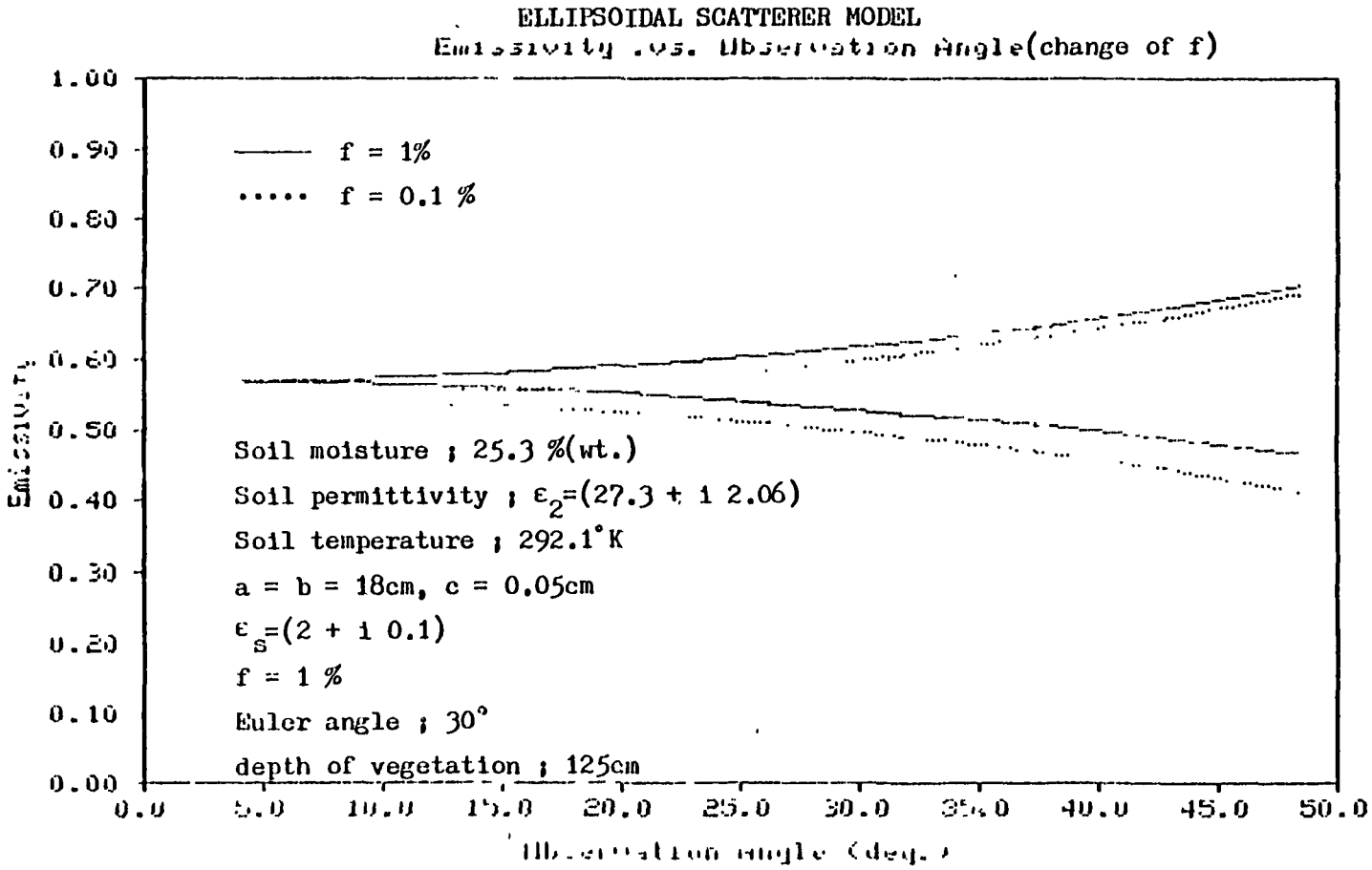

Fig. 23. Sensitivity plot of ellipsoidal scatterer model with different fractional volumes at soil moisture 25.3 %.

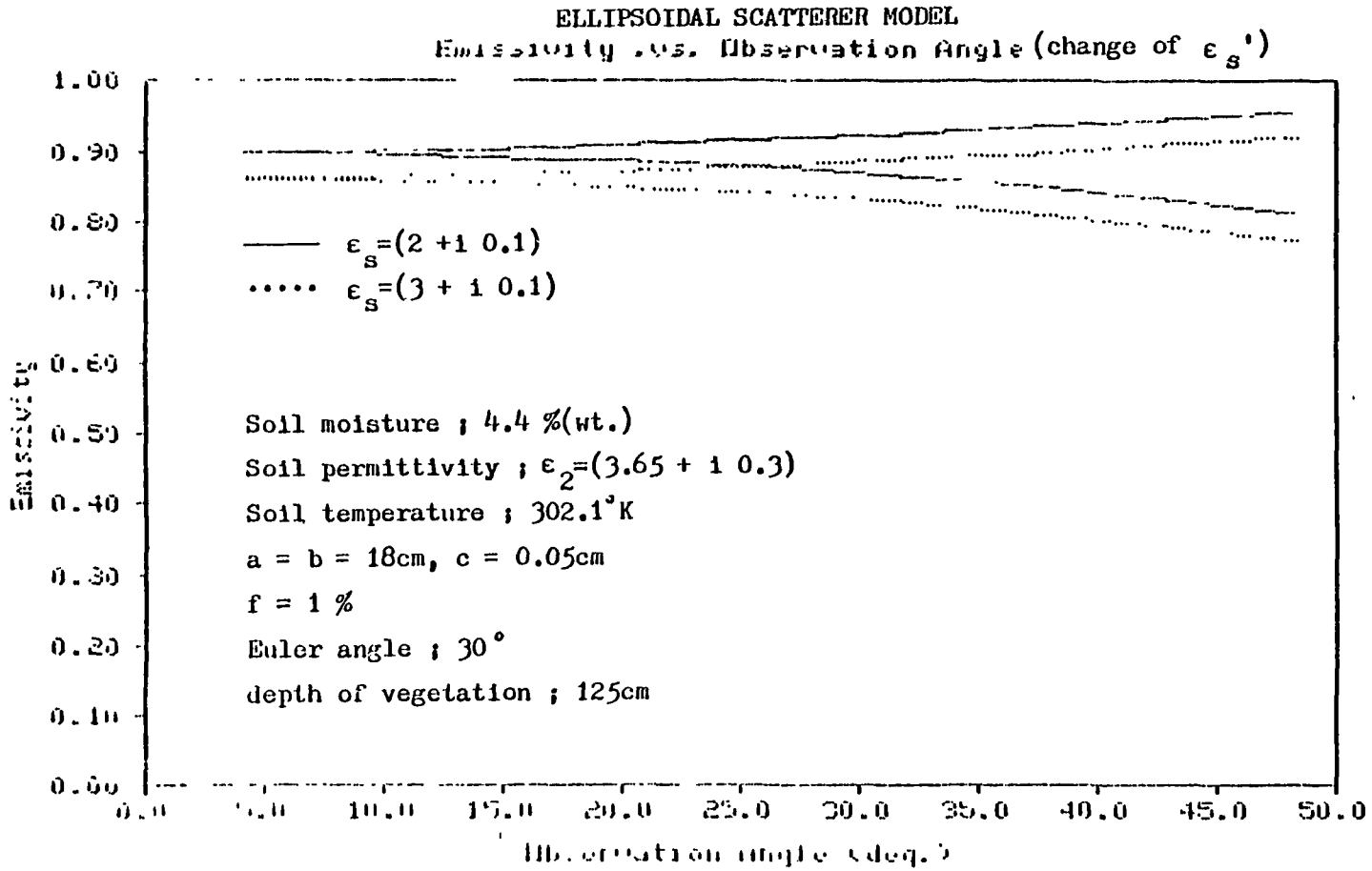

Fig. 24. Sensitivity plot of ellipsoidal scatterer model with different ε_s' at soil moisture 4.4 %.

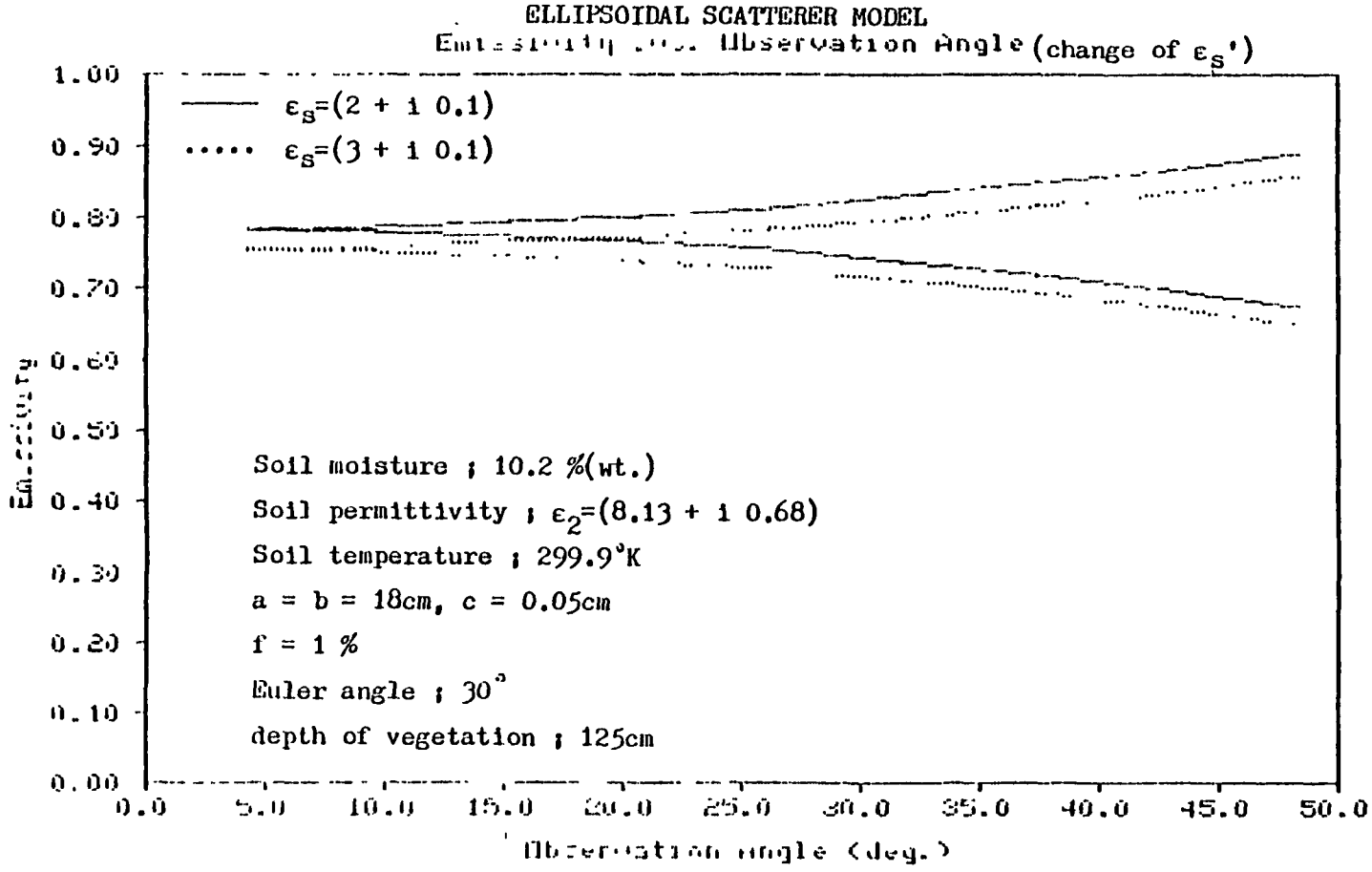

Fig. 25. Sensitivity plot of ellipsoidal scatterer model with different ε_s' at soil moisture 10.2 %.

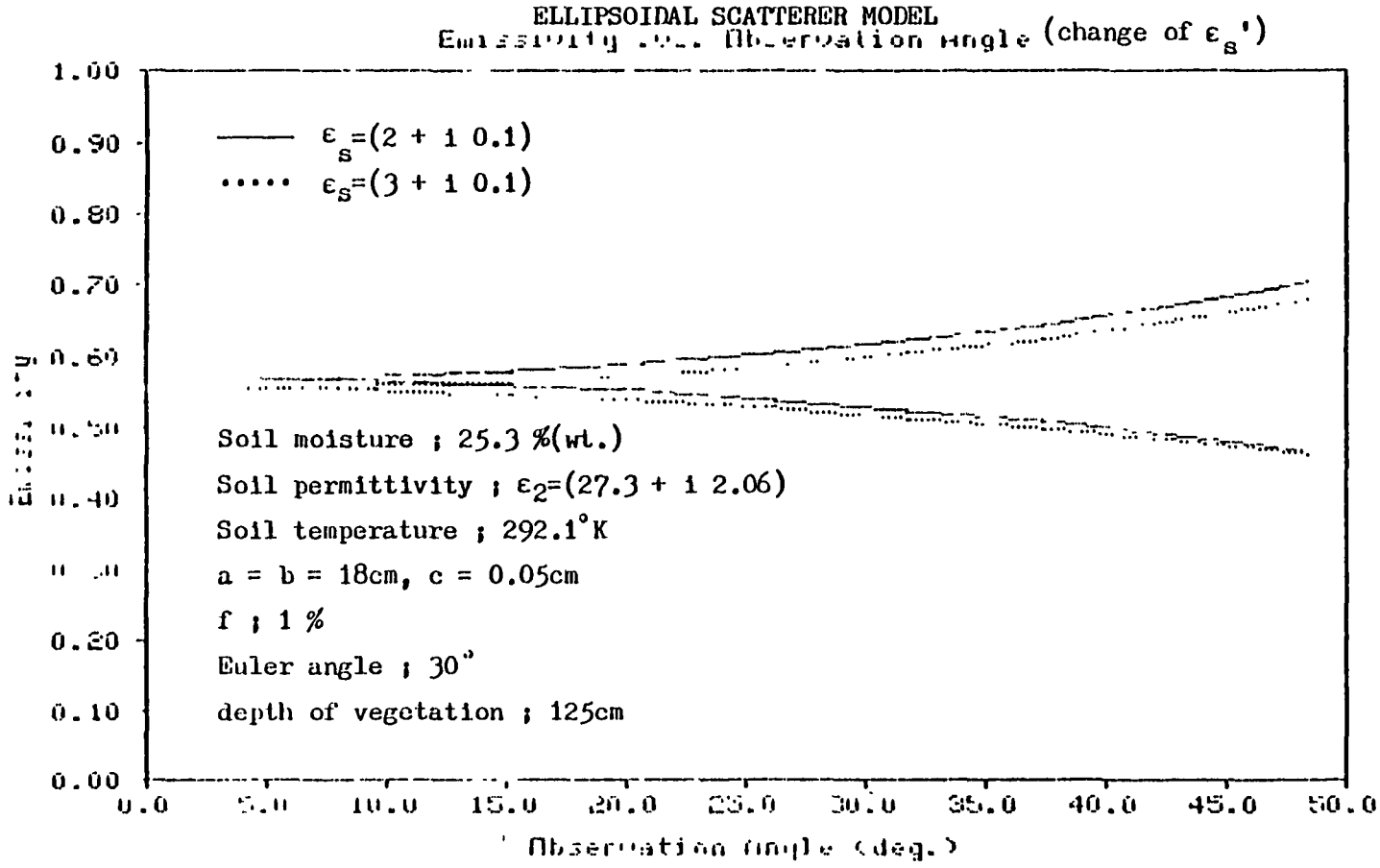

Fig. 26. Sensitivity plot of ellipsoidal scatterer model with different ε_s' at soil moisture 25.3 %.

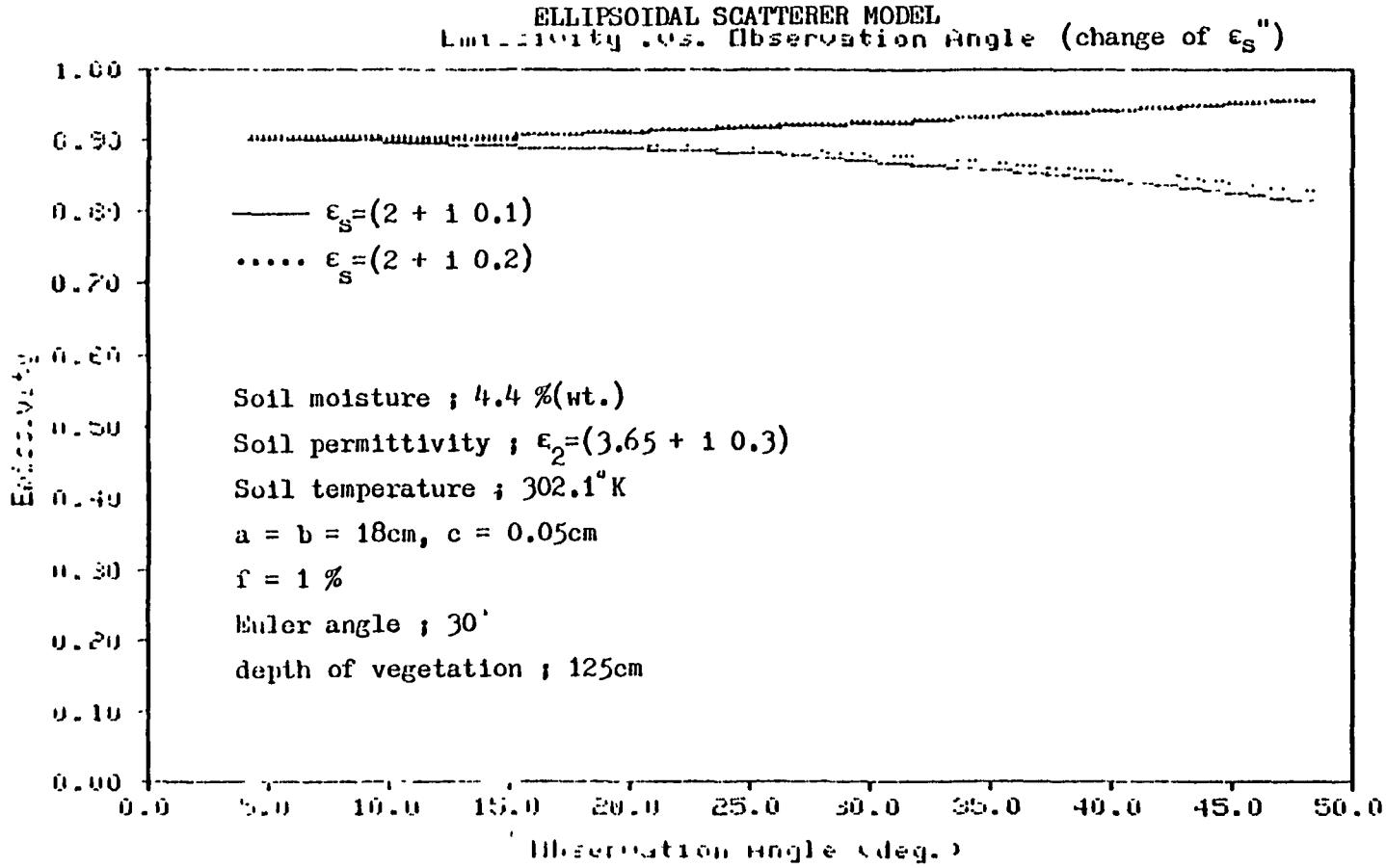

Fig. 27. Sensitivity plot of ellipsoidal scatterer model with different ϵ_s" at soil moisture 4.4 %.

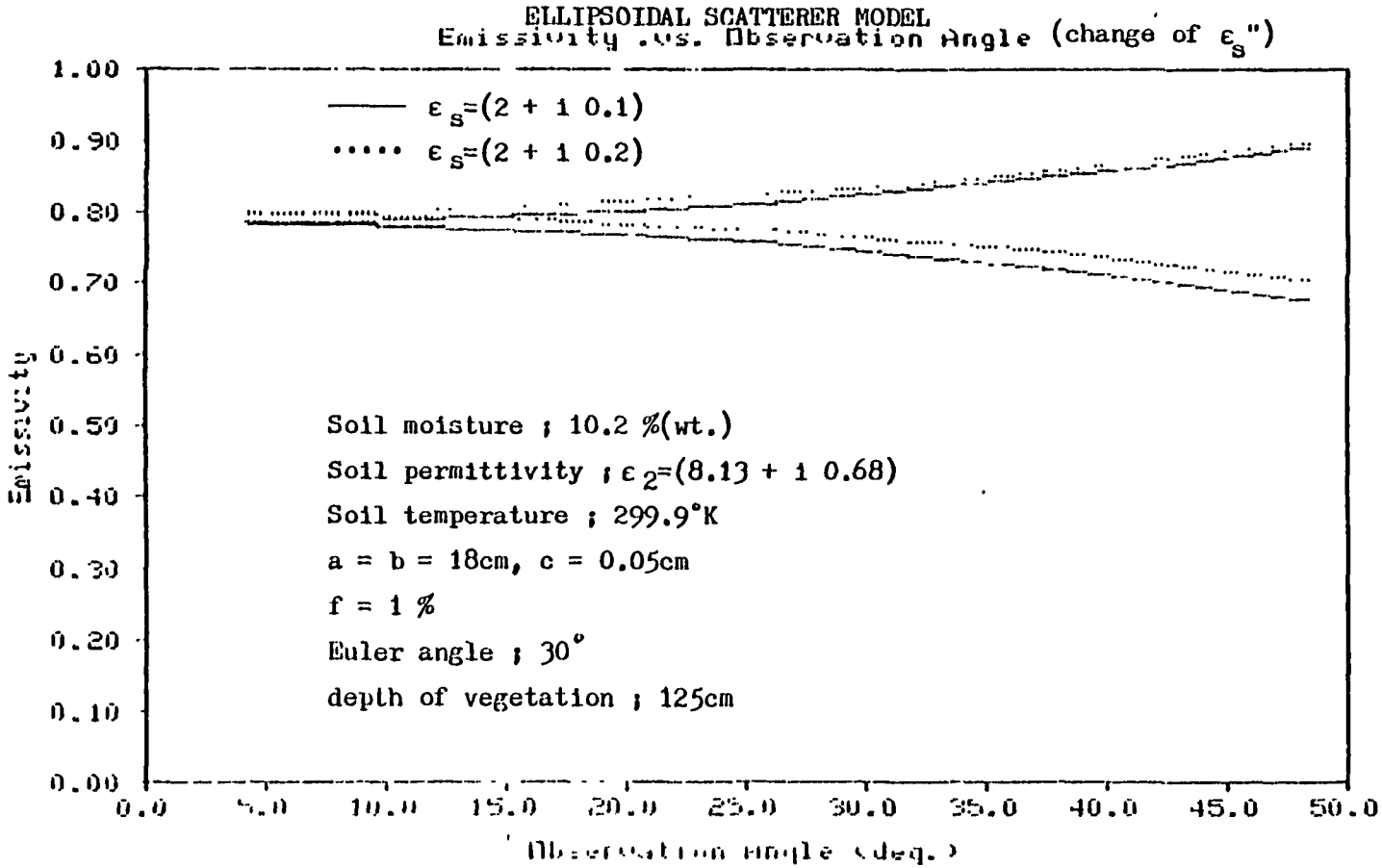

Fig. 28. Sensitivity plot of ellipsoidal scatterer model with different ϵ_s" at soil moisture 10.2 %.

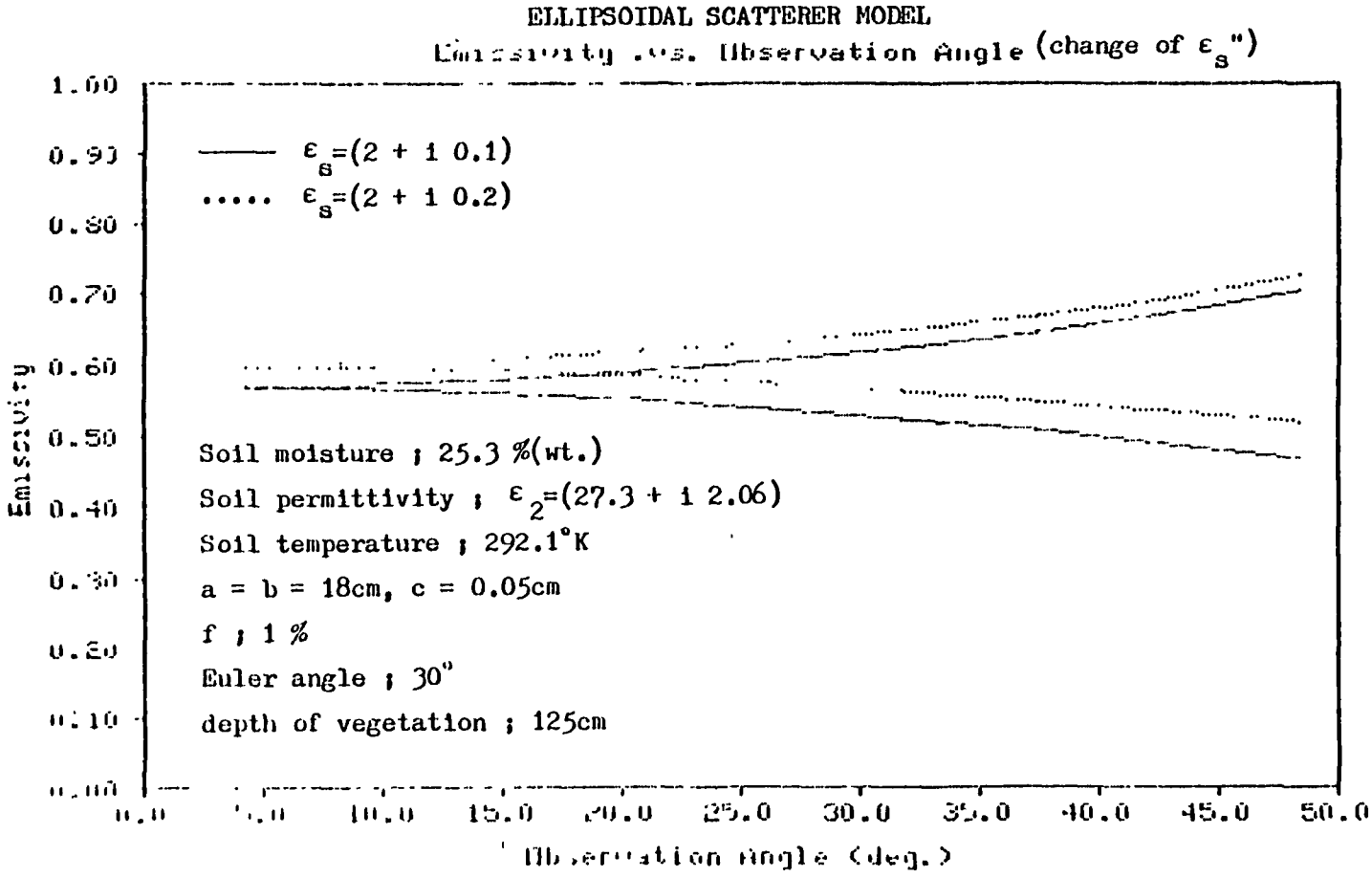

Fig. 29. Sensitivity plot of ellipsoidal scatterer model with different ε_s" at soil moisture 25.3 %.

volume from 0.1% to 1%, the emissivity was not affected as much as with the cylindrical scatterer model. Note that in the case of the cylindrical scatterer model, the fractional volume was changed from 0.01% to 0.1%.

The effects of scatterer permittivity at different soil moisture contents are shown in Figs. 24-29. An increase in the value of the real part from 2 to 3 decreased the emissivity. An increase in the imaginary part from 0.1 to 0.2 increased the emissivity as shown in Figs. 27-29. For each change of the real part, the change of emissivity was almost the same at each soil moisture content. The emissivity was more affected by changes in the imaginary part at the higher soil moisture content than for the dry soil case.

Composite Form of Cylindrical and Ellipsoidal Scatterer

Now we apply the radiative transfer theory to the scattering medium containing both of the cylindrical scatterers and ellipsoidal scatterers with different volume densities. Suppose that the permittivities of both the scatterers are the same. Then, the radiative transfer equations can be derived by combining the formulations obtained in previous sections C and D.

For $0 < \theta < \pi$,

$$\cos\theta \frac{d}{dz} I_v(\theta,z) = k_{av}^{(t)}(\theta)\, CT - k_v^{(t)}(\theta)\, I_v(\theta,z)$$

$$Q_2(\theta)\, I_v(\theta,z) + \int_0^{\pi} d\theta' \sin\theta' \int_0^{2\pi} d\phi'$$

$$[(v,v')\, I_v(\theta',z) + (v,h')\, I_h(\theta',z)] \qquad (95)$$

$$\cos\theta \frac{d}{dz} I_h(\theta,z) = k_{ah}^{(t)}(\theta)\, CT - Q_2(\theta)\, I_v(\theta,z)$$

$$-k_h^{(t)}(\theta)\, I_h(\theta,z) + \int_0^{\pi} d\theta' \sin\theta' \int_0^{2\pi} d\phi'$$

$$[(h,v')\, I_v(\theta',z) + (h,h')\, I_h(\theta',z)] \qquad (96)$$

with

$$k_{av}^{(t)}(\theta) = k_{av}^{(c)}(\theta) + k_{av}^{(e)}(\theta) \qquad (97)$$

$$k_{ah}^{(t)}(\theta) = k_{ah}^{(c)}(\theta) + k_{ah}^{(e)}(\theta) \qquad (98)$$

$$k_v^{(t)}(\theta) = k_{ev}^{(c)}(\theta) - Q_1(\theta) + k_{ev}^{(e)}(\theta) \qquad (99)$$

$$k_h^{(t)}(\theta) = k_{eh}^{(c)}(\theta) - Q_3(\theta) + k_{eh}^{(e)}(\theta) \qquad (100)$$

where subscripts c and e represent the cylindrical model and ellipsoidal model, respectively.

The radiative transfer equations (95) and (96) subject to the boundary conditions in section B can be solved by numerical approach, and the results are illustrated in Chapter V.

NUMERICAL APPROACH

For the general case, the integro-differential radiative transfer equations must be solved by a numerical approach. The radiative transfer equations are rewritten letting $\mu = \cos\theta$. Then, following Chandrasekhar [48], the integrals in the radiative transfer equations are replaced by a Gaussian quadrature [Appendix D], which is an appropriately weighted sum over 2n intervals between the 2n zeros of the even-order Legendre polynomials $P_{2n}(\mu)$. We obtain, for $\tau = \pm 1, \pm 2, .., \pm n$

$$\mu_i \frac{d}{dz} I_{vi}(z) = K_{avi}\, CT - K_{evi}\, I_{vi}(z) + \sum_{j=-n}^{n} a_j [(v_i, v_j)\, I_{vj}(z) + v_i, h_j)\, I_{hj}(z)] \tag{101}$$

$$\mu_i \frac{d}{dz} I_{hi}(z) = K_{ahi}\, CT - K_{ehi}\, I_{vi}(z) + \sum_{j=-n}^{n} a_j [(v_i, v_j)\, I_{vj}(z) + h_i, h_j)\, I_{hj}(z)] \tag{102}$$

where

$$I_{\beta i}(z) = I_{\beta}(\mu_i, z) \tag{103}$$

$$K_{x\beta i} = K_{x\beta}(\mu_i) \tag{104}$$

$$(\alpha_i, \beta_j) = (\alpha(\mu_i),\ \beta(\mu_j)) \tag{105}$$

α and β denote h or v, x denotes a or e, μ_i are the zeros of $P_{2n}(\mu)$, and a_j are the Christoffel weighting functions. There are 2n μ_j's and 2n a_j's. They obey the relation

$$a_j = a_{-j} \tag{106}$$

$$\mu_j = \mu_{-j} \tag{107}$$

Relations (101) and (102) constitute a system of 4n ordinary differential equations with constant coefficients.

To solve for the homogeneous solutions to (101) and (102), let

$$I_{\beta i}(z) = I_{\beta i}\, e^{\alpha z} \tag{108}$$

Substitute (108) in (101) and (102) with T equal to zero in order to determine the 4n eigenvalues of α and the corresponding 4n eigenvectors. In matrix notation

$$\bar{\bar{\alpha}}\bar{\mu} \cdot \bar{I}_u = -\bar{\bar{K}}_e \cdot \bar{I}_u + \bar{\bar{F}} \cdot \bar{\bar{a}} \cdot \bar{I}_u + \bar{\bar{B}} \cdot \bar{\bar{a}} \cdot \bar{I}_d \tag{109}$$

$$-\bar{\bar{\alpha}}\bar{\mu} \cdot \bar{I}_d = -\bar{\bar{K}}_e \cdot \bar{I}_d + \bar{\bar{B}} \cdot \bar{\bar{a}} \cdot \bar{I}_u + \bar{\bar{F}} \cdot \bar{\bar{a}} \cdot \bar{I}_d \tag{110}$$

where $\bar{I}_u$ and $\bar{I}_d$ are two 2n x 1 matrices

$$\bar{I}_u = \begin{bmatrix} I_{v1} \\ \cdot \\ \cdot \\ I_{vn} \\ I_{h1} \\ \cdot \\ \cdot \\ I_{hn} \end{bmatrix} \qquad \bar{I}_d = \begin{bmatrix} I_{v-1} \\ \cdot \\ \cdot \\ I_{v-n} \\ I_{h-1} \\ \cdot \\ \cdot \\ I_{h-n} \end{bmatrix} \tag{111}$$

the matrices $\bar{\bar{\mu}}$, $\bar{\bar{k}}_e$, and $\bar{\bar{a}}$ are 2n x 2n diagonal matrices

$$\bar{\bar{\mu}} = \begin{bmatrix} \mu_1 & & & & & & 0 \\ & \ddots & & & & & \\ & & \mu_n & & & & \\ & & & \mu_1 & & & \\ & & & & \ddots & & \\ 0 & & & & & \ddots & \\ & & & & & & \mu_n \end{bmatrix} \tag{112}$$

$$\bar{\bar{k}}_e = \begin{bmatrix} k_{evi} & & & & & & 0 \\ & \ddots & & & & & \\ & & k_{evn} & & & & \\ & & & k_{ehl} & & & \\ & & & & \ddots & & \\ 0 & & & & & \ddots & \\ & & & & & & k_{ehn} \end{bmatrix} \tag{113}$$

$$\bar{\bar{a}} = \begin{bmatrix} a_1 & & & & & & 0 \\ & \ddots & & & & & \\ & & a_n & & & & \\ & & & a_1 & & & \\ & & & & \ddots & & \\ 0 & & & & & \ddots & \\ & & & & & & a_n \end{bmatrix} \tag{114}$$

and the matrices $\bar{\bar{F}}$ and $\bar{\bar{B}}$ are forward and backward scattering phase functions with dimensions of 2n x 2n.

$$\overline{\overline{F}} = \begin{bmatrix} (v_1,v_1) & \cdots & (v_1,v_n) & (v_1,h_1) & \cdots & (v_1,h_n) \\ \vdots & & \vdots & \vdots & & \vdots \\ (v_n,v_1) & \cdots & (v_n,v_n) & (v_n,h_1) & \cdots & (v_n,h_n) \\ (h_1,v_1) & \cdots & (h_1,v_n) & (h_1,h_1) & \cdots & (h_1,h_n) \\ \vdots & & \vdots & \vdots & & \vdots \\ (h_n,v_1) & \cdots & (h_n,v_n) & (h_n,h_1) & \cdots & (h_n,h_n) \end{bmatrix} \tag{115}$$

$$\overline{\overline{B}} = \begin{bmatrix} (v_1,v_{-1}) & \cdots & (v_1,v_{-n}) & (v_1,h_{-1}) & \cdots & (v_1,h_{-n}) \\ \vdots & & \vdots & \vdots & & \vdots \\ (v_n,v_{-1}) & \cdots & (v_n,v_{-n}) & (v_n,h_{-1}) & \cdots & (v_n,h_{-n}) \\ (h_1,v_{-1}) & \cdots & (h_1,v_{-n}) & (h_1,h_{-1}) & \cdots & (h_1,h_{-n}) \\ \vdots & & \vdots & \vdots & & \vdots \\ (h_n,v_{-1}) & \cdots & (h_n,v_{-n}) & (h_n,h_{-1}) & \cdots & (h_n,h_{-n}) \end{bmatrix} \tag{116}$$

From the symmetry relations for scattering phase functions, note that

$$\overline{\overline{F}}^t = \overline{\overline{F}} \tag{117}$$

$$\overline{\overline{B}}^t = \overline{\overline{B}} \tag{118}$$

where superscript t denotes the transpose of the matrix.

We can reduce the number of homogeneous equations from 4n to 2n by defining

$$\bar{I}_+ = \bar{I}_u + \bar{I}_d \tag{119}$$

$$\bar{I}_- = \bar{I}_u - \bar{I}_d \tag{120}$$

Adding (109) and (110),

$$\overline{\overline{\alpha\mu}} \cdot \bar{I}_- = \overline{\overline{A}} \cdot \bar{I}_- \tag{121}$$

and subtracting (109) from (110)

$$\overline{\overline{\alpha\mu}} \cdot I_+ = \overline{\overline{W}} \cdot I_- \tag{122}$$

where

$$\bar{\bar{A}} = -\bar{\bar{K}}_e + \bar{\bar{F}} \cdot \bar{\bar{a}} + \bar{\bar{B}} \cdot \bar{\bar{a}} \tag{123}$$

$$\bar{\bar{W}} = -\bar{\bar{K}}_e + \bar{\bar{F}} \cdot \bar{\bar{a}} - \bar{\bar{B}} \cdot \bar{\bar{a}} \tag{124}$$

Combining (121) and (122), we obtain the eigenvalue problem.

$$\bar{\bar{\mu}}^{-1} \cdot \bar{\bar{W}} \cdot \bar{\bar{\mu}}^{-1} \cdot \bar{\bar{A}} - \alpha^2 \bar{\bar{I}}) \cdot \bar{I}_+ = 0 \tag{125}$$

where $\bar{\bar{I}}$ is an identity matrix. Thus is α is an eigenvalue so is $-\alpha$. After the eigenvalue and eigenvector problem is solved, the solution is written in the following form

$$\bar{I}_+ = \sum_{\ell=1}^{2n} \{ P_\ell \bar{I}_{+\ell} e^{a_\ell z} + P_{-\ell} \bar{I}_{+\ell} e^{-\alpha_\ell z} \} \tag{126}$$

where a_ℓ is the square root of the ℓ-th eigenvalue in (125) and $\bar{I}_{+\ell}$ the corresponding eigenvectors. The constants P_ℓ and $P_{-\ell}$ are to be determined from the boundary conditions.

Also, $\bar{I}_-$ is determined from (121). The result is

$$\bar{I}_- = \sum_{\ell=1}^{2n} \{ P_\ell \bar{I}_{-\ell} e^{\alpha_\ell z} + P_{-\ell} \bar{I}_{-\ell} e^{-\alpha_\ell z} \} \tag{127}$$

where

$$\bar{I}_{-\ell} = \frac{1}{\alpha_\ell} \bar{\bar{\mu}}^{-1} \cdot \bar{\bar{A}} \cdot \bar{I}_{+\ell} \tag{128}$$

Finally, from (119) and (120),

$$\bar{I}_u = \sum_{\ell=1}^{2n} \{ P_\ell \bar{I}_{u\ell} e^{\alpha_\ell z} + P_{-\ell} \bar{I}_{d\ell} e^{-\alpha_\ell z} \} \tag{129}$$

$$\bar{I}_d = \sum_{\ell=1}^{2n} \{ P_\ell \bar{I}_{d\ell} e^{\alpha_\ell z} + P_{-\ell} \bar{I}_{u\ell} e^{-\alpha_\ell z} \} \tag{130}$$

where

$$\bar{I}_{u\ell} = \frac{1}{2}(\bar{I}_{+\ell} + \bar{I}_{-\ell}) \tag{131}$$

$$\bar{I}_{d\ell} = \frac{1}{2}(\bar{I}_{+\ell} - \bar{I}_{-\ell}) \tag{132}$$

The particular solutions to (101) and (102) are, for $i=\pm1,\ldots,\pm n$,

$$\bar{I}^{p}_{ui} = CT \tag{133}$$

$$\bar{I}^{p}_{di} = CT \tag{134}$$

Therefore, the complete solution is

$$\bar{I}_u = \sum_{\ell=1}^{2n} \{P_\ell \ \bar{I}_{u\ell} e^{\alpha_\ell z} + P_{-\ell} \bar{I}_{d\ell} e^{-\alpha_\ell z}\} + CT \tag{135}$$

$$\bar{I}_d = \sum_{\ell=1}^{2n} \{P_\ell \ \bar{I}_{d\ell} e^{\alpha_\ell z} + P_{-\ell} \bar{I}_{u\ell} e^{-\alpha_\ell z}\} + CT \tag{136}$$

The 4n unknown constants P_ℓ and $P_{-\ell}$ are to be determined from the following boundary conditions.

$$\bar{I}_d\,(z=0) = \bar{\bar{r}}_{10} \cdot \bar{I}_u\,(z=0) \tag{137}$$

$$\bar{I}_u\,(z=-d) = \bar{\bar{r}}_{12} \cdot \bar{I}_d\,(z=-d) + \bar{\bar{t}}_{12} \cdot C\bar{T}_2 \tag{138}$$

where

$$\bar{\bar{\gamma}}_{10} = \begin{bmatrix} r_{v101} & & & & 0 \\ & \ddots & & & \\ & & r_{v10n} & & \\ & & & r_{h101} & \\ 0 & & & & \ddots \\ & & & & & r_{h10n} \end{bmatrix} \tag{139}$$

$$\underline{\underline{\gamma}}_{12} = \begin{bmatrix} \gamma_{v121} & & & & & \\ & \ddots & & & & \\ & & \gamma_{v12n} & & & \\ & & & \gamma_{h121} & & \\ & 0 & & & \ddots & \\ & & & & & \gamma_{h12n} \end{bmatrix} \tag{140}$$

$$\underline{\underline{t}}_{21} = \begin{bmatrix} t_{v211} & & & & & \\ & \ddots & & & 0 & \\ & & t_{v21n} & & & \\ & & & t_{h211} & & \\ & 0 & & & \ddots & \\ & & & & & t_{h21n} \end{bmatrix} \tag{141}$$

$$\underline{\bar{T}}_2 = \begin{bmatrix} \underline{T}_2 \\ \underline{T}_2 \\ \vdots \\ \underline{T}_2 \end{bmatrix} \tag{142}$$

DATA MATCHING

In this section, the theoretical results from the composite form of the cylindrical and ellipsoidal models are used to match the experimental data collected from the vegetated field. In data matching, the main objective was to find the set of parameters that are consistent with the ground truth observations and that also matches the experiment measurements.

Of the several parameters, the most important are the permittivity of underlying soil and the fractional volumes. The first step of data matching is to find the permittivity of the soil. Following Schmugge [49], the permittivity formula is a linear function of soil moisture.

$$\varepsilon_2' = \begin{cases} -9.9 + 1.38\ Sm & \text{for } Sm \geq 11.5 \\ 2.56 + 0.3\ Sm & \text{for } Sm < 11.5 \end{cases} \tag{143}$$

$$\varepsilon_2'' = \begin{cases} -1.44 + 0.185 Sm & \text{for } Sm \geq 11.5 \\ 0.06 \cdot Sm & \text{for } Sm < 11.5 \end{cases} \tag{144}$$

where ε_2' and ε_2'' are real and imaginary parts of soil permittivity, respectively, and Sm is the soil moisture.

Soil permittivity also can be calculated from the definition of emissivity for bare smooth soil (CS field).

$$e(\theta) = 1 - r_{10}(\theta) \tag{145}$$

The reflectivity $r_{10}(\theta)$ is given in (23) and (24). In this case, the imaginary part of the soil permittivity is small compared to the real part and is neglected.

In Fig. 30, the real parts of soil permittivity computed using measurements of emissivity and equations (23), (24) and (145) are plotted as a function of soil moisture by weight. The permittivity calculated from the 1974 experimental radiometric measurements as an observation angle 20° are close to the permittivity values computed with equations (143) and (144).

Figs. 31-33 show the theoretical computations of brightness temperature using the permittivity based on the bare soil measurements made at 20°. These results are well matched to the experimental measurements from field CS at various soil moistures and the other observation angles. In Figs. 31-33, soil moistures are 4.3%, 10.5% and 25.9%, respectively, and the corresponding soil permittivities are $\varepsilon_2 = (3.56 + i0.39)\varepsilon_0$, $(8.25 + i0.98)\varepsilon_0$ and $(28.12 + i3.36)\varepsilon_0$, respectively.

Another important parameter is the permittivity of the scatterers. Since soil moisture content effects to the moisture content in plant, it is natural to assume that the permittivity of the scatterers is a function of soil moisture. It is shown below that the vegetation permittivity must be a function of soil moisture in order to match observations to theoretical predictions.

The permittivity of the scatterers is $\varepsilon_2 = (2 + i0.1)\varepsilon_0$ at a soil moisture content of 25.3%. This value was obtained with using cylindrical scatterer model only. Emissivities were first computed using the composite form (stalks and leaves) of the theoretical model with the constant value of scatterer permittivity given above and compared to the measurements obtained from the sorghum field (BS field). Figs. 34-37 show comparisons of the theoretical simulations and the

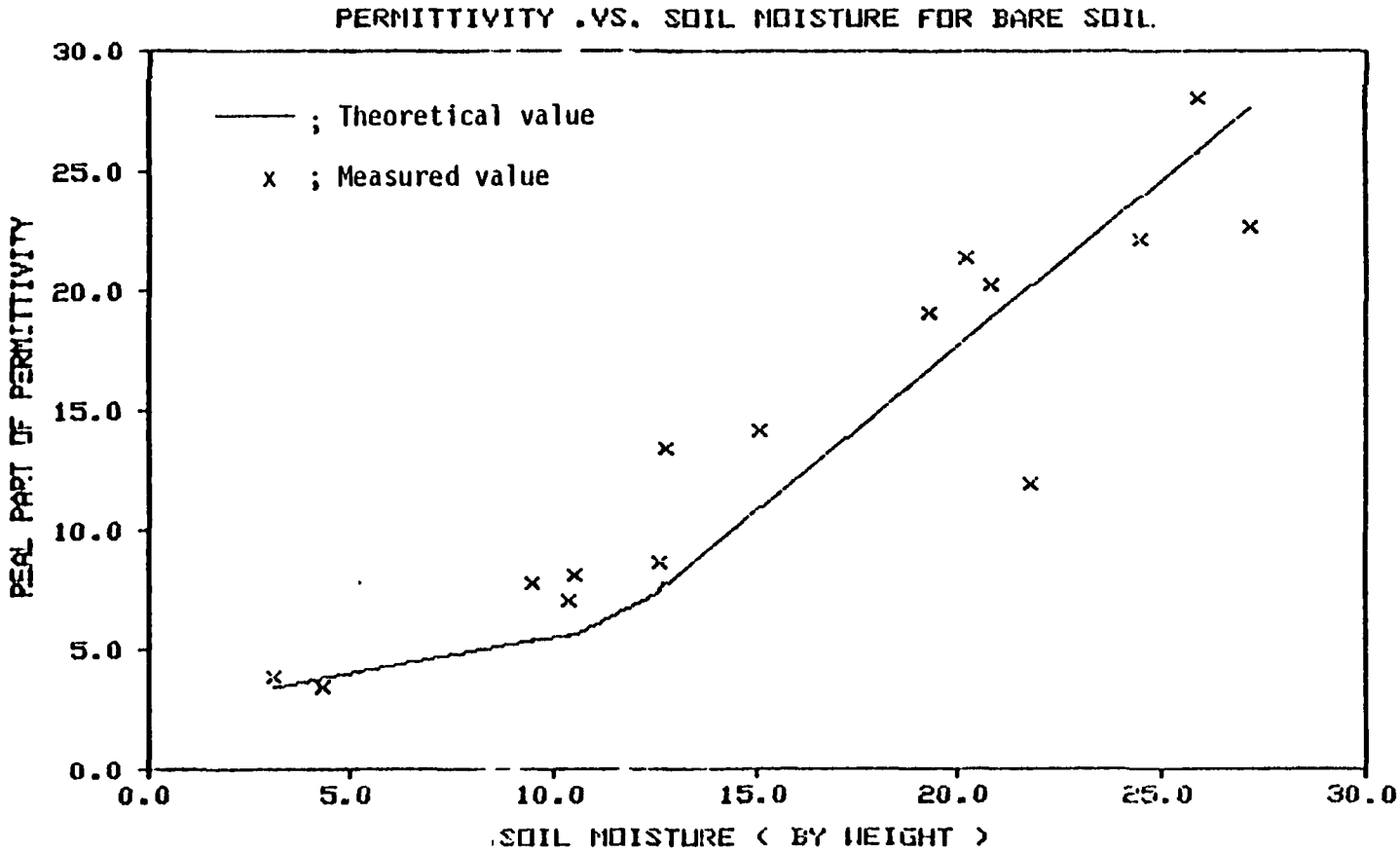

Fig. 30. Comparison of theoretical and measured soil permittivities.

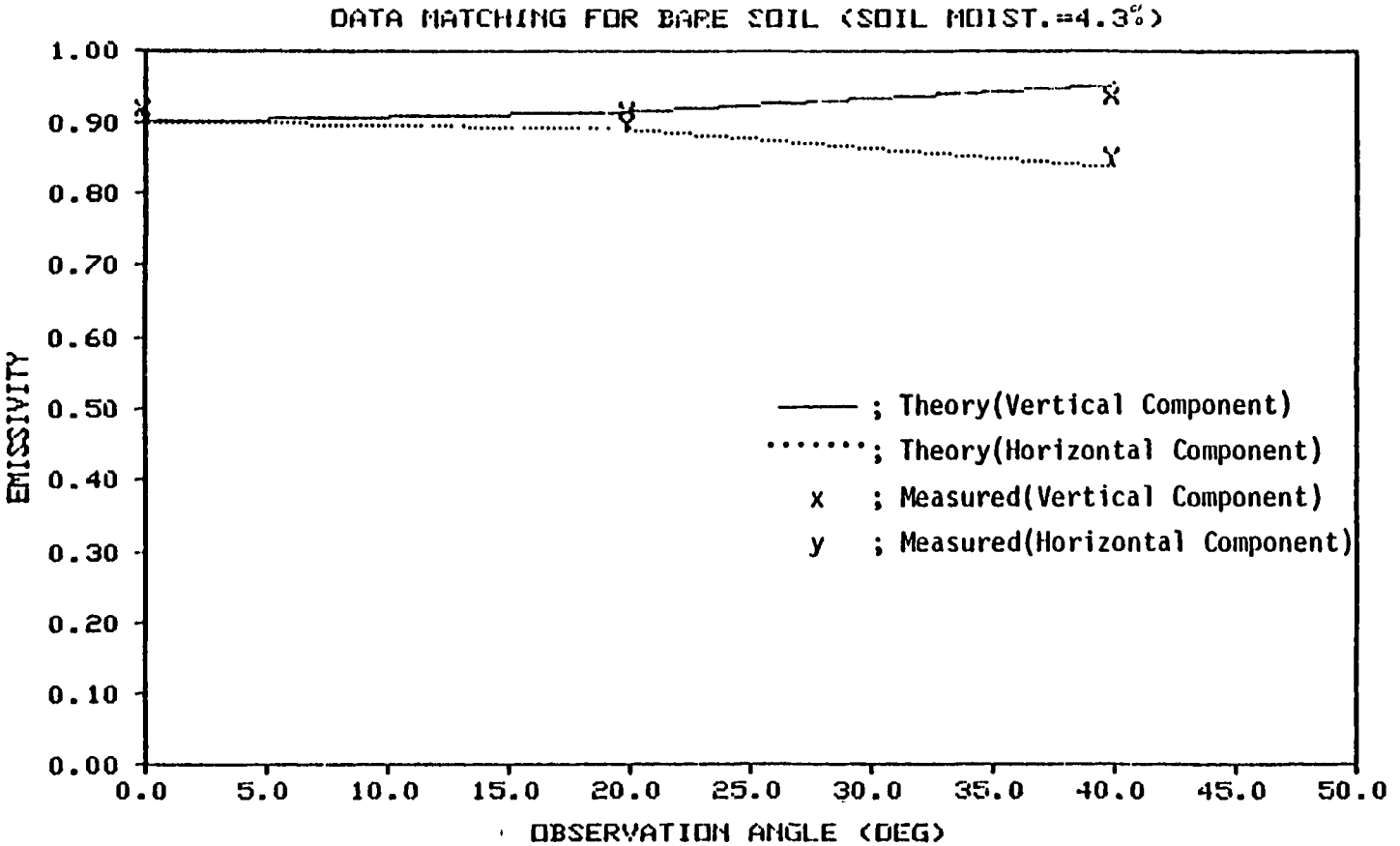

Fig. 31. Data matching for bare soil at soil moisture 4.3 %.

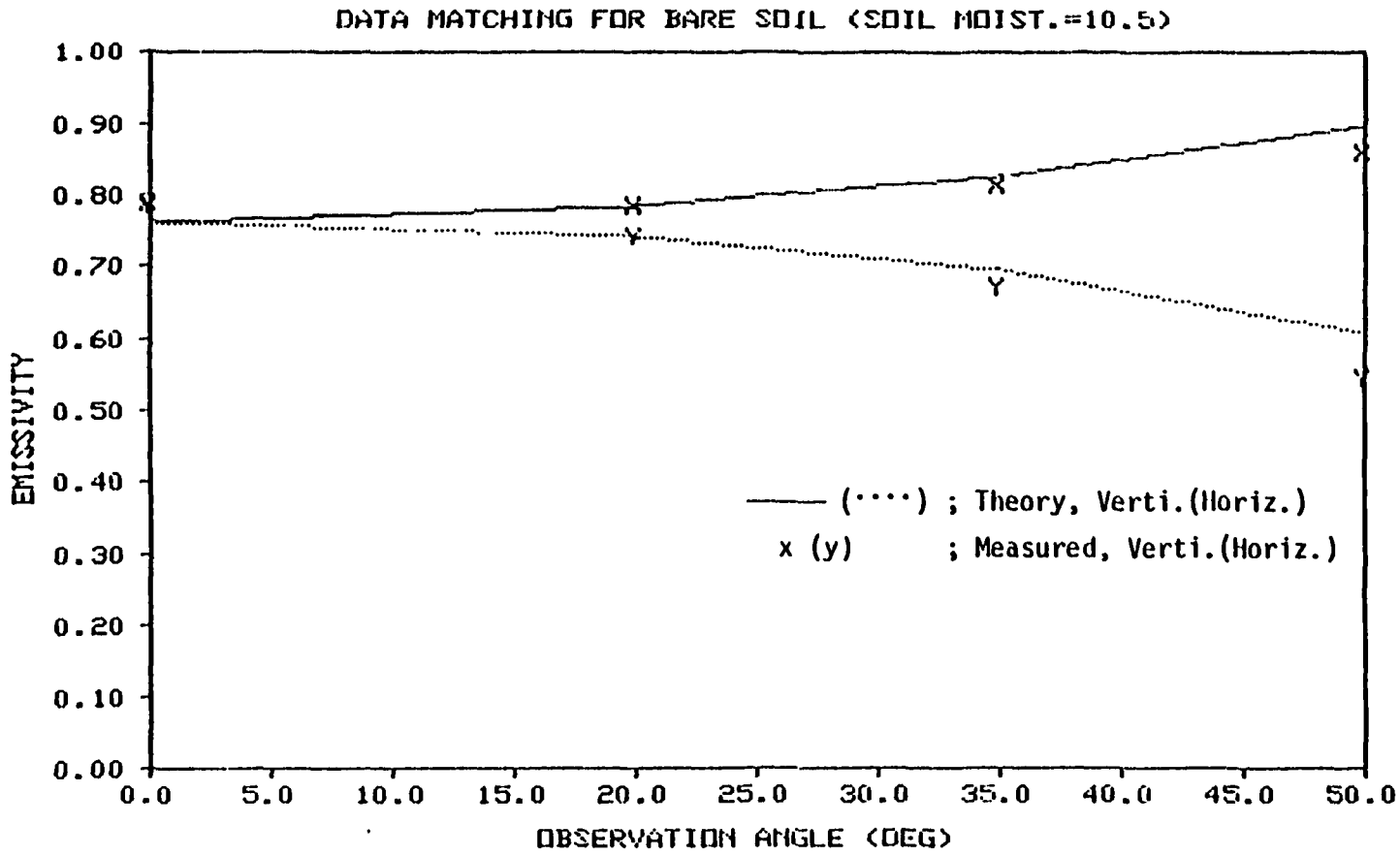

Fig. 32. Data matching for bare soil at soil moisture 10.5 %.

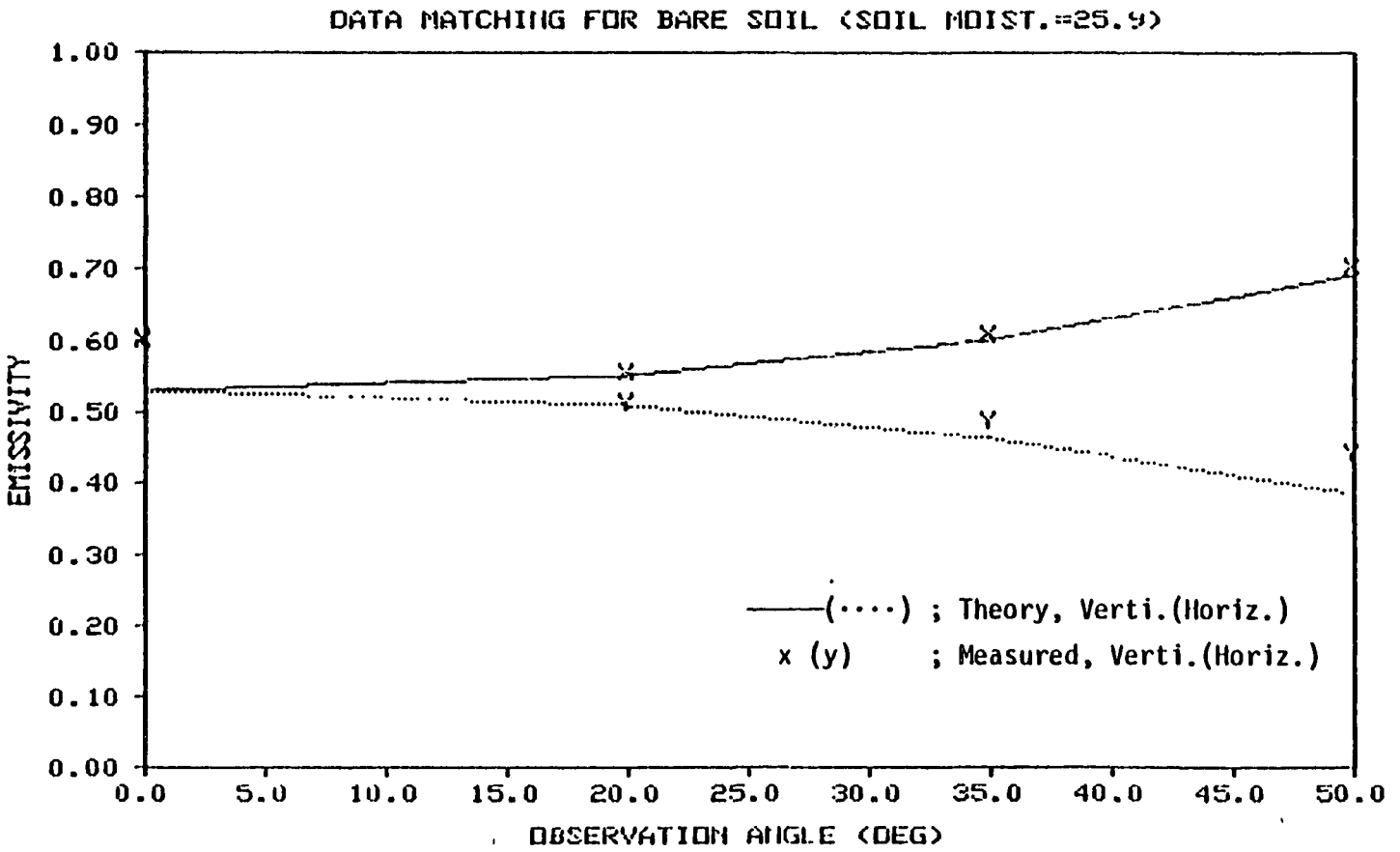

Fig. 33. Data matching for bare soil at soil moisture 25.9 %.

experimental measurements for a vegetated field, and for comparison, experimental results of a bare field both for soil moisture contents of 4.4%, 8.7%, 10.2% and 25.3%, respectively. The corresponding soil permittivities were $\varepsilon_2 = (3.65 + i0.3)\varepsilon_0$, $(7.21 + i0.58)\varepsilon_0$, $(8.13 + i0.68)\varepsilon_0$ and $(27.3 + i2.06)\varepsilon_0$, respectively and soil surface temperatures were 301.2°K, 301.3°K, 299.9°K and 292.1°K, respectively. In all cases, the same input parameters are used. For the cylindrical scatterers (stalks), the radius and length were 1 cm and 125 cm, resepectively, For the ellipsoidal scatterers (leaves), a, b, and c were 18 cm, 18 cm and 0.05 cm, respectively. The corresponding leaf area was $324\ \pi\ cm^2$ which corresponds to the length 64.8 cm and width 5 cm of a sorghum leaf. The average inclination angle of the leaf distribution was chosen as 30° from the vertical direction. This is within the range of most populations of sorghum such as P 407, SC 170 and Caprock. The fractional volume of the cylindrical and ellipsoidal scatterers were 0.1% and 0.9%, respectively.

Fig. 37 shows the highest soil moisture content case. The theoretical results are well matched to the measurement data. The lower soil moisture content cases shown in Figs. 34-36 demonstrate that the theoretical results are higher than the measured data. The reason for this is that the permittivity of the scatterers, $\varepsilon_s = (2 + i.01)\varepsilon_0$, was chosen at the soil moisture content of 25.3% and not allowed to vary as the soil moisture varied.

Since the change of soil moisture content affects the moisture content in sorghum, it is necessary that the permittivity of the scatterers be changed as the soil moisture changes. From the sensitivity

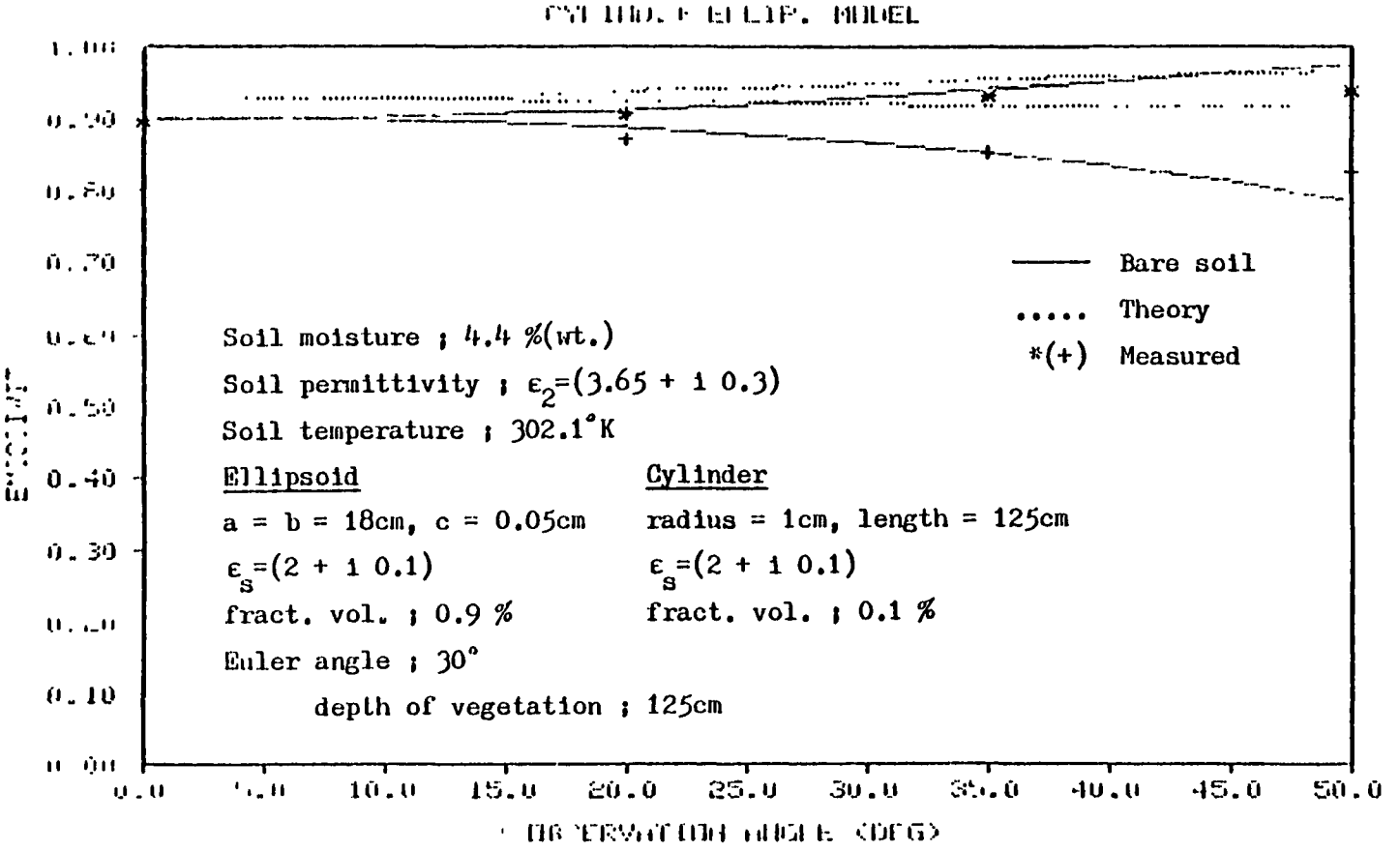

Fig. 34. Data matching for sorghum field at soil moisture 4.4 %.

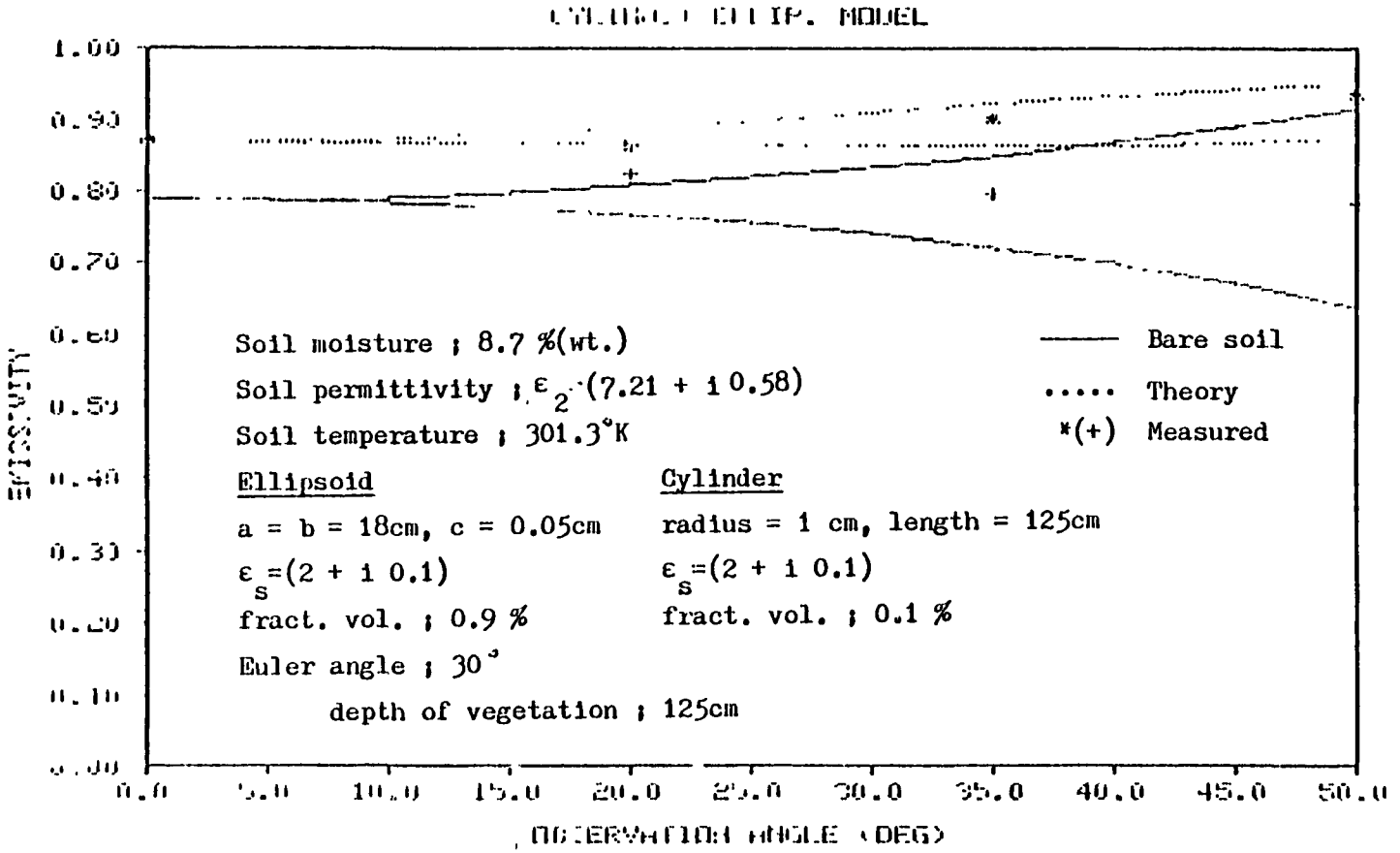

Fig. 35. Data matching for sorghum field at soil moisture 8.7 %.

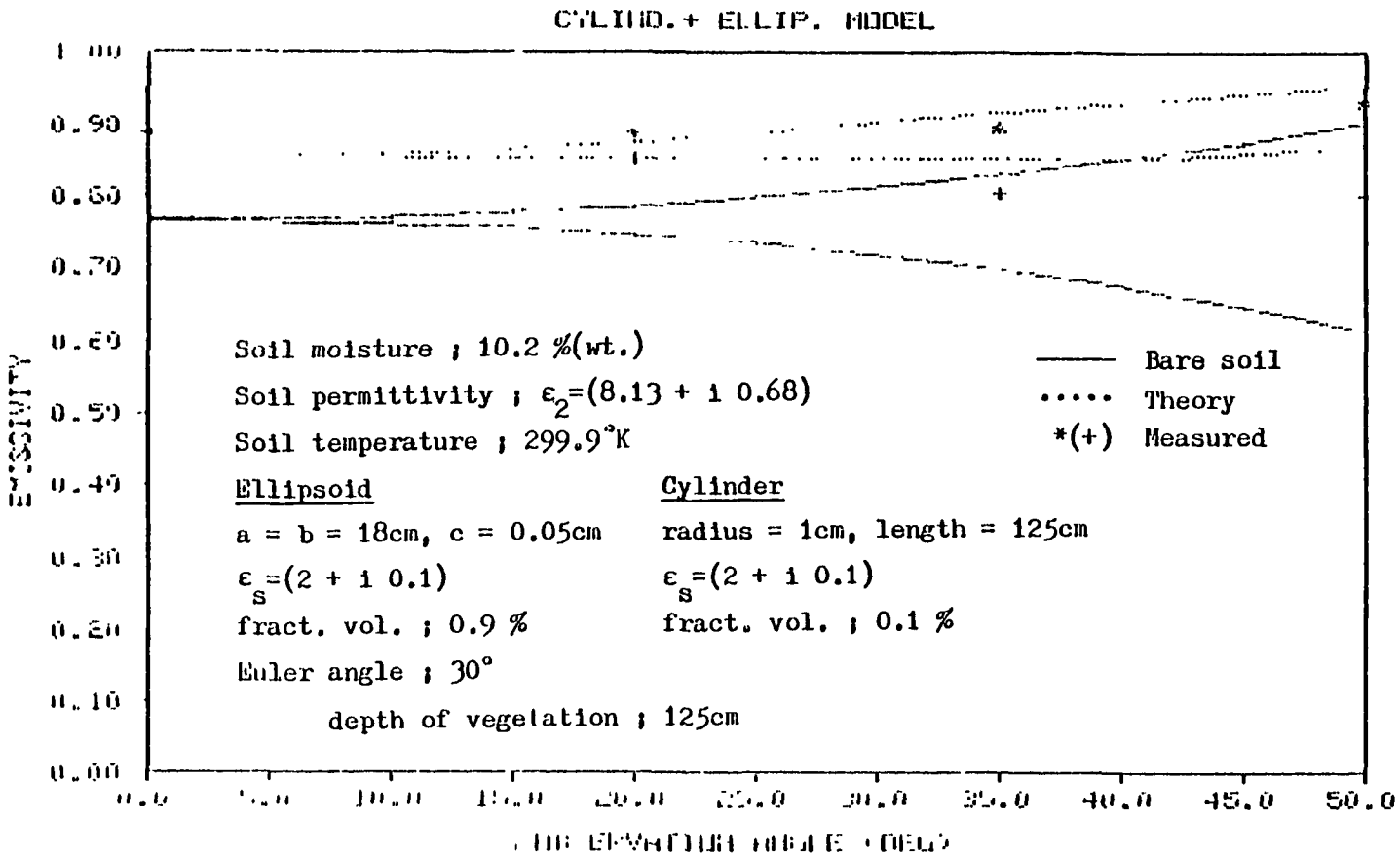

Fig. 36. Data matching for sorghum field at soil moisture 10.2 %.

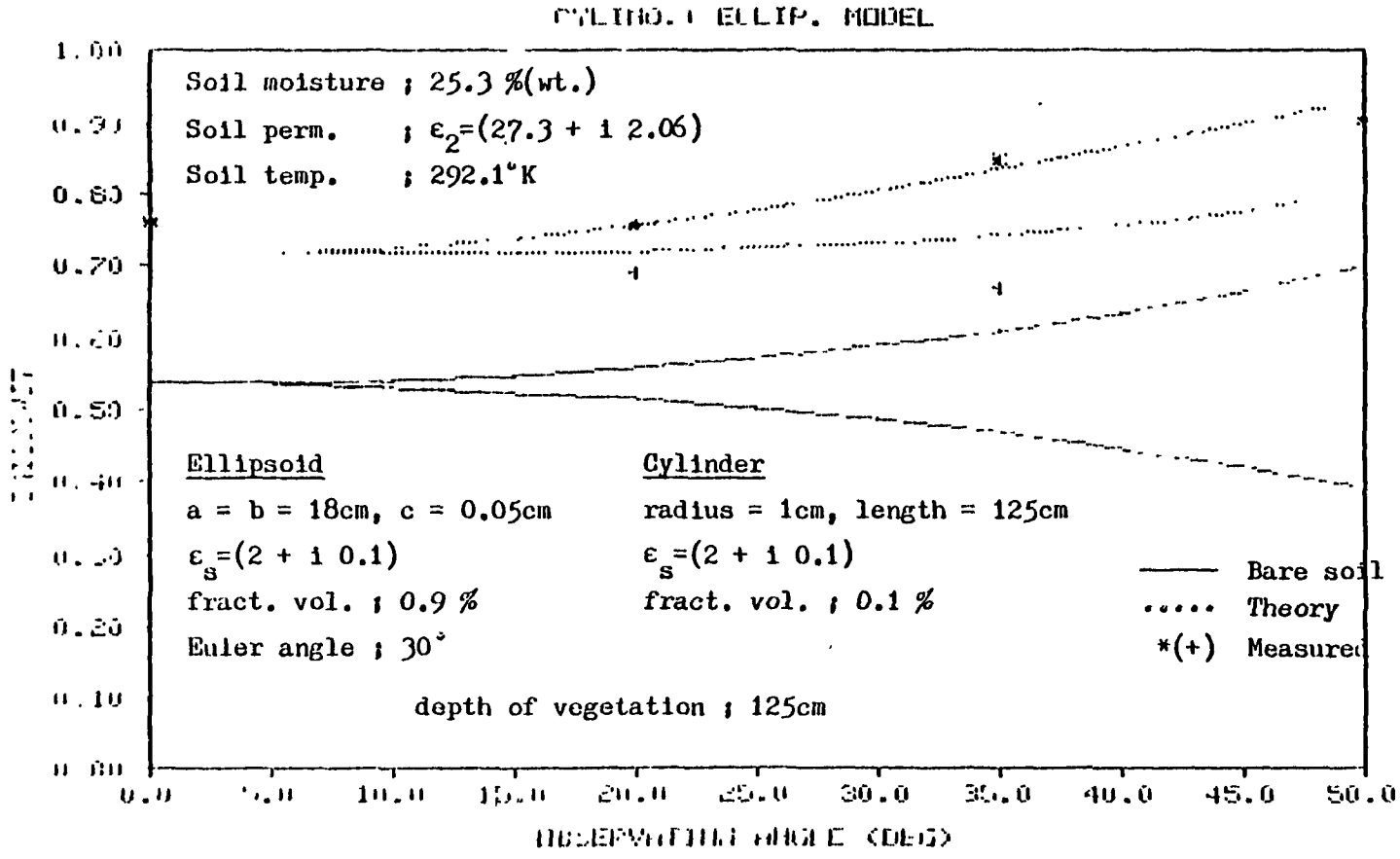

Fig. 37. Data matching for sorghum field at soil moisture 25.3 %.

analysis, it was shown that an increase of the real part of the permittivity results in a decraase of emissivity and that an increase of the imaginary part of the permittivity results in an increase of emissivity. Here we assume that the permittivity of the scatterers is linearly dependent upon the soil moisture content by weight. For soil moistures of 4.4%, 8.7% and 10.2% which are approximately 1/6, 1/3 and 2/5 of 25.3%, respectively, the imaginary parts of scatterer permittivity were chosen as 1/6, 1/3 and 2/3 of 0.1 which is the value of 25.3% soil moisture content case. With this assumption Figs. 38-40 show that the theoretical results are well matched to the measurement data.

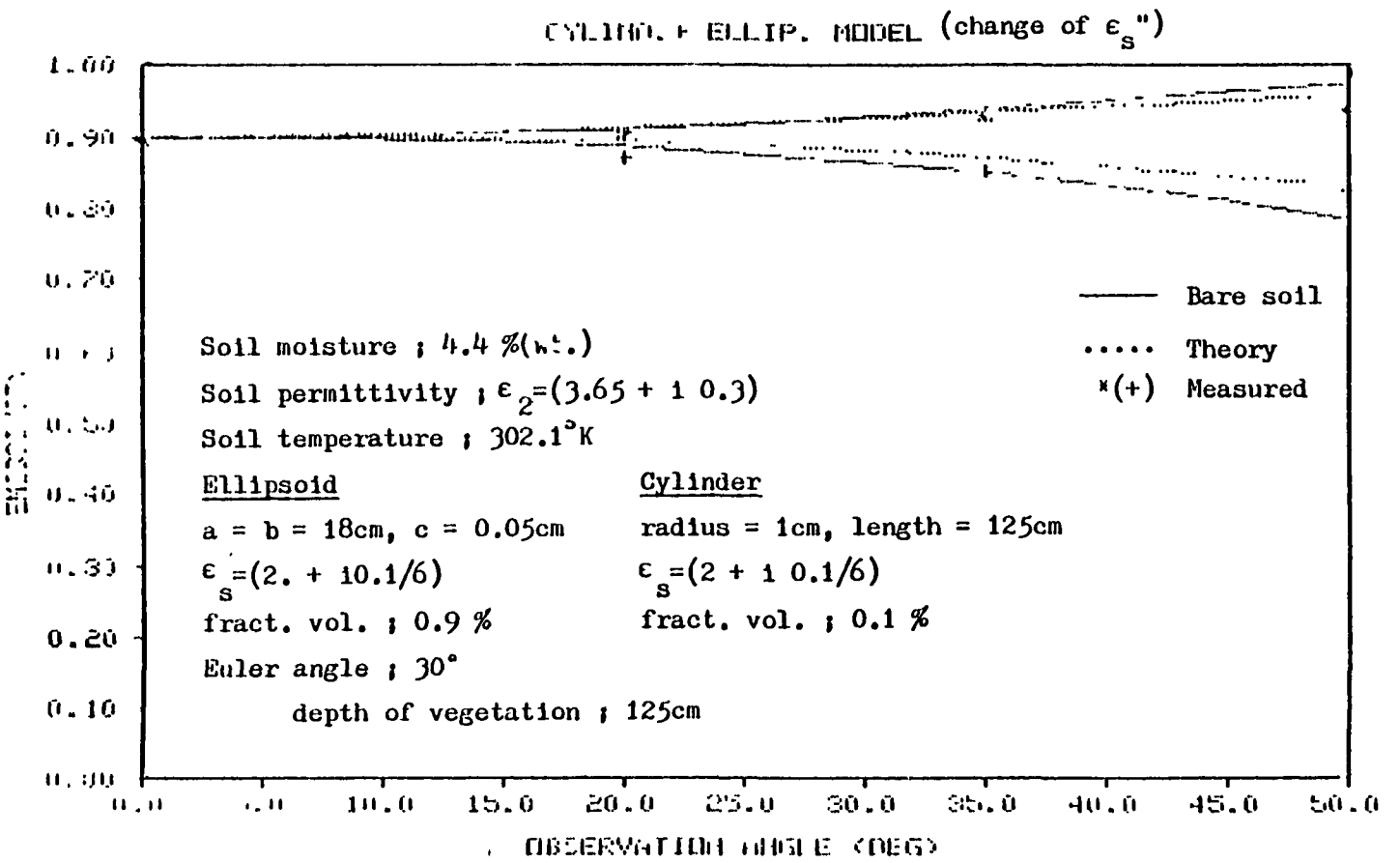

Fig. 38. Modified data matching for sorghum field at soil moisture 4.4 %.

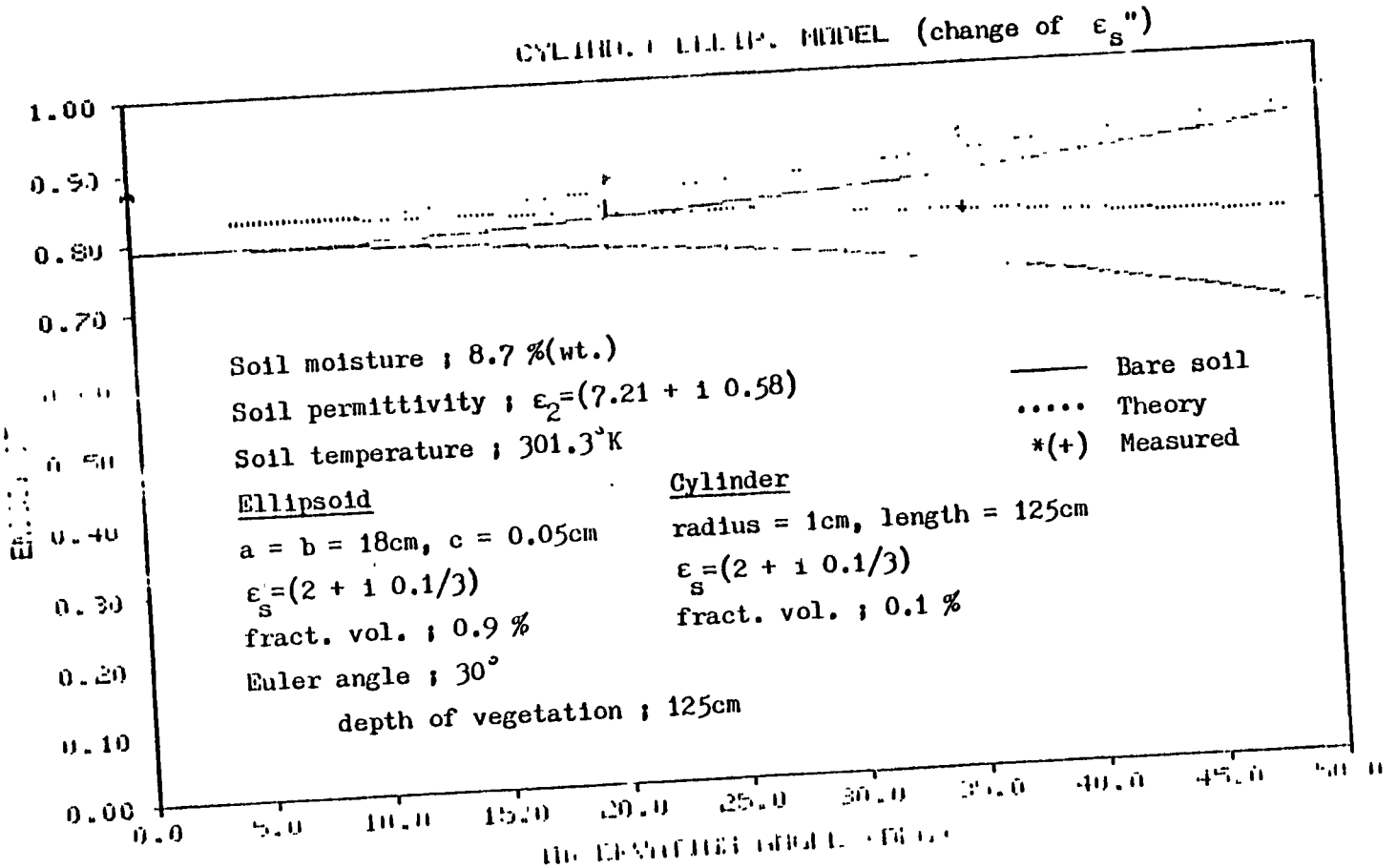

Fig. 39. Modified data matching for sorghum field at soil moisture 8.7 %.

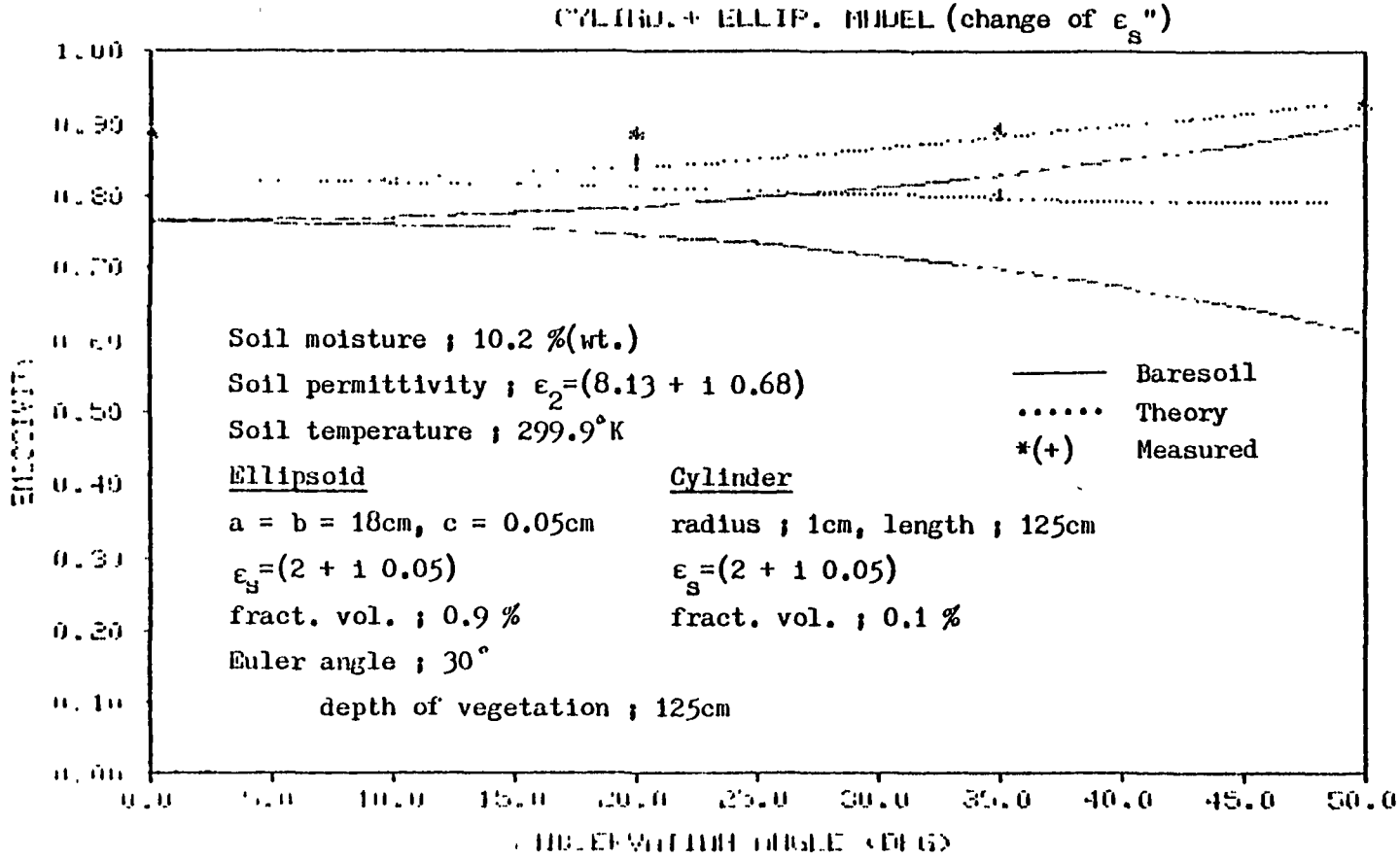

Fig. 40. Modified data matching for sorghum field at soil moisture 10.2 %.

CONCLUSION

As an application of passive microwave remote sensing, a theoretical model has been developed to study the effect of volume scattering from a vegetation canopy. A vegetation canopy was modeled as a homogeneous medium containing a cylindrical scatterer model representing the stalks and an ellipsoidal scatterer model representing the leaves. Radiative transfer theory with the composite form of each discrete scatterer model was used to obtain the brightness temperature from the scattering layer. A numerical technique using Gaussian quadrature method was utilized to do this. The theoretical results have been used to match measured data obtained from a vegetated field. From these results, it can be seen that the agreement is reasonable and the model can now be used to simulate the effect of vegetation canopies of differing height, structure, and volume density. Important observations resulting from this work are as follows:

(1) The soil permittivity calculated from the experimental radiometric measurements at an observation angle of 20° are close to Schmugge's formula.

(2) The effect of fractional volume changes in the cylindrical scatterers (stalks) is much larger than fractional volume changes in the ellipsoidal scatterers (leaves).

(3) Emissivity is not affected by a 20% change of leaf area which corresponds to a 10% change of each semi axis of the ellipsoid.

(4) An increase of ε_s', the real part of scatterer permittivity, results in a decrease of emissivity.

(5) An increease of ε_s'', the imaginary part of scatterer permittivity, results in an increase of emissivity.

(6) The permittivity of the scatterer is assumed to be linearly dependent upon the soil moisture, which means that for dry soil, moisture content in vegetation also reduces and then, reduces the permittivity of vegetation. Therefore, it is necessary to develop the permittivity of vegetation as a function of soil moisture.

The task of developing a theoretical model of vegetation is by no means complete. We have assumed that the underlying soil is a homogeneous half-space. This can immediately be extended to consider the case of a multi-layered medium below the vegetation.

REFERENCES

[1] W. H. Peake, "Theory of radar return from terrain," IRE International Convention Record, vol. 7, Part 1: 27, 1959.

[2] T. Tamir, "On radio wave propagation in forest environments," IEEE Trans. on Antennas and Propagation, vol. AP-15, no. 6, Nov. 1967.

[3] D. I. Sachs and P. L. Wyatt, "A conducting slab model for electromagnetic propagation within a jungle medium," Radio Science, vol. 3, no. 2, 125-134, February 1968.

[4] L. Du, "Scattering and absorption by large leaves at microwave frequencies," Technical Report 2440-6, Electro Science Laboratory, Ohio State University, Columbus, Ohio, January 1969.

[5] R. Sibley, "Microwave emission and scattering from vegetated terrain," Technical Report RSC-44, Remote Sensing Center, Texas A&M University, College Station, Texas, August 1973.

[6] S. Rosenbaum and L. W. Bowles, "Clutter return from vegetation areas," IEEE Transactions on Antennas and Propagation, vol. AP-22, no. 2, 227-236, March 1974.

[7] R. W. Newton, S. L. Lee, J. W. Rouse, Jr., and J. F. Paris, "On the Feasibility of remote monitoring of soil moisture with microwave sensors," Proc. Ninth International Symposium on Remote Sensing of Environment, University of Michigan, Ann Arbor, Michigan, April 1974.

[8] S. L. Lee, "Dual frequency microwave radiometer measurements of soil moisture for bare and vegetated rough surfaces," Technical Report RSC-56, Remote Sensing Center, Texas A&M University, College Station, Texas, August 1974.

[9] R. W. Newton, "Passive microwave data report; Joint soil moisture experiment at Texas A&M University; June 26-July 21, 1974," Tech. Report RSC-65, Remote Sensing Center, Texas A&M University, College Station, Texas, January 1975.

[10] R. W. Newton and S. L. Lee, "Ground data report; Joing soil moisture experiment at Texas A&M University; June 26-July 21, 1974," Technical Report RSC-61, Remote Sensing Center, Texas A&M University, College Station, Texas, October 1974.

[11] R. W. Newton and E. A. Tesch, "Joint soil moisture experiment; Ground based measurements at Texas A&M University; July 13-July 25, 1975," Tech. Report RSC-71, Remote Sensing Center, Texas A&M University, College Station, Texas, January 1976.

[12] R. W. Newton, "Microwave remote sensing and its application to soil moisture detection," Technical Report RSC-81, Remote Sensing Center, Texas A&m University, College Station, Texas, January 1977.

[13] P. P. Bativala and J. Cihlar, "Joint soil moisture experiment (Texas); Documentation of radar backscatter and ground truth data," RSL Tech. Report 264-1, Remote Sensing Lab, University of Kansas, Lawrence, Kansas, April 1975.

[14] F. T. Ulaby, "Radar response to vegetation," IEEE Trans. on Ant. and Prop., vol. AP-23, no. 1, January 1975.

[15] F. T. Ulaby and P. P. Batlivala, "Diurnal variation of radar backscatter from a vegetation canopy," IEEE Trans. on Ant. Prop., AP-24, no. 1, 11-17, Jan. 1976.

[16] A. K. Fung and T. J. Ulaby, "A scatter model for leafy vegetation," paper presented at the Conference on Aspects of Effective Scattering in Radio Communications, Advisory Group for Aero space Res. and Div., Cambridge, Mass., 1977.

[17] K. P. Kirdiashev, A. A. Chukhlantsev, and A. M. Shutko, "Microwave radiation of earth's surface in the presence of vegetation cover," Radio Eng. Electron. Phy. Engl. Transl., 24, 256-264, 1979.

[18] J. R. Wang, R. W. Newton, and W. Rouse, Jr., "Passive microwave remote sensing of soil moisture; The effect of tilled row structure," IEEE Trans. Geosci. Remote Sensing, GE18, 296-302, 1980b.

[19] F. T. Ulaby, R. K. Moore, and A. K. Fung, "Microwave remote sensing Fundamentals and radiometry," Chap. 4, Addision-Wesley, Reading, Mass., 1981.

[20] H. K. Burke and T. J. Schmugge, "Effects of varying soil moisture contents and vegetation canopies on microwave emissions," IEEE Trans. Geosci. Remote Sensing, GE20, 268-274, 1982.

[21] T. J. Jackson, T. J. Schmugge, and J. R. Wang, "Passive microwave sensing of soil moisture under vegetation canopies," Water Resour. Res., 18, 1137-1142, 1982.

[22] F. T. Ulaby, M. Razani, and M. C. Dobson, "Effects of vegetation cover on the microwave radiometric sensitivity of soil moisture," Rep. RSL TR-460-6, Remote Sensing Lab., Univ. of Kansas, Lawrence, Kansas, 1982.

[23] J. R. Wang, J. E. McMurtrey, E. T. Engman, T. J. Jackson, T. J. Schmugge, W. I. Gould, W. S. Glazar and J. E. Fuchs, "Radiometric measurements over bare and vegetated fields at 1.4 GHz and 5 GHz frequencies," Remote Sensing Environ., 12, 291-311, 1982.

[24] T. Mo, B. J. Choudhury, T. J. Schmugge, and J. R. Wang, "A model for microwave emission from vegetation-covered fields," Journal of Geophys. Res., vol. 87, no. c13 11229-11237, December, 1982.

[25] A. S. Gurvich, V. I, Kalinin, and D. T. Matveyev, "Influence of the internal structure of glaciers on their thermal radio emission," Atmos. Oceanic Phys., 9, 712-717, 1973.

[26] L. Tsang and J. A. Kong, "The brightness temperature of a half-space random medium with nonuniform temperature profile," Radio Science, 10, no. 12, 1025-1033, Dec. 1075.

[27] L. Tsang and J. A. Kong, "Emissivity of a half-space random media," Radio Science, 11, 593-598, July 1976.

[28] L. Tsang and J. A. Kong, "Thermal microwave emission from half-space random medium," Radio Science, 11, 599-609, July 1976.

[29] L. Tsang and J. A. Kong, "Microwave remote sensing of a two-layer random medium," IEEE Trans. on Ant. Prop., AP-24, no. 3, 283-287, May 1976.

[30] L. Tsang and J. A. Kong, "Thermal microwave emission from a random inhomogeneous layer over a homogeneous medium using the method of invariant imbedding," Radio Science, 12, no. 2, 185-194, March 1977.

[31] B. Djermakoye and J. A. Kong, "Radiative transfer theory for the remote sensing of layered random media," Journal of Appl. Phys., accepted for publication, 1979.

[32] A. Stogryn, "Electromagnetic scattering by random dielectric constant fluctuations in a bounded medium," Radio Science, 9, 509-518, May 1974.

[33] L. Tsang and J. A. Kong, "Radiative transfer theory for active remote sensing of half-space random media," Radio Science, 13, 763-773, Sept.-Oct. 1978.

[34] A. K. Fung and H. S. Fung, "Application of first-order renormalization method to scattering from a vegetation-like half-space," IEEE Trans. on Geoscience Electronics, GE-15, no. 4, 189-195, Oct. 1977.

[35] M. Zuniga and J. A. Kong, "Active remote sensing of random media," Journal of Apl. Phys., 51, 74-79, 1980.

[36] M. Zuniga, J. A. Kong, and L. Tsang, "Depolarization effects in the active remote sensing of random media," IEEE Trans. on Geoscience Electronics, accepted for publication, 1979.

[37] M. Zuniga, T. Habashy, and J. A. Kong, "Active remote sensing of layered random media," IEEE Trans. on Geoscience Electronics, 17, 296-302, 1979.

[38] A. W. England, "Thermal microwave emission from a half space containing scatterers," Radio Science, 9, 447-454 April 1974.

[39] A. W. England, "Thermal microwave emission from a scattering layer," Journal of Geophysical Res., 80, 4484-4496, Nov. 1975.

[40] L. Tsang and J. A. Kong, "Theory for thermal microwave emission from a bounded medium containing spherical scatterers," Journal of Appl. Phys., 48(8), 3593-3599, 1977.

[41] L. Tsang, J. A. Kong, E. Njoku, D. H. Staelin, and J. W. Waters, "Theory for microwave thermal emission from a layer of cloud or rain," IEEE Trans. Antennas Propagat., AP-25(5), 650-657, 1977.

[42] T. C. Chang, T. Gloersen, T. Schmugge, T. T. Wilhert, and H. J. Zwally, "Microwave emission from snow and glacier ice," J. Glaciol., 16, 23-39, 1976.

[43] R. J. Shin, J. A. Kong, and L. Tsang, "Radiative transfer theory for active remote sensing of homogeneous layer scatterers," in National Radio Science Meeting, URSI Conference Record, Boulder, Colorado, November 5-8, 1979.

[44] R. Lang, "Electromagnetic backscattering from a sparse distribution of loss dielectric scatterers," Radio Science, 16, 15-30, 1981.

[45] L. Tsang, M. C. Kubacsi, and J. A. Kong, "Radiative transfer theory for active remote sensing of a layer of small ellipsoidal scatterers," Radio Science, Vol. 16, no. 3, 321-329, May-June 1981.

[46] L. D. Landau and E. M. Lifshitz, "Mechanics," 110-112, Addison-Wesley, Reading, Mass., 1960.

[47] U. D. Havelka, "The effect of leaf type, plant density, and YOW spacing on canopy architecture and plant morphology in grain sorghum," Sorghum Bicolor, L. Moerch, Doctorial Dissertation, Texas A&M University, College Station, Texas, August 1971.

[48] S. Chandrasekhar, "Radiative transfer," Dover, New York, 1960.

[49] T. Schmugge, T. Wilheit, W. Webster, Jr., and P. Gloersen, "Remote sensing of soil moisture with microwave radiometers-II," Technical Note G-76114, Goddard Space Flight Center, Greenbelt, Maryland, June 1976.

[50] J. A. Kong, "Theory of electromagnetic waves," Wiley Interscience, 1975.

[51] C. T. Tai, "Dyadic Green's functions in electromagnetic theory," Intext Educational, Scranton, PA., 1971.

[52] J. A. Stratton, "Electromagnetic theory," 207-213, McGraw-Hill, New York, 1941.

[53] M. Abramowitz and I. A. Stegun, "Handbook of Mathematical functions," Dover, New York, 1965.

APPENDIX A

Table 1. Ground Truth Data for Bare Soil.

Data Set	Soil Moisture by Weight (%)	Soil Temperature (°K)
CS 1	3.1	313.4
CS 2	4.3	288.4
CS 3	27.2	300.5
CS 4	21.8	304.5
CS 5	19.3	296.0
CS 6	20.8	300.9
CS 7	25.9	304.9
CS 8	24.5	298.9
CS 9	20.2	305.8
CS 10	12.8	299.9
CS 11	15.1	302.1
CS 12	12.6	299.5
CS 13	9.5	302.1
CS 14	10.5	302.3
CS 15	10.4	300.2

Table 2. Ground Truth Data for Sorghum Field.

Data Set	Soil Moisture by Weight (%)	Soil Temperature (°K)
BS 1	25.3	292.1
BS 2	13.8	291.2
BS 3	11.7	303.9
BS 4	10.2	299.9
BS 5	8.7	301.3
BS 6	4.8	310.1
BS 7	4.4	302.1

Table 3. Brightness Temperature as a function of Observation Angle, θ, for Bare Soil.

Data Set	θ = 0°		θ = 20°		θ = 35°		θ = 50°	
	$T_{BV}(^{o}K)$	$T_{BH}(^{o}K)$	$T_{BV}(^{o}K)$	$T_{BH}(^{o}K)$	$T_{BV}(^{o}K)$	$T_{BH}(^{o}K)$	$T_{BV}(^{o}K)$	$T_{BH}(^{o}K)$
CS 1	284.23	284.11	283.01	277.42	x	x	x	x
CS 2	265.63	265.87	264.70	258.02	x	x	x	x
CS 3	199.98	201.52	179.08	167.87	198.24	159.70	220.84	142.68
CS 4	219.22	214.83	218.16	179.61	201.92	164.29	201.92	151.09
CS 5	206.52	205.36	186.08	173.11	197.68	159.75	222.25	146.11
CS 6	212.89	206.51	185.41	174.77	198.60	163.89	221.30	149.46
CS 7	183.25	185.18	169.54	156.80	186.25	148.85	215.44	135.53
CS 8	191.66	191.17	179.44	166.27	194.56	151.87	222 11	134.57
CS 9	202.10	205.02	185.60	167.22	194.30	155.07	227.33	141.28
CS 10	218.82	218.60	208.43	195.00	217.74	195.06	241.70	177.45
CS 11	216.09	217.21	206.70	193.44	218.11	177.91	244.44	162.68
CS 12	234.20	234.12	232.28	219.38	241.75	198.84	251.64	170.59
CS 13	245.92	244.12	240.27	229.73	247.52	210.86	255.67	180.77
CS 14	238.60	237.60	237.77	224.36	246.57	203.05	260.05	265.16
CS 15	246.71	246.94	244.23	236.83	251.74	220.78	260.20	196.31

Table 4. Brightness Temperature as a function of Observation Angle, θ, for Sorghum Field.

Data Set	$\theta = 0^o$		$\theta = 20^o$		$\theta = 35^o$		$\theta = 50^o$	
	$T_{BV}(^oK)$	$T_{BH}(^oK)$	$T_{BV}(^oK)$	$T_{BH}(^oK)$	$T_{BV}(^oK)$	$T_{BH}(^oK)$	$T_{BV}(^oK)$	$T_{BH}(^oK)$
BS 1	222.46	223.45	221.28	201.88	248.44	196.09	265.18	202.16
BS 2	249.33	251.13	265.61	218.97	261.40	220.64	272.99	221.88
BS 3	249.92	254.16	256.54	230.42	275.29	222.78	283.36	225.04
BS 4	266.80	261.99	260.42	249.06	271.73	240.14	283.14	236.28
BS 5	262.98	261.99	260.42	249.06	271.73	240.14	283.14	236.28
BS 6	273.05	273.02	274.00	263.61	283.57	255.33	288.59	247.08
BS 7	270.71	270.50	273.69	263.60	281.39	257.54	283.80	249.30

APPENDIX B

Derivation of scattering functions, scattering coefficients and extinction coefficients for a homogeneous medium containing cylindrical scatterers.

Consider a plane wave with the electric field

$$\bar{E}'(r) = (\hat{v}'E_v + \hat{h}'E_h') e^{i\bar{k}_1' \cdot \bar{r}} \tag{B1}$$

incident on a long cylinder of radius a, length ℓ and permittivity ε_s, as shown in Fig. B1. The unit vectors $\hat{h}'$, and $\hat{v}'$ denotes the direction of the electric fields for horizontal and vertical polarizations. The unit vectors $\hat{h}'$, $\hat{v}'$ and $\hat{k}'$ form an orthogonal coordinate system,

$$\hat{h}' = (\hat{z}' \times \hat{k}')/|\hat{z}' \times \hat{k}'| \tag{B2}$$

$$\hat{v}' = \hat{h}' \times \hat{k}' \tag{B3}$$

In spherical coordinates

$$\hat{k}' = \hat{x} \sin\theta' \cos\phi' + \hat{y} \sin\theta' \sin\phi' + z \cos\theta' \tag{B4}$$

$$\hat{h}' = -\hat{x} \sin\phi' + \hat{y} \cos\phi' \tag{B5}$$

$$\hat{v}' = \hat{x} \cos\theta' \cos\phi' + \hat{y} \cos\theta' \sin\phi' - \hat{z} \sin\theta' \tag{B6}$$

The scattered wave takes the form

$$\bar{E} = \hat{v} E_v + \hat{h} E_h \tag{B7}$$

where

$$\hat{k} = \hat{x} \sin\theta \cos\phi + \hat{y} \sin\theta \sin\phi + \hat{z} \cos\theta \tag{B8}$$

$$\hat{h} = -\hat{x} \sin\phi + \hat{y} \cos\phi \tag{B9}$$

$$\hat{v} = \hat{x} \cos\theta \cos\phi + \hat{y} \cos\theta \sin\phi - \hat{z} \sin\theta \tag{B10}$$

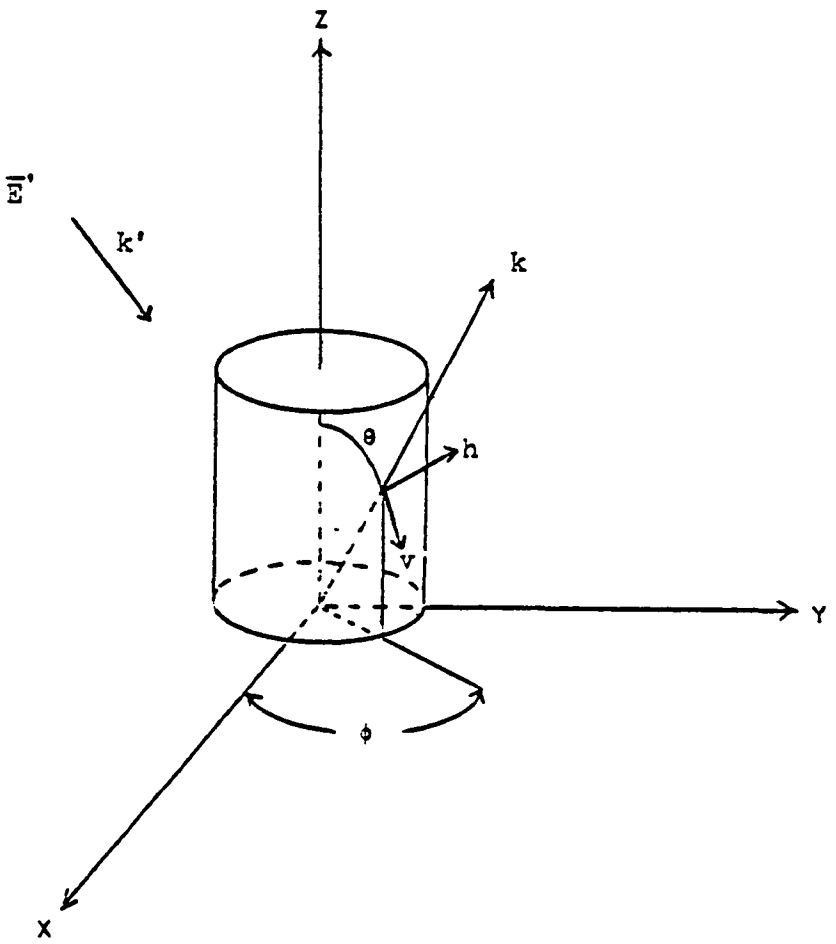

Fig. B1. Geometry used in derivation of scattered fields from a cylindrical scatterer.

The amplitudes of scattered field are related to those of incident field by

$$\begin{bmatrix} E_v \\ E_h \end{bmatrix} = \frac{e^{ik_1 r}}{r} \begin{bmatrix} f_{vv} & f_{vh} \\ f_{hv} & f_{hh} \end{bmatrix} \begin{bmatrix} E'_v \\ E'_h \end{bmatrix} \tag{B11}$$

By the solution of homogeneous Helmholtz equation in cylindrical coordinates, the longitudinal components of electric and magnetic fields internal to the surface of cylinder take the form of

$$E_z^{int} = \sum_{m=-\infty}^{\infty} A_m J_m (k_{s\rho} \rho) e^{im(\phi-\phi')} e^{ik_{1z} z} \tag{B12}$$

$$H_z^{int} = \sum_{m=-\infty}^{\infty} B_m J_m (k_{s\rho} \rho) e^{im(\phi-\phi')} e^{ik_{1z} z} \tag{B13}$$

where $J_m(k_{s\rho}\rho)$ denote the Bessel function of first kind of order m and,

$$k_{s\rho} = \sqrt{k_s^2 - k_{1z}^2} \tag{B14}$$

$$k_{1z} = k_1 \cos \theta \tag{B15}$$

$$k_s = \omega \sqrt{\mu_0 \varepsilon_s} \tag{B16}$$

$$k_1 = \omega \sqrt{\mu_0 \varepsilon_1} \tag{B17}$$

Similarly, the longitudinal components of the scattered fields take the form of

$$E_z = \sum_{m=-\infty}^{\infty} C_m H_m^{(1)}(k_{1\rho} \rho) e^{im(\phi-\phi')} e^{ik_{1z} z} \tag{B18}$$

$$H_z = \sum_{m=-\infty}^{\infty} D_m H_m^{(1)} (k_{1\rho} \rho) e^{im(\phi-\phi')} e^{ik_{1z} z} \tag{B19}$$

where $H_m^{(1)}(k_{1\rho}\rho)$ denote the Hankel function of first kind of m and,

$$k_{1\rho} = k_1 \sin\theta \tag{B20}$$

The scattered wave can be solved from Maxwell's equation by applying Huygen's principle [50] and by matching the boundary conditions. The Huygen's principle is such that with a knowledge of the tangential fields over a surface due to original sources, the fields everywhere external to the surface can be calculated through the use of equivalent new sources. Under the assumption that the tangential electric and magnetic fields are known on the surface s' enclosing a radiation source, the scattered electric field $\bar{E}(r)$ outside s' takes the form:

$$\bar{E}(\bar{r}) = \oint_{s'} ds' \{ i\omega\mu \bar{\bar{G}}(\bar{r},\bar{r}') \cdot [\hat{n} \times \bar{H}(\bar{r}')] + \bar{\nabla} \times \bar{\bar{G}}(\bar{r},\bar{r}') \cdot [\hat{n} \times \bar{E}(\bar{r}')] \tag{B21}$$

where $\bar{\bar{G}}(\bar{r},\bar{r}')$ is the dyadic Green's function [51] and,

$$\bar{\bar{G}}(\bar{r},\bar{r}') = (\bar{\bar{I}} + \frac{1}{k_1^2} \bar{\nabla}\bar{\nabla}) \frac{e^{ik_1|\bar{r}-\bar{r}'|}}{4\pi |\bar{r}-\bar{r}'|} \tag{B22}$$

With the far field approximation, the amplitudes of scattered field are related to those of incident field by

$$\begin{bmatrix} E_v \\ E_h \end{bmatrix} = \frac{i\ell}{\pi} \frac{e^{ik_1 r}}{r} \begin{bmatrix} -A & -B \\ B & -C \end{bmatrix} \begin{bmatrix} E'_v \\ E'_h \end{bmatrix} \tag{B23}$$

with

$$A = \sum_{m=-\infty}^{\infty} C_m^{TM} e^{im(\phi-\phi')} \cdot F(\theta,\theta') \tag{B24}$$

$$B = \sum_{m=-\infty}^{\infty} C_m^{ME} e^{im(\phi-\phi')} \cdot F(\theta,\theta') \tag{B25}$$

$$C = \sum_{m=-\infty}^{\infty} C_m^{TE} \, e^{jm(\phi-\phi')} \cdot F(\theta,\theta') \tag{B26}$$

where

$$C_m^{TM} = -\{P_m V_m - q^2{}_m \, J_m(k_{1\rho}a) \, H_m^{(1)}(k_{1\rho}a) \, (J_m(k_{s\rho}a))^2\}/X_m \tag{B27}$$

$$C_m^{TE} = -\{M_m N_m - q^2{}_m \, J_m(k_{1\rho}a) \, H_m^{(1)}(k_{1\rho}a) \, (J_m(k_{s\rho}a))^2\}/X_m \tag{B28}$$

$$C_m^{ME} = \frac{2k}{\pi k_{1\rho}{}^2 a} \, \frac{q_m [J_m(k_{s\rho}a)]^2}{X_m} \tag{B29}$$

and

$$F(\theta,\theta') = \frac{\sin\left[k_1 \frac{\ell}{2}(\cos\theta'-\cos\theta)\right]}{k_1 \frac{\ell}{2}(\cos\theta'-\cos\theta)} \tag{B30}$$

with

$$X_m = P_m N_m - q_m{}^2 \, [J_m(k_{s\rho}a)]^2 \, [H_m^{(1)}(k_{1\rho}a)]^2 \tag{B31}$$

$$V_m = \frac{k_1}{\varepsilon_1}\left\{\frac{\varepsilon_s}{k_{s\rho}} J_m(k_{1\rho}a) \, J_m'(k_{s\rho}a) - \frac{\varepsilon_1}{k_{1\rho}} J_m'(k_{1\rho}a) \, J_m(k_{s\rho}a)\right\} \tag{B32}$$

$$P_m = k_1\left\{\frac{1}{k_{s\rho}} H_m^{(1)}(k_{1\rho}a) \, J_m'(k_{s\rho}a) - \frac{1}{k_{1\rho}} H_m^{(1)\prime}(k_{1\rho}a) \, J_m(k_{s\rho}a)\right\} \tag{B33}$$

$$q_m = \frac{mk_{1z}}{a}\left\{\frac{1}{k_{s\rho}{}^2} - \frac{1}{k_{1\rho}{}^2}\right\} \tag{B34}$$

$$M_m = k_1\left\{\frac{1}{k_{s\rho}} J_m(k_\rho a) \, J_m'(k_{s\rho}a) - \frac{1}{k_{1\rho}} J_m'(k_{1\rho}a) \, J_m(k_{s\rho}a)\right\} \tag{B35}$$

$$N_m = \frac{k_1}{\varepsilon_1}\left\{\frac{\varepsilon_s}{k_{s\rho}} H_m^{(1)}(k_{1\rho}a) \, J_m'(k_{s\rho}a) - \frac{\varepsilon_1}{k_{1\rho}} H_m^{(1)\prime}(k_{1\rho}a) \, J_m(k_{s\rho}a)\right\} \tag{B36}$$

We now derive the scattering functions. Define the radial Poynting vector as follows:

$$S_v = \frac{1}{\eta} < |E_v|^2 > \tag{B37}$$

$$S_h = \frac{1}{\eta} < |E_h|^2 > \tag{B38}$$

The Stokes parameters are related to the radial Poynting vector by

$$I_v = \frac{1}{\cos\theta\ \Delta V}\ r^2\ S_v \tag{B39}$$

$$I_h = \frac{1}{\cos\theta\ \Delta V}\ r^2\ S_h \tag{B40}$$

where θ is the angle between the direction of propagation and the outward normal to the elementary area ΔA. We then use (B23) to write down the components of radial Poynting vector for the scattered field in terms of incident Stokes parameters.

$$S_v = \frac{\ell^2}{\pi^2\gamma^2}\left[\ |A|^2 \quad |B|^2\right] \begin{bmatrix} I_v' \\ I_h' \end{bmatrix} \tag{B41}$$

$$S_h = \frac{\ell^2}{\pi^2\gamma^2}\left[\ |B|^2 \quad |C|^2\right] \begin{bmatrix} I_v' \\ I_h' \end{bmatrix} \tag{B42}$$

Let us now consider a plane wave with the electric field vector given by (B1) incident on a volume ΔV of homogeneous medium containing n cylindrical scatterers with radius a, length ℓ and permittivity ε_s. Relating Stokes parameters of the scattered field to those of incident field by making use of (B39)-(B42), we obtain

$$\begin{bmatrix} I_v \\ I_h \end{bmatrix} = \frac{n}{\Delta V}\ \frac{\ell^2}{\pi^2} \begin{bmatrix} |A|^2 & |B|^2 \\ |B|^2 & |C|^2 \end{bmatrix} \begin{bmatrix} I_v' \\ I_h' \end{bmatrix} \tag{B43}$$

where we made use of the fact that $\Delta V = A\Delta s$. From the above expression we can easily identify scattering functions

$$(v,v') = N_a \frac{\ell^2}{\pi^2 \cos\theta'} |A|^2 \tag{B44}$$

$$(v,h') = N_a \frac{\ell^2}{\pi^2 \cos\theta'} |B|^2 \tag{B45}$$

$$(h,v') = (v,h') \tag{B46}$$

$$(h,h') = N_a \frac{\ell^2}{\pi^2 \cos\theta'} |C|^2 \tag{B47}$$

where N_a in the above equation is the number of scatterers per unit volume.

Once we have obtained the scattering function matrix, we can calculate the scattering coefficient k_s, which is the functional loss of power per unit length due to scattering.

$$k_{sv} = \int d\Omega' \, [(v,v') + (h,v')] \tag{B48}$$

$$k_{sh} = \int d\Omega' \, [(v,h') + (h,h')] \tag{B48}$$

The extinction coefficient which is the fractional loss of power per unit length due to absorption and scattering per scatterer, can be found by using the optical theorem. The rate of extinction is by definition of optical theorem,

$$W = -\frac{2\pi}{nk_1} \text{ Imag } [E' \, E^* \, \hat{k}' \cdot \hat{k}] \tag{B50}$$

where E^* is the complex conjugate of the scattered field E. Since the extinction power is given by $W \cdot \Delta A \cdot N$ and incident power is $\Delta A |E'|^2 \cos\theta / \eta'$.

$$k_{ev}(\theta') = -\frac{4N_a \ell}{k_1 \cos\theta'} \sum_{m=-\infty}^{\infty} R_e(C_m^{TM}) \tag{B51}$$

$$k_{eh}(\theta') = -\frac{4N_a \ell}{k_1 \cos\theta'} \sum_{m=-\infty}^{\infty} R_e(C_m^{TE}) \tag{B52}$$

The radiative transfer equation for cylindrical scatterers can be simplified considerably by applying the small radii approximations (i.e. $k_1 a << 1$) into (B24)-(B26).

$$A(\Omega,\Omega') = F(\theta,\theta') \left[C_0^{TM} + 2\, C_1^{TM} \cos(\phi-\phi')\right] \tag{B53}$$

$$B(\Omega,\Omega') = F(\theta,\theta')\, 2\, i\, C_1^{ME} \sin(\phi-\phi') \tag{B54}$$

$$C(\Omega,\Omega') = F(\theta,\theta')\, 2\, C_1^{TE} \cos(\phi-\phi')] \tag{B55}$$

with C_0^{TM}, C_1^{TM}, C_1^{ME}, and C_1^{TE} expressed in (42)-(45).

We can also simplify (B30) with the long cylinder approximation as follow:

$$\lim_{k_1 \ell \to \infty} \int_0^{\pi} d\theta' \sin\theta' F^2(\theta,\theta') = \frac{2\pi}{k_1 \ell} \tag{B56}$$

And with the same approximation in (B56)

$$\int_0^{\pi} d\theta' \sin\theta' F^2(\theta,\theta') f(\theta') = \frac{2\pi}{k_1 \ell} f(\theta) \tag{B56}$$

where $f(\theta)$ is any smoothly varying function of θ. Using these approximations, we can find that the specific intensities for different θ are decoupled and the radiative transfer equation assume the form of (31) and (32) with the coefficients given in (33)-(38).

APPENDIX C

Derivation of scattering phase function, scattering coefficients and absorption coefficients for ellipsoidal scatterers.

Consider an incident plane wave

$$\bar{E}' = [\hat{v}' E_v' + \hat{h}' E_h'] e^{i\bar{k}_1' \cdot \bar{r}} \tag{C1}$$

impinging on an ellipsoidal scatterer of permittivity $\varepsilon_s = \varepsilon_s' + i \varepsilon_s''$ embedded in a medium of permittivity ε_1. The amplitude of the scattered field are related to those of the incident field by

$$\begin{bmatrix} E_v(\Omega) \\ E_h(\Omega) \end{bmatrix} = \frac{e^{ik_1 r}}{r} \begin{bmatrix} f_{vv}(\Omega,\Omega') & f_{vh}(\Omega,\Omega') \\ f_{hv}(\Omega,\Omega') & f_{hh}(\Omega,\Omega') \end{bmatrix} \begin{bmatrix} E'_v(\Omega') \\ E'_h(\Omega') \end{bmatrix} \tag{C2}$$

If the axes of the ellipsoid are oriented in the $\hat{x}_b$, $\hat{y}_b$ and $\hat{z}_b$ directions, then the internal induced dipole moment $\bar{p}^{int}$ inside the ellipsoid is [52]

$$\bar{p}^{int} = v_0 (\varepsilon_s - \varepsilon_1) \left[\frac{E_{xb} \hat{x}_b}{1+v_d A_1} + \frac{E_{yb} \hat{y}_b}{1+v_d A_2} + \frac{E_{zb} \hat{z}_b}{1+v_d A_3} \right] \tag{C3}$$

where v_0 is the volume of the ellipsoid, and

$$v_d = \frac{abc}{2} (\varepsilon_s - \varepsilon_1) \tag{C4}$$

$$A_1 = \int_0^\infty \frac{ds}{(s+a^2)R_s} \tag{C5}$$

$$A_2 = \int_0^\infty \frac{ds}{(s+b^2)R_s} \tag{C6}$$

$$A_3 = \int_0^\infty \frac{ds}{(s+c^2)R_s} \tag{C7}$$

$$R = [\,(s + a^2)(s + b^2)(s + c^2)\,]^{1/2} \tag{C8}$$

In (C3)

$$E_{xb} = (\hat{v}'\cdot\hat{x}_b)\, E_v' + (\hat{h}'\cdot\hat{x}_b)\, E_h' \tag{C9}$$

$$E_{yb} = (\hat{v}'\cdot\hat{y}_b)\, E_v' + (\hat{h}'\cdot\hat{y}_b)\, E_h' \tag{C10}$$

$$E_{zb} = (\hat{v}'\cdot\hat{z}_b)\, E_v' + (\hat{h}'\cdot\hat{z}_b)\, E_h' \tag{C11}$$

The equivalent induced current is $J^{ind} = -i\omega\bar{p}^{int}\,\delta(r)$. This is an equivalent Herzian dipole, the radiated fields of which can be calculated easily, is in the form of (C2). The coefficients $f_{vv}(\Omega,\Omega')$, $f_{vh}(\Omega,\Omega')$, $f_{hv}(\Omega,\Omega')$ and $f_{hh}(\Omega,\Omega')$ are given by

$$f_{vv}(\Omega,\Omega') = \frac{\omega^2\mu}{4\pi} v_0\,(\varepsilon_s-\varepsilon_1)\left[\frac{(\hat{v}\cdot\hat{x}_b)(\hat{x}_b\cdot\hat{v}')}{1+v_dA_1} + \frac{(\hat{v}\cdot\hat{y}_b)(\hat{y}_b\cdot\hat{v}')}{1+v_dA_2} + \frac{(\hat{v}\cdot\hat{z}_b)(\hat{z}_b\cdot\hat{v}')}{1+v_dA_3}\right] \tag{C12}$$

$$f_{vh}(\Omega,\Omega') = \frac{\omega^2\mu}{4\pi} v_0\,(\varepsilon_s-\varepsilon_1)\left[\frac{(\hat{v}\cdot\hat{x}_b)(\hat{x}_b\cdot\hat{h}')}{1+v_dA_1} + \frac{(\hat{v}\cdot\hat{y}_b)(\hat{y}_b\cdot\hat{h}')}{1+v_dA_2} + \frac{(\hat{v}\cdot\hat{z}_b)(\hat{z}_b\cdot\hat{h}')}{1+v_dA_3}\right] \tag{C13}$$

$$f_{hv}(\hat{\Omega},\hat{\Omega}') = \frac{\omega^2\mu}{4\pi} v_0 (\varepsilon_s-\varepsilon_1) \left[\frac{(\hat{h}\cdot\hat{x}_b)(\hat{x}_b\cdot\hat{v}')}{1+v_d A_1} + \frac{(\hat{h}\cdot\hat{y}_b)(\hat{y}_b\cdot\hat{v}')}{1+v_d A_2} + \frac{(\hat{h}\cdot\hat{z}_b)(\hat{z}_b\cdot\hat{v}')}{1+v_d A_3}\right] \quad (C14)$$

$$f_{hh}(\hat{\Omega},\hat{\Omega}') = \frac{\omega^2\mu}{4\pi} v_0 (\varepsilon_s-\varepsilon_1) \left[\frac{(\hat{h}\cdot\hat{x}_b)(\hat{x}_b\cdot\hat{h}')}{1+v_d A_1} + \frac{(\hat{h}\cdot\hat{y}_b)(\hat{y}_b\cdot\hat{h}')}{1+v_d A_2} + \frac{(\hat{h}\cdot\hat{z}_b)(\hat{z}_b\cdot\hat{h}')}{1+v_d A_3}\right] \quad (C15)$$

In (C12)-(C15), $\hat{v}'$ and $\hat{h}'$ are, respectively, the vertical polarization vector and horizontal polarization vector for incident wave and $\hat{v}$ and $\hat{h}$ are, respectively, the vertical polarization vector and horizontal polarization vector for scattered wave as shown in Appendix B.

Then, with the radial Poynting vectors defined in (B37) and (B38), and the relation between the Stokes parameters and the radial Poynting vectors as shown in (B41) and (B42), we can obtain the scattering matrix for passive remote sensing.

$$(v,v') = n_0 < \left|f_{vv}(\hat{\Omega},\hat{\Omega}')\right|^2 > \quad (C16)$$

$$(v,h') = n_0 < \left|f_{vh}(\hat{\Omega},\hat{\Omega}')\right|^2 > \quad (C17)$$

$$(h,v') = n_0 < \left|f_{hv}(\hat{\Omega},\hat{\Omega}')\right|^2 > \quad (C18)$$

$$(h,h') = n_0 < \left|f_{hh}(\hat{\Omega},\hat{\Omega}')\right|^2 > \quad (C19)$$

The angular bracket in (C16)-(C19) stands for ensemble average over the Eulerian angles, and n_0 stands for the number of ellipsoids per unit volume.

The scattering coefficient which are the fractional loss of power per unit length due to scattering are

$$k_{sv}(\Omega') = \int d\Omega\,[(v,v') + (h,v')] \tag{C20}$$

$$k_{sh}(\Omega') = \int d\Omega\,[(h,v') + (h,h')] \tag{C21}$$

The absorption coefficients is n_0 times the fractional loss of power due to absorption per scatterer and defined as

$$k_a(\Omega') = n_0 \frac{\int dv \frac{1}{2}\varepsilon''\omega|E^{int}|^2}{\frac{|E'|^2}{2\eta}} \tag{C22}$$

With this definition, the absorption coefficients for ellipsoids are

$$k_{av}(\Omega') = \sqrt{\frac{\mu_0}{\varepsilon_1}}\, n_0\, v_0\, \varepsilon_s''\, w \left\langle \left[\frac{(\hat{x}_b\cdot\hat{v}')^2}{|1+v_d A_1|} + \frac{(\hat{y}_b\cdot\hat{v}')^2}{|1+v_d A_2|} + \frac{(\hat{z}_b\cdot\hat{v}')^2}{|1+v_d A_3|} \right] \right\rangle \tag{C23}$$

$$k_{ah}(\Omega') = \sqrt{\frac{\mu_0}{\varepsilon_1}}\, n_0\, v_0\, \varepsilon_s''\, w \left\langle \left[\frac{(\hat{x}_b\cdot\hat{h}')^2}{|1+v_d A_1|} + \frac{(\hat{y}_b\cdot\hat{h}')^2}{|1+v_d A_2|} + \frac{(\hat{z}_b\cdot\hat{h}')^2}{|1+v_d A_3|} \right] \right\rangle \tag{C23}$$

where the angular brackets represent ensemble average over the Eulerian angle of rotation and can be obtained by multiplying with the probability density function $p(\alpha,\beta,\gamma)$ and integrating over α between 0 and 2π, β between 0 and 2π and γ between 0 and 2π.

APPENDIX D

Gaussian Quadrature Formula

Consider an integral

$$I = \int_a^b dx\ f(x)\ W(x) \tag{D1}$$

to be evaluated approximately by using m values of f(x) in the interval (a,b):

$$\int_a^b dx\ f(x)\ W(x) = \sum_{j=1}^{m} a_j\ f(x_j) \tag{D2}$$

where W(x) is a weighting function. The problem is to choose x_j and determine a_j in such manner that the integral is best approximated by the least number of terms (smallest m).

Suppose the m values of f(x) are taken at the positions

$$[x_j] = [x_1, x_2, \ldots, x_m] \tag{D3}$$

Using the Lagrange interpolation formula we can construct a polynomial $\emptyset(x)$ of a degree less than or equal to m-1, which will take the same values at the points $[x_j]$ as f(x) does. Thus

$$\emptyset(x) = \sum_{j=1}^{m} f(x_j)\ \frac{F(x)}{(x-x_j)\ F'(x_j)} \tag{D4}$$

where

$$F(x) = \prod_{j=1}^{m} (x-x_j) \tag{D5}$$

is a polynomial of degree m whose zeros are at $[x_j]$, and

$$F'(x_j) = \left[\ \frac{d}{dx} F(x)\ \right]_{x=x_j} = \sum_{\substack{i=1 \\ i\neq j}}^{m} (x_j-x_i) \tag{D6}$$

We define the integral

$$I_1 = \int_a^b dx\ W(x)\ \phi(x) \tag{D7}$$

Substituting (D4) into (D7)

$$I_1 = \sum_{j=1}^{m} a_j\ f(x_j) \tag{D8}$$

where

$$a_j = \frac{1}{F'(x_j)} \int_a^b dx\ \frac{F(x)W(x)}{x-x_j} \tag{D9}$$

Clearly, if f(x) is a polynomial of degree less than or equal to m-1, then

$$\phi(x) = f(x) \tag{D10}$$

and, therefore

$$I_1 = I \tag{D11}$$

We note that (D10) and (D11) hold irrespective of the choices of $[x_j]$.

We shall now show that with a judicious choice of $[x_j]$

$$I_1 = I \tag{D12}$$

when f(x) is a polynomial of degree 2m-1 or less.

Let f(x) be a polynomial of degree 2m-1. Since, for j=1,...,m

$$f(x_j) = \phi(x_j) \tag{D13}$$

$$F(x_j) = 0 \tag{D14}$$

we can write

$$f(x) = \phi(x) + F(x) \sum_{\ell=0}^{m-1} C_\ell\ x^\ell \tag{D15}$$

where C_ℓ are constants. Since $F(x)$ is a polynomial of degree m, the series in the second term in (D15) is a polynomial of degree 2m-1. By proper choice of C_ℓ, any function which can be described by a polynomial of degree 2m-1 can be represented by (D15). Substituting in (D15) into (D1)

$$I = \sum_{j=1}^{m} a_j \, f(x_j) + \sum_{\ell=0}^{m-1} C_\ell \int_a^b dx \, F(x) \, W(x) \, x^\ell \tag{D16}$$

Now choosing $[x_j]$, and thus $F(x)$, such that

$$\int_a^b dx \, F(x) \, W(x) \, x^\ell = 0 \qquad \ell = 0, \ldots, m-1 \tag{D17}$$

then the second term on the right side of (D16) vanishes and

$$I = I_1 \tag{D18}$$

If the polynomial $F(x)$ can be determined from (D17), then x_j are the zeros of $F(x)$ and a_j can then be determined from (D9).

For the integrals in the radiative transfer equations $W(x) = 1$, $a = -1$, $b = +1$. It is also recognized that the Legendre polynomial $P_m(x)$ is orthogonal to all x^ℓ, and therefore choose

$$F(x) = P_m(x) \tag{D19}$$

and x should be the zeros of the Legendre polynomial $P_m(x)$.

Thus

$$\int_{-1}^{1} f(x) \, dx = \sum_{j=1}^{m} a_j \, f(x_j) \tag{D20}$$

where

$$a_j = \frac{1}{P_m'(x_j)} \int_{-1}^{1} \frac{P_m(x)}{(x-x_j)} \, dx \tag{D21}$$

This is called Gaussian quatrature formula. The numerical technique of using Gaussian quadrature formula to replace the integral in the radiative transfer equations and solving the resulting system of first order differential equations is called the method of Gaussian quadrature.

For our problem, it is convenient to choose an even order, m=2N, Legendre polynomial. Using μ instead of x,

$$\int_{-1}^{1} f(\mu)\, d\mu = \sum_{j=-N}^{N} a_j\, f(\mu_j) = \sum_{j=1}^{N} a_j\, [f(\mu_j) + f(-\mu_j)] \qquad (D22)$$

and for $j = 1,\ldots,N$

$$P_{2N}(\mu_j) = P_{2N}(-\mu_j) \qquad (D23)$$

$$a_j = \frac{1}{P'_{2N}(\mu_j)} \int_{-1}^{1} \frac{P_{2N}(\mu)}{(\mu-\mu_j)}\, d\mu \qquad (D24)$$

$$a_j = a_{-j} \qquad (D25)$$

$$\mu_j = -\mu_{-j} \qquad (D26)$$

The values of a_j and μ_j for different values of N are tabulated and readily available [53].